ASSESSMENT OF TORSIONAL RESONANCE IN TURBINE-GENERATOR SHAFT DUE TO MULTIPLE EAF OPERATION

MD. MINARUL ISLAM

DEPARTMENT OF ELECTRICAL AND ELECTRONIC ENGINEERING
BANGLADESH UNIVERSITY OF ENGINEERING AND TECHNOLOGY
DHAKA-1000, BANGLADESH

JULY 2013

Assessment of Torsional Resonance in Turbine-Generator Shaft Due to Multiple EAF Operation

by

Md. Minarul Islam

A thesis submitted to the Department of the Electrical and Electronic Engineering of Bangladesh University of Engineering and Technology in partial fulfillment of the requirements for the degree of

MASTER OF SCIENCE IN ELECTRICAL AND ELECTRONIC ENGINEERING

Department of Electrical and Electronic Engineering

BANGLADESH UNIVERSITY OF ENGINEERING AND TECHNOLOGY

DHAKA-1000, BANGLADESH

July 2013

The thesis titled **"Assessment of Torsional Resonance in Turbine-Generator Shaft Due to Multiple EAF Operation"** submitted by Md. Minarul Islam, Roll No. 0409062136P, Sesson: April 2009, has been accepted as statisfactory in partial fulfillment of the requirement for the degree of **Master of Science in Electrical and Electronic Engineering** on 13 July, 2013.

BOARD OF EXAMINERS

1	____________________________ Dr. Abdul Hasib Chowdhury Associate Professor Department of Electrical and Electronic Engineering BUET, Dhaka-1000, Bangladesh	Chairman (Supervisor)
2	____________________________ Dr. Pran Kanai Saha Professor and Head Department of Electrical and Electronic Engineering BUET, Dhaka-1000, Bangladesh	Member
3	____________________________ Dr. Md. Quamrul Ahsan Professor Department of Electrical and Electronic Engineering BUET, Dhaka-1000, Bangladesh	Member
4	____________________________ Dr. Enamul Basher Professor Department of Electrical and Electronic Engineering BUET, Dhaka-1000, Bangladesh	Member
5	____________________________ Dr. Kazi Mujibur Rahman Professor Department of Electrical and Electronic Engineering BUET, Dhaka-1000, Bangladesh	Member
6	____________________________ Dr. Md. Fayyaz Khan Professor Department of Electrical and Electronic Engineering United International University (UIU), Dhaka	Member (External)

Declaration

It is hereby declared that this thesis titled **"Assessment of Torsional Resonance in Turbine-Generator Shaft Due to Multiple EAF Operation"** or any part of it has not been submitted elsewhere for the award of any degree or diploma.

Signature of the candidate

Md. Minarul Islam

Acknowledgement

First of all, the author is grateful to almighty ALLAH for overcoming all the difficulties and problems that he faced during this work and for bringing this thesis into reality. The author wants to show his sincere gratitude to all individuals, who provided support, advice and encouragement during his student life in all the institutions.

The author is delighted to express his heartiest gratitude and sincerest indebtness to his supervisor, Dr. Abdul Hasib Chowdhury, Associate Professor, Department of Electrical and Electronic Engineering, Bangladesh University of Engineering and Technology, Dhaka. He guided the author and provided information, useful suggestion, criticism and encouragement that enabled the author to carry out this work.

The author is deeply grateful to Mr. Sahbun Nur Rahman, Deputy Manager, System Planning, Power Grid Company of Bangladesh Ltd. for all his supporting grid data.

Last but not the least, the author wants to express his indebtness to his parent, his wife and his brother for their all time support and encouragement during the work.

ABSTRACT

The oscillating torques between different mass sections of turbine-generator shaft are amplified at resonance, which indicates that the oscillating torques absorb more energy from the system. This may cause violent swing motion creating torsional stress and even catastrophic failure in the mechanical system. The torsional stressing may arise as a result of torsional resonance induced by pulsating components in the electrical torque of the generator. Hence, the interaction between the electrical system and the turbine-generator has to be analysed in advance to assess the severity of torsional stress to the shaft system to ensure undisturbed operation.

The frequencies of torsional oscillations are in the subsynchronous range. There are many sources of subsynchronous frequencies in the electrical network such as capacitor compensated transmission line, EAF loads, load-commutated inverters, PWM voltage-source inverters etc. These equipments induce pulsating components in the air-gap torque of synchronous machine and through which the torsional oscillating torques are amplified during torsional resonance.

The EAF load causes power quality problems such as flicker, voltage imbalances, harmonics and interharmonics. If the subsynchronous frequencies created by EAF leads to resonance, the respective matched torsional modes of the turbine-generator system are excited causing torsional oscillating torques amplification. The magnitude of torsional resonance depends on the proximity of stimulating frequency and natural frequency, on the magnitude and duration of the excitation and on the damping of the excited natural mode.

Torsional oscillating torques amplification due to multiple EAF operations at the same point of common coupling (PCC) or at close proximity has not been studied yet. Investigation of torsional excitation due to multiple EAF operations is the main focus of this thesis.

In this work, the three-phase EAFs are modeled using MATLAB/Simulink from mathematical model of electric arc, where the resistances of the EAFs varied deterministically in the frquency range of 1.2-45.5 Hz to meet the actual characteristics of EAF.

For the test system, EAFs are connected to the same PCC and their effects on turbine-generator shaft are measured with/without resonant excitation of torsional modes. For both cases, FFT technique is used to quantify torsional torques between different mass sections of the rotor shaft.

As the interaction between EAF operation and turbine-generator mechanical system is in subsynchronous frequency range, this allows the shaft system to be designed by a simple lumped-mass model. Steam turbine-generator shafts having five torsional masses such as a generator rotor, two low-pressure, an intermediate-pressure and a high pressure turbine sections are considered for simulation.

Eigenvalue analysis technique and FFT are used to find the torsional frequencies and modes of the turbine-generator rotor shaft system.

Finally, the Chittagong region of the Bangladesh Power System (BPS) with two steel mills using AC EAFs are modeled and simulated. The region is modeled with all the large power plants in the region included and the national grid as an equivalent generation at the Comilla-North bus.

Contents

LIST OF TABLES

LIST OF FIGURES

List of Abbreviations

BLWN	Band Limited White Noise
BPS	Bangladesh Power System
CVS	Controlled Voltage Source
DRI	Direct Reduced Iron
EAF	Electric Arc Furnace
FFT	Fast Fourier Transform
GTG	Gas Turbine Generator
HP	High Pressure
HVDC	High Voltage Direct Current
IHA	Iterative Harmonic Analysis
IP	Intermediate Pressure
LCI	Load Commutated Inverter
LP	Low Pressure
OCC	Open Circuit Characteristic Curve
PCC	Point of Common Coupling
PWM	Pulse Width Modulation
SPSR	Supersynchronous Resonance
SSR	Subsynchronous Resonance
SVC	Static Voltage Controller
VFD	Variable Frequency Drive
VSI	Voltage Source Inverter

List of Principle Symbols

$\boldsymbol{A}$	State matrix
D	Damping constant
e	Induced voltage
E_t	Terminal voltage
E_q	Internal voltage
$G(s)$	Stator to field transfer function
H	Inertia constant
I_{ig}	Ignition current
I_{ex}	Extinction current
I_n	Amplitude of modulation current of frequency f_n
K	Torsional stiffness
L	Inductance
P_1	Power radiated in the form of heat to the external environment
P_2	Power , increasing the internal energy of arc
P_t	Power output from generator
P_{r0}	Arc column power
Q_t	Reactive power
R	Resistance
r	Arc radius
T_e	Air gap torque
T'_{d0}	*d*-axis transient OC time constant
T'_{q0}	*q*-axis transient OC time constant
T''_{d0}	*d*-axis subtransient OC time constant
T''_{q0}	*q*-axis subtransient OC time constant
V_{ig}	Ignition voltage
V_{ex}	Extinction voltage
X	Reactance
X_d	*d*-axis synchronous reactance
X_q	*q*-axis synchronous reactance
X'_d	*d*-axis transient reactance
X'_q	*q*-axis transient reactance
X''_d	*d*-axis subtransient reactance
X''_q	*q*-axis subtransient reactance

X_l	Stator leakage reactance
ξ	Damping ratio
λ	Eigenvalue
ρ	Resistivity
τ_a	Arc time constant
ψ	Instantaneous flux linkage
ω_r	Angular speed of rotor in electrical rad/sec.

CHAPTER 1

INTRODUCTION

1.1. Introduction

The tendency of a system to oscillate with greater amplitude at some frequencies than at others is termed as resonance. Frequencies at which the response amplitude is a relative maximum are termed as resonance frequencies. Even small periodic driving forces at resonance may produce large amplitude of oscillations which means that at resonance the oscillations absorb more energy from the system. It may lead to violent swing motions and even catastrophic failure in the mechanical system.

A steam/gas turbine-generating unit consists of many mass sections assembled in a shaft. At time of operation, there are oscillations/vibrations among the masses termed as torsional oscillations. If frequencies, generated from any source in the network, match the frequecies of torsional oscillations, it cause torsional resonance. In many studies, it has been discussed that interaction between the electrical system and the turbine-generator may induce torsional stress to the shaft system whose magnitude and risk of damage have to be carefully analysed in advance to ensure undisturbed operation and to preclude any damage from the unit. The torsional stressing may arise as a result of torsional resonance induced by pulsating components in the electrical torque of the generator.

The frequencies of the torsional oscillations are in the subsynchronous range. There are many sources of subsynchronous frequencies in the electrical network such as capacitor compensated transmission line, electric arc furnace (EAF) loads, load-commutated inverters, pulse width modulated (PWM) voltage-source inverters etc. These equipments induce pulsating components in the air-gap torque of synchronous machine and through which the torsional oscillating torques are amplified during torsional resonance. Torsional excitation/amplification causes reduction of fatigue-life and even severe damages to turbine-generator shaft. Both the assessment of impacts of EAF on turbine generator shaft and the modeling of EAF to assess the impact are important. The core fucus of this work is to assess torsional resonance due to EAF operation.

1.2. Torsional Oscillation Problems Influenced by EAFs

The EAF load, because of its non-linear, non-stationary and unpredictable characteristics, causes power quality problems such as flicker, voltage imbalances, harmonics and interharmonics. The source of harmonics in EAF is the non-linear voltage-current characteristic of the arc due to the arc length variations occuring during scrap melting. The harmonics and interharmonics could cause heating and damage to rotating machine or accelerate mechanical fatigue damage within the rotating machine. If the subsynchronous frequencies of the network match closely to the turbine-generator torsional mode frequencies, the respective matched torsional modes are excited which cause torsional oscillating torques amplification. The magnitude of torsional resonance depends on the proximity of stimulating frequency and natural frequency, on magnitude and duration of the excitation and on damping of the excited natural mode. Such torque amplifications may cause crack in generator shaft near turbine end, failure of brushless exciter and failure of unit retaining ring. Therefore, assessment of torsional torques amplification due to multiple EAF operations at the same point of common coupling (PCC) is the main focus of this work.

In this section, a review of torsional resonance in turbine-generator shaft caused by different sources in the electrical network is presented.

In [1], it has been shown that load-commutated inverters (LCIs) and puslewidth-modulated (PWM) voltage-source inverters (VSIs) produce interharmonics. They can interact with the mechanical system at torsional natural frequencies of rotating machine. These interactions can lead to gear damage, shaft fatigue lifetime reduction and system blackouts. Mechanical failures have been consistently reported due to machine air-gap torques supplied by PWM drives.

In [2], Lambrecht et el. investigated pulsating components in the electrical torque of the generator inducing torsional resonance. Different electrical disturbances were considered to invesitgate the risk of torsional resonance and the investigation revealed that torsional stimulation due to resonance could occur in subsynchronous frequency range. They showed that series-compensated transmission system could cause torsional resonance.

In [3], gas turbine generators (GTGs) and large variable frequency drives (VFDs) have been discussed. Here, the VFDs are used as compressor drivers. The torsional modes of GTG can be excited by the interharmonic currents produced by the VFDs. It is shown that in islanded opereation the GTGs cannot provide any electrical damping to the torsional vibration which implies that strict interharmonic limits should be applied in the design. In [4], it has been studied that the shaft of a subsynchronous cascade drives was twisted and the coupling hub broke into two pieces due to torsional resonance. The subsynchronous dirves are used for large compressor and fan drives. The torsional resonance caused excessive mechanical torques which damaged the shaft.

Torsional vibrations on the turbine-generator shafts and blades due to real and reactive power variations at an EAF has been studied in [5]. It was found that the real power fluctuation of EAF was the source of subsynchronous frequency component of the air-gap torque which imposed considerable resonant torque on turbine shaft and blades. Changing distance between EAF and generating unit could not reduce the torsional impact.

The fatigue life loss in turbine-generator shaft due to long-term effect of non-characteristic subharmonic currents in a HVDC is analysed in [6]. The asynchronous operation in HVDC links disturbs rotor frequency. This disturbing frequencies are in subsynchronous range. The potential long-term failure of shaft is due to electrical disturbances. It has also been shown that although the shaft could withstand the most severe impact due to three-phase to ground fault, it still can not guarantee long-term safety operations even under normal operating conditions. In [7], Tsai et el. investigated partial power transmission in healthy phases during the dead time between single-pole tripping and line reclosing. This gives rise to significantly negative sequence current flowing into the nearby turbine-generator and may lead to supersynchronous resonance (SPSR) effect on low pressure (LP) turbine blades and even result in fatigue damage.

The torsional oscillations on the shaft of a small scale steam turbine-generator due to current unbalance produced by EAF operation has been discussed in [8]. If the unbalance is severe and sustained, the oscillations might not be ignored. The oscillations might be remarkable if there is any torsional mode having frequency close to the double system frequency.

In [9-13], it has been discussed that torsional natural frequencies of turbine-generator shaft exist because of its physical properties. Series capacitor compensated transmission line is prone to produce subsynchronous frequencies, and it can excite torsional oscillations in turbine-generators. Series capacitors also have a tendency to amplify the shaft stress during major network transient events. This can lose fatigue life of turbine-generator shaft, and in extreme case, the shaft may be broken/twisted. In [14], Ramey et el. investigated that the higher frequency components in air-gap torque have dominant effects on small components such as turbine blades and the lower frequency components realy stimulate the torsional oscillation in the main shaft sections.

To investigate the torsional resonance caused by the operation of EAF, it is necessary to model EAF which represents characteristics proximity to actual EAF. It has been reported that although three-phase EAF model is necessary to analyse problems caused by EAF, a single-phase furnace model can be used.

A new time domain controlled voltage source (CVS) model for EAF is developed in [15], which is based on piece wise linear approximation of the *V-I* characteristic of the arc furnace load. The arc resistance is varied with sinusoidal and band limited white noise variation to incorporate the dynamic variation of the arc. Deterministic load models are useful for harmonic studies while the random load models are useful for power qualitiy studies like voltage flicker.

A new frequency domain arc furnace model for iterative harmonic analysis (IHA) using Newton method is developed in [16]. A general set of non-linear equations is derived which represents the arc furnace characteristic under continuous and discontinuous evolution of arc current. In order to reproduce the actual behaviour of the furnace, a three-phase arc furnace configuration is developed.

An arc furnace model is developed in [17] which includes two main voltage disturbances associated with arc furnace: flicker and harmonics. Stocastic nature of arc *I-V* characteristic is incorporated in this model. Although a single phase model is enough to describe furnace behaviour, a three phase model has been developed to fully represent the unbalances occured in real plants and which play a vital role in the behaviour of compensation devices such as SVCs. In [18], it has been discussed that the flicker and harmonic currents are adverse effects introduced by EAFs. An EAF model is developed using chaotic and deterministic elements. The arc voltage is simulated by solving the corresponding differential equation which describes dynamic behaviour of EAF load. Using Chua's chaotic circuit, a low frequency chaotic signal is generated which is used to modulate the arc voltage. The proposed model is connected to the system as a controlled voltage source.

In [19], it has been discussed that the random property of arc melting process and the control system contribute to the thermal and electrical dynamic which may affect supply system adversely. For harmonic analysis and flicker compensation, an adaptive arc furnace model is proposed. The model is divided into three parts: the supply system, the non-linear EAF load model and the controller model. The supply system is represented by a set of linear differential equations. The EAF is represented by a current controlled non-linear resistance which is controlled by the average arc length condition. A rectangular approximation of arc voltage is adopted by the controller.

In [20], three EAF models have been compared. In the first model, the most important non-linearities of EAF system were considered which were the saturation and hysteresis effect on the transformer, the power cable, and the arc phenomenon inside the furnace. A quasi-empirical model was proposed to analyse the EAF. In the second model, the transformer reactance was considered linear excluding saturation and hysteresis effect. In the third model, the wave-shape of the arc voltage-current was considered to be piece-wise linear and the resistance of the impedance was neglected. From the comparison of simulation result, the first model was chosen as the most important representation for EAF.

In [21], it has been discussed that EAF affects the power quality due to its non-linear characteristic. In [22], Solanics et el. showed that harmonic and unbalanced currents produced from EAF can contribute to generator rotor heating and also may interact with the turbine-generator shaft torsioanl system. The large electrical drives also cause those problems. The resulting torsional stresses on turbine-generator unit are functions of the EAF behaviour, turbine-generator characteristics, the utility power system characteristic and how the EAF is connected to the power system grid.

The impact of six kinds of small power system disturbances on the torsional torques and fatigue life expenditure induced in turbine-generator shafts and blades is presented in [23]. The investigated generating unit was connected to the infinite bus and also feeding various loads. The six disturbances are EAF loads, infinite bus voltage sag, power system unbalance, HVDC sub-harmonic currents, load rejection, and mechanical torque pulsation.

The problem of integrating steel mills to a power system is discussed in [24]. In [25], Robert et el. discussed unusual power oscillations which were observed at two power plants located near large EAFs. Correlations between EAFs, influence of SVCs and power oscillations of generating units were then investigated.

EAF models and its characteristics are discussed in [26-28]. It has been discussed that EAFs are sources of flicker in the range of 0.5 to 30 Hz due to random arc behavior during the meltdown of the scraps. It is reported that voltage fluctuation from 0.3% to 0.5% in the frequency range 6-10 Hz causes incandescent lamp flickering which cause uneasiness to eyes. In [29], Logar et el. discussed an approach to the mathematical modeling of 3-phase AC EAF processes for control-design and process-optimization purposes. The EAF is considered as the combination of electrical, thermal, chemical, hydraulic and several energy-balance sub-systems. Since electrical and hydraulic sub-systems are very complex and critical, these two sub-models are discussed for complete EAF model.

Evidently, the impact on the torsional torque due to the operation of multiple numbers of EAFs at the same PCC or at close electrical proximity has not been studied in details yet. Furthermore, the study of the effect of relative position of the generator, PCC and EAF on the turbine-generator shaft system are of importance.

1.3. Thesis Objective

The main objective of the thesis is to assess the impact of simultaneous operation of multiple EAF on multi-stage turbine-generator shaft. The specific objectives are as follows:

(1) To quantify the torsional torque amplification and find out its severity due to operation of multiple EAFs at the same PCC and at close proximity.

(2) To assess the impact of multiple EAF operation on the generators in the Chittagong region of the Bangladesh Power System (BPS).

1.4. Organization of the Thesis

This thesis contains seven chapters including introductory chapter and conclusion chapter. Chapter 1 reviews characteristics of EAF, reason of torsional resonance, and clarify the reason of this thesis. Chapter 2 explains EAFs with a little bit history, its description, classification, its energy requirement in operation, and steel making cycles. Chapter 3 explains defferent AC EAF model and selection of EAF model for this thesis. It also describes performance equations of synchronous generator. Chapter 4 explains eigenvalue analysis technique and its use of finding torsional modes of turbine-generator shaft. Chapter 5 describes a test system for investigating resonant excitation of torsional modes. Chapter 6 describes the analysis of torsional resonance in turbine-generator shaft of generating unit located in Chittagong region due to operation of EAFs connected to Banagladesh Power System. Chapter 7 draws conclusion from this work and propose the extension of this work, scope of future work etc.

CHAPTER 2

ELECTRIC ARC FURNACE

2.1. Introduction

An EAF is used to convert electrical energy to thermal energy in the form of an electric arc to melt the steel scraps held by the furnace. The arc, established between an electrode and the scraps, is characterized by a high current and a low voltage. The difference between arc furnaces and induction furnaces is that the scraps are directly exposed to an electric arc in EAF and the current in the furnace electrode passes through the scraps. Due to shortage of scrap materials, some countries use direct reduced iron (DRI) to meet steel demand. But DRI is characteriezed by high porosity, low thermal and electrical conductivities which cause problem in melting phase limiting production capacity of induction furnace [33]. On the other hand, EAF can produce steel from 100% scrap metal feedstock and even it can use DRI as input without decreasing production capacity.

In 1810, Sir Humphrey Davy conducted an experiment on electric arc and Pepys investigated welding in 1815. In 1853, Pinchon attempted to build up an electro-thermic furnace and in the year 1878-79, William Siemens obtained patents for an EAF. Paul Heroult developed the first EAF which was installed in a commercial plant in the United States in 1907. Electric arc furnaces were vastly used to produce steel alloys in World War II and after that steelmaking in EAF began to expand.

Continuous inovations in the design and operation of EAF have contributed significantly to the overall total steel production in the world. It is estimated that 36% of total steel yield is produced by the EAF route and this share is being expected to reach to 50% by 2030 [33] as the global steel demand is increasing and energy requirement of EAF is reduced.

2.2. Description of an EAF

A schematic of EAF in figure 2.1 shows its cross-section having three electrodes, molten bath, tapping spout, refractory brick movable roof, brick shell, and a refractory-lined bowl-shaped hearth. Primarily, the furnace can be divided into three sections such as

- The shell: consists of the lower steel bowl and sidewalls
- The hearth: consists of the refractory that lines the lower bowl
- The roof: it may be refractory-lined or water-cooled, and supports the refractory delta in its center, through which one or more graphite electrodes enter.

Besides furnace structure, there are also electrode support and electrical system, and the furnace platform on which EAF rests.

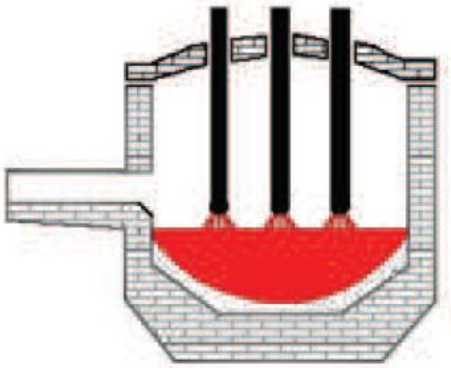

Figure 2.1 Cross-section of an EAF [33]

2.3. Classification of EAF

Based on steel production, three-phase arc furnaces are classified as follows:

(1) furnaces used only as melting units,

(2) furnaces used for both melting and refining, and

(3) furnaces used for refining only.

The furnace in which conversion of scraps primarily necessitates melting is termed as 'melting' unit. The 'melting and refining' unit is a furnace in which it is necessary not only to melt scraps but also to do some metallurgical change and produce a material different in chemical and metallurgical qualities from the initial scraps. The refining furnace is defined as the unit where hot metal is loaded either from an open hearth, bessemer vessel, and the hot metal is changed metallurgically to produce a product diffrent from the initial scraps. The classification are overlapped considerably.

Based on power supply, EAFs are classified as alternating current (AC) EAF and direct current (DC) EAF.

2.3.1 AC EAF

There are three electrodes in a typical AC furnace. The electric arc, formed between the steel scraps and the electrodes, is used to heat the scraps both by current passing through the scraps and by the radiated thermal energy by the arc. An automatic system controls the electrodes to maintain nearly constant current and power input during the melting of the scraps, even though scraps may move under the electrodes as it becomes liquid pool. Because of electrodes movement and high temperature, the power supply cables from furnace transformer to electrodes are flexible and heavy water-cooled. A complete assembly of EAF is shown in figure 2.2.

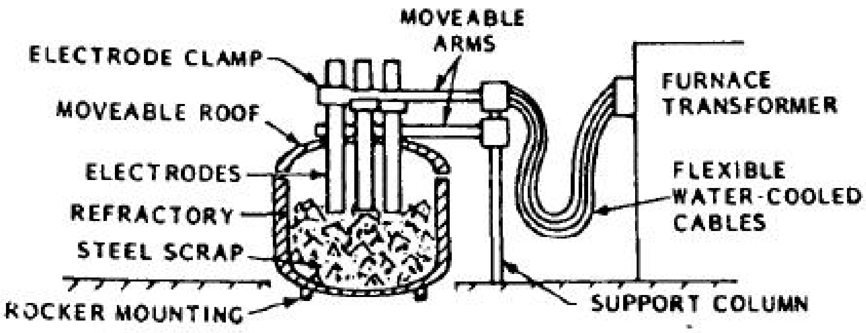

Figure 2.2 EAF assembly [26]

Figure 2.3 shows an electrical circuit of AC furnace. Energy loss in the secondary circuit depends on the resistance and current. So, sometimes it is recommended to operate the furnace at higher voltage as possible. But it is limited by arc flare to the sidewall of the furnace and the existing furnace electrics. By connecting a supplementary reactors in series at primary side of furnace transformer the operating voltage of secondary side can be increased which allows furnace operation with a theoretical maximum power factor nearly 70% [26, 34]. The series reactor may drop the secondary voltage which may reduce the power transferred to the arc. For this reason, the secondary voltage is increased to approximately 800 to 1100 volts allowing operation of the furnace at higher arc voltage and lower electrode current. The benefits of using reactors in series are (1) more stable arc than for standard operations, (2) electrode consumption reduced by 10%.

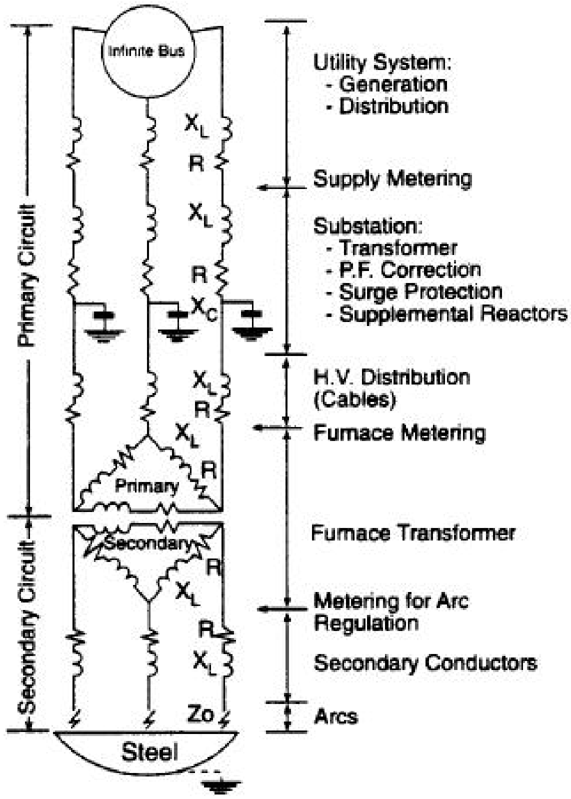

Figure 2.3 Electrical circuit of an AC EAF [34]

2.3.2 DC EAF

The arrangement of the DC furnace is shown in figure 2.4 which shows that some extra electrical equipements such as rectifier, bottom electrode and a DC reactor are necessary for DC furnace. There are only graphite electrode with the return electrode which is installed in the bottom of the furnace.

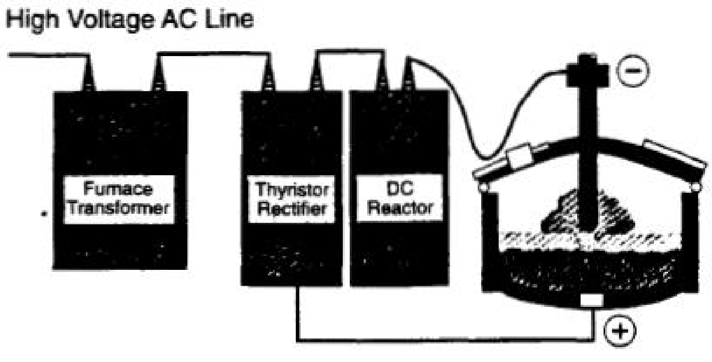

Figure 2.4 Arrangement of a DC EAF [34]

Several types of return electrodes are available such as conductive refractories, multi-pin metalic conductor and single-pin metalic conductor. A mixture of steel scraps and slags helps in providing initial electrical path during startup from cold conditions. Once this initial scrap is melted in, the furnace can be loaded with scrap for steel production.

2.4. Energy Requirements in EAF

From figure 2.5, it is seen that about 70% of the total energy required for EAF is electrical while the remainder is chemical. The chemical energy comes form oxidation elements such as carbon, iron, and silicon and the burning of natural gas with oxy-fuel burners. The liquid steel goes out from furnace with about 53% of the total energy, while the rest is lost to cooling, slag and waste gas.

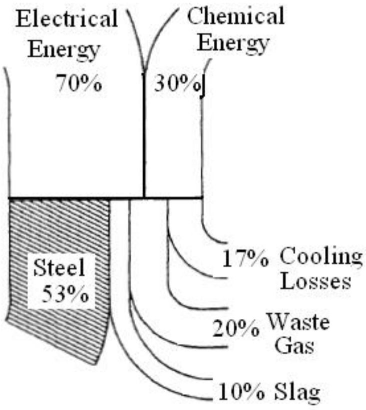

Figure 2.5 Energy patterns in an EAF [33]

A 60 MVA transformer may be used for a mid-size EAF. The secondary voltage of the furnace transformer ranges 400-900 Volts and a secondary current in excess of 44 kA. An EAF requires approximately 440 KWh/tone of steel; the theoretical minimum amount of energy requirement is 300 KWh/tone steel. The performance of EAF is improved greatly at a fast pace. Due to impressive innovations, the tap-to-tap time has been shortened to 30-40 min. for 100-130 ton furnace operating with scraps. Accordingly, the productivity of EAF is increased and electrical energy requirement is reduced from 580-650 to 320-350 KWh/ton.

2.5. Steel Making Cycle

The typical six heat cycles shown in figure 2.6 are commonly used in steel making process using EAF. The cycles are

a) Arc ignition period (start of power supply)
b) Boring period
c) Molten metal formation period
d) Main melting period
e) Meltdown period and
f) Meltdown heating period.

The electrodes are controlled by regulator and mechanical drives. With the help of its automatic control system, electrodes are lowered down to a point above the scraps and current is initiated to the electrodes. After that, the electrodes are bored through the steel scrap in order to form a pool of liquid metal. During meltdown, the steel scrap itself protects the furnace lining from the high intensity electric arc. Afterward, by increasing applying power to its maximum the arc is lengthened so that maximum thermal energy can be obtained to melt down the scrap with minimum time.

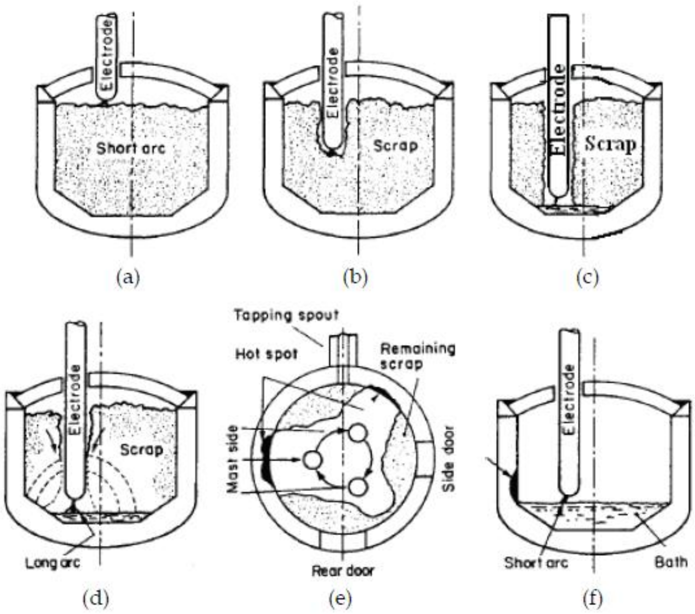

Figure 2.6 Steel making cycle [33]

In the final cycle, when the scraps are completely melted down, the electric arc is shortened in order to reduce radiation heat losses and to protect refractory from damage and hot spots. After meltdown, oxygen is introduced to oxidize the charged carbon. The oxydation process is a significant source of energy. In addition, the carbon monoxide that evolves helps to drive out the nitrogen and hydrogen from the metal. It also foams slag which helps to reduce heat loss.

2.6. Problem due to EAF Operation

The EAF load is non-linear, non-stationary and unpredictable and cause power quality problems such as flicker, voltage imbalances, harmonics and interharmonics [15-21]. The cause of harmonic is mainly related to the non-linear voltage-current characteristic of the arc due to the arc length variations occuring during melting [26-28]. The harmonics and interharmonics could cause heating and damage to rotating machine or accelerate mechanical fatigue damage within the rotating machine [22]. If the subsynchronous frequencies of the network match closely to the turbine-generator torsional mode frequencies, the respective matched torsional modes are excited which cause torsional torque amplification [23-25, 35-36]. The magnitude of torsional resonance depends on the proximity of stimulating frequency and natural frequency, on the magnitude and duration of the excitation and on the damping of the excited natural mode [2]. Such torque amplifications may cause crack in generator shaft near turbine end, failure of brushless exciter and/or failure of unit retaining ring [22].

2.7. Possible Causes of Resonant Excitation in the Shaft System

The possible causes, mentioned in [2] other than operation of EAFs, of torsional resonance in turbine-generator shaft are listed in Table 2.1. Table 2.1 also shows the various frequency ranges and mode or torsional resonance in correlation to the faults and causes of excitation which are conceivable to occur during power system operation.

From the Table 2.1, it is seen that the potential sources of excitation are in the subsynchronous range. All natural frequencies between 10 Hz and 0.9 f_N are liable to subsynchronous excitation by pulsations in the electrical torque as a result of series-compensated transmission systems, use of subsynchronous converter cascades, from high voltage direct current transmission or from other excitation sources. Again, as EAFs produce frequencies in the subsynchronous range, it should be taken in consideration to control its operation for the safety of turbine-generator shaft.

Table 2.1: Risk of resonance due to torsional stimulation [2]

Range of exciting frequencies	**Natural frequency in range of exciting frequencies**	**Mode of torsional stimulation**	**Faults or causes of stimulation**	**Risk of resonance**
	No	Unidirectional surge	Load rejection, Normal line switching, High-speed reclosing, Terminal short-circuit, Faulty synchronization	No
0.3 to 2 Hz	No	Slow power swing	Fault clearing and high-speed reclosing with extended fault clearing time	No
5 to 10 Hz	Yes	Sub-synchronous	Pole slipage at $sf_N \approx f_{el}$	Yes
10 Hz to $<0.9f_N$			SSR due to series-compensated transmission system, Power converter induced oscillating electrical moment	
0.9 to $1.1f_N$	Must be avoided	System frequency	Terminal short-circuit, Faulty synchronization, Clearing of multi-phase faults	Yes
$>1.1f_N$ $<1.9f_N$	Yes	Super-synchronous	Not known	No
1.9 to $2.1f_N$	Allowable, if not stimulated by generator	Double system frequency	High-speed reclosing of L-G and L-L system faults, Delayed clearing of L-G and L-L faults in and close to the power station, Unbalanced load	Yes
$>2.1f_N$	Yes	Super-double synchronous	Not known	No

f_N represents system frequency.

CHAPTER 3

COMPONENT MODELING

3.1 Introduction

The major two components such as EAF and synchronous generator are modeled in this chapter. There are many models of EAFs in the literature which are studied and made choice among them for this work. Detailled descriptions of synchronous generator modeling are available in [30] and only the necessary performance equations for modeling it using MATLAB are paraphrased here.

3.2 EAF Modeling

The electrical supply system may be affected substantially by steel making process using electric arc. Because the process is nonstationary stochastic, it may contribute to the electrical and thermal dynamic. A precise model for three-phase arc furnace is required to analyse its characteristics including interharmonics, harmonics, flicker and subsynchronous frequencies. Because of its unpredictatable characteristics, it is very difficult to model EAF load appropriately. On the other hand, there are many external factors such as melting stage, scrap materials, electrode position, the electrode arm control, the supply system voltage and impedance, which affect operation of the furnace [37]. It is desired to include all these factors in designing model of EAF which can be expected to have the characteristics of practical EAF. There are many EAF models which are primarily classified as (1) Time domain analysis model and (2) Frequency domain analysis model.

3.2.1 Time Domain Analysis Model

In this model, all the waveforms obtained from EAF operation are time dependent functions. To find the frequency components in the waveforms, Fast Fourier Transform (FFT) is performed. This model can be subdivided into different models which are described in the following subsections.

3.2.1.1 Voltage Source Model

In this model, EAF can be represented by a Thevenin equivalent circuit where the equivalent impedance is the furnace load impedance including electrodes. There are different options of modeling the voltage source. A possible way of designing voltage source is to form it by empirical major harmonic components.

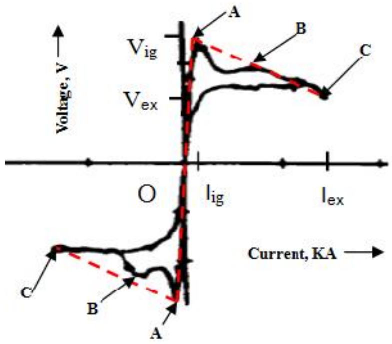

Figure 3.1 Piece-wise linear approximation of an actual EAF load

There are several models based on voltage source, where the resistances in different period of furnace operation are considered constant. These models can be obtained mathematically by using piece-wise linear approximation of the actual *V-I* characteristic curve as shown in figure 3.1. Those approximate models are described below.

A. ***Model 1:***

The actual *V-I* characteristic of EAF can be linearized by two lines as shown in Figure 3.1. The slopes of the lines OA and AC represent resistances during pre-ignition and arc established period expressed as R_1 and R_2 respectively.

$$R_1 = \frac{V_{ig}}{I_{ig}}, \; R_2 = \frac{V_{ex} - V_{ig}}{I_{ex} - I_{ig}} \tag{3.1}$$

The arc voltage is given by equation (3.2). Figure 3.2(a) shows the simulated *V-I* characteristic of model 1.

$$v(t) = \begin{cases} R_1 i(t); & 0 \le |i(t)| \le I_{ig} \\ R_2 i(t) + V_{ig}(1 - \frac{R_2}{R_1}); & I_{ig} < |i(t)| \le I_{ex} \end{cases} \tag{3.2}$$

B. ***Model 2:***

This model is established based on linear approximation of *V-I* characteristics of the static resistance EAF model as described in [38]. The arc voltages are expressed by equation (3.3).

$$v(t)=\begin{cases} R_1 i(t); & 0 \le |i(t)| \le I_1 \quad and \quad |i_1(t)| > 0 \\ R_2(i(t)-I_1)+V_1; & I_1 < |i(t)| \le I_2 \quad and \quad |i_1(t)| > 0 \\ R_3(i(t)-I_2)+V_2; & I_3 \le |i(t)| \le I_2 \quad and \quad |i_1(t)| < 0 \\ R_4(i(t)-I_3)+V_3; & I_4 < |i(t)| < I_3 \quad and \quad |i_1(t)| < 0 \\ R_5 i(t); & 0 \le |i(t)| \le I_4 \quad and \quad |i_1(t)| < 0 \end{cases} \tag{3.3}$$

where, $R_1 = \frac{V_1}{I_1}$, $R_2 = \frac{V_1 - V_2}{I_1 - I_2}$, $R_3 = \frac{V_2 - V_3}{I_2 - I_3}$, $R_4 = 0$ (assumed), $R_5 = \frac{V_4}{I_4}$ and $i_1(t)$ is the first derivative of the supply current to the furnace. Figure 3.2(b) shows the simulated *V-I* characteristic of model 2.

C. *Model 3:*

In this model, the voltage drop after ignition is considered as exponentially decaying. V_e represents voltage at the end of exponential portion of the curve which is also equal to V_2. As usual, $i_1(t)$ is the first derivative of the supply current to furnace. The arc voltages are expressed as

$$v(t)=\begin{cases} R_1 i(t); & 0 \le |i(t)| \le I_1 \quad and \quad |i_1(t)| > 0 \\ V_e + (V_1 - V_e)\exp(-(i(t)-I_1)/I_1); & I_1 < |i(t)| \le I_2 \quad and \quad |i_1(t)| > 0 \\ R_2(i(t)-I_2)+V_2; & I_2 \le |i(t)| \le I_3 \quad and \quad |i_1(t)| < 0 \\ R_3(i(t)-I_3)+V_3; & I_4 \le |i(t)| \le I_3 \quad and \quad |i_1(t)| < 0 \\ R_4 i(t); & 0 \le |i(t)| \le I_4 \quad and \quad |i_1(t)| < 0 \end{cases} \tag{3.4}$$

where, $R_1 = \frac{V_1}{I_1}$, $R_2 = \frac{V_2 - V_3}{I_2 - I_3}$, $R_3 = 0$ (assumed) , $R_4 = \frac{V_4}{I_4}$. Figure 3.2(c) shows the simulated *V-I* characteristic of model 3.

D. *Model 4: Mayr's Arc Model*

In this model, the expression of arc voltage and arc current are given by the following equations

$$i_a = \sqrt{2} I \sin \omega t \tag{3.5}$$

$$v_a = \frac{2V_0 \sin \omega t}{1 - \frac{\sin(2\omega t + \theta_a)}{\sqrt{1 + (2\xi\tau_a)^2}}} \tag{3.6}$$

where, $V_0 = \frac{P_{r0}}{\sqrt{2I}}$, $\tan\psi_a = \frac{1}{2\omega\tau_a}$, P_{r0} is the arc column power at the moment of interruption, τ_a is the arc time constant. The *V-I* characteristic of model is shown in figure 3.2(d).

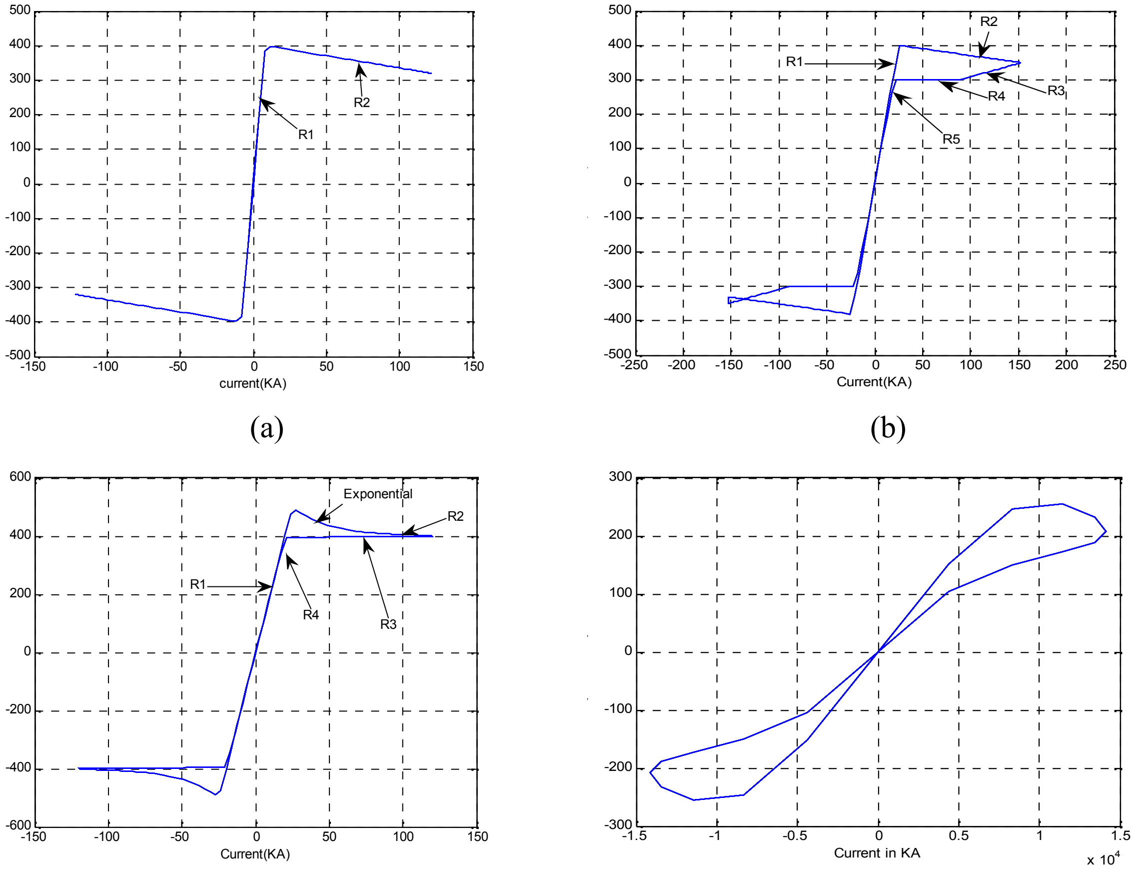

(c) (d)

Figure 3.2 *V-I* characteristics of EAF (a) *model 1* when R_1 and R_2 are constant, (b) *model 2* with all static resistances, (c) *model 3* with all static resistances, (d) *model 4*

This voltage source model loses the random behavior of arc furnace.To account the random characteristic, it is more precise to design the furnace by amplitude modulated waves. After every zero-crossing of the arc current, the arc must be reignited and a new value of the voltage amplitude is taken. So we can express the arc voltage as function of arc current. This model is statistically more acceptable [39].

3.2.1.2 Nonlinear Time Varying Voltage Source Model

In this model, the arc voltage is adapted as a nonlinear function of the arc length. Deterministic or stocastic laws are incorporated in the variation of arc length. In deterministic law, the arc length is considered to be varied sinusoidally which is the worst-case approximation. In stocastic law, a white-noise time variation of arc lenght is considered. The frequency range for both the laws is considered in the flicker range of 0.5 to 25 Hz. Both laws are applicable to an unbalanced or balanced EAF [27].

3.2.1.3 Current Source Model

An EAF is generally modeled as current source for harmonics and interharmonics studies where the current can be expressed as follows

$$i_{eaf}(t) = \sum_{n=1}^{\infty} A_n \sin(n\omega t) + \sum_{n=0}^{\infty} B_n \cos(n\omega t) \tag{3.7}$$

The above equation is a fourier series where the coefficients may change randomly in every period. The coefficients can be expressed as function of;

(i) Actual arc furnace current measured from the steel industry

(ii) Interharmonics and harmonics of practical EAF currents

(iii) Probability distributions of current harmonics

(iv) Ratio of the reactive power variation to the active power variation.

To design filter and to calculate voltage distortions resulting from harmonic/interharmonic current injected to the system, this model match more perfectly. It includes the stocastic behaviour of the furnace more appropriately. Based on chaos theory, another related model is described in [40] which can produce data from selected parameters. This model can be used for planning of EAF installation or for studies of impact from installed EAF.

3.2.1.4 Nonlinear Resistance Model

There are many models based on the approximation of the *V-I* characteristic of the arc as shown in figure 3.1. The approximation can be done by piece-wise linearization or nonlinear estimation [20]. The accuracy of the model completely depends on the simplification of the *V-I* characteristic. In this model, the numerical analysis technique is applied to solve the differential equation describing the furnace system with the estimated *V-I* characteristic. This model does not support the time-varying behaviour of the EAF. As an example, one nonlinear resistance model is described below.

With some assumptions the actual arc melting process can be divided into three periods which are described in [20]. In this model, the arc resistances are represented as a current controlled nonlinear resistace. The mathematical expression of the *R-I* characteristics curves are as follows

$$R_{arc} = \begin{cases} R_g; & 0 \le |i(t)| < I_{ig} \quad and \quad |i_1(t)| > 0 \\ \dfrac{V_d + (V_{ig} - V_d)\exp(-(i(t) - I_{ig})/\tau_1)}{i(t)}; & |i(t)| \ge I_{ig} \quad and \quad |i_1(t)| > 0 \\ \dfrac{V_t + (V_{ig} - V_t)\exp(-(i(t)/\tau_2)}{i(t) + I_{ig}}; & |i_1(t)| < 0 \end{cases} \tag{3.8}$$

where, $V_d \approx \dfrac{V_{ig}}{1.15}$, $R_g = \dfrac{V_{ig}}{I_{ig}}$, $V_t = \dfrac{V_d(I_{max} + I_{ig})}{I_{max}}$, τ_1 and τ_2 are time constants or exponential decaying periods of arc resistance. Although V_d is function of arc length it is assumed as constant for a given V_{ig}. Figure 3.3 represents the simulated characteristic of this arc model.

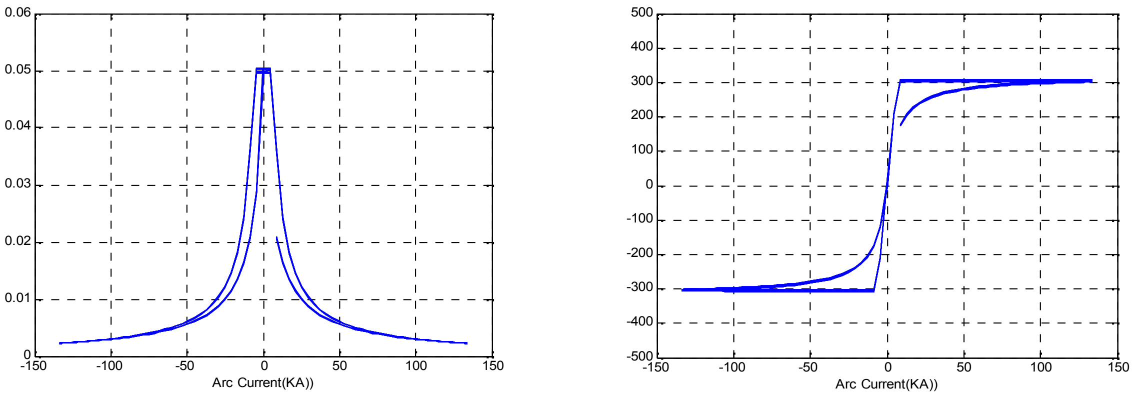

(a) (b)

Figure 3.3 Characteristic curve of EAF (a) *R-I* characteristic, (b) *V-I* characteristic

3.2.1.5 Nonlinear Time Varying Resistance Model

The operation of EAF can be explained by three states such as open circuit, short circuit and normal operation. An approximate Gaussian distribution can be used to model the arc resistance during normal operation. The random variation in arc resistance causes flicker. The arc resistance in EAF can be modelled as randomly changing around the nominal value in a periodical manner [41].

Some recent time varying resistance models relate arc resistance to the power consumed by EAF. The static model depends only on consumed power and *V-I* characteristics of EAF. The dynamic models are considered of sinusoidal and BLWN variation of arc resistance in different period of furnace operation [15]. The dynamic model can also be obtained from the dynamic behavior of electric arc. These dynamic models of EAF are described in the following section.

3.2.1.6 Dynamic Models from Variation of Arc Resistances

The resistance of the EAF varies as arc length varies depending on the operating condition (supply of active power) of the arc furnace load [17].

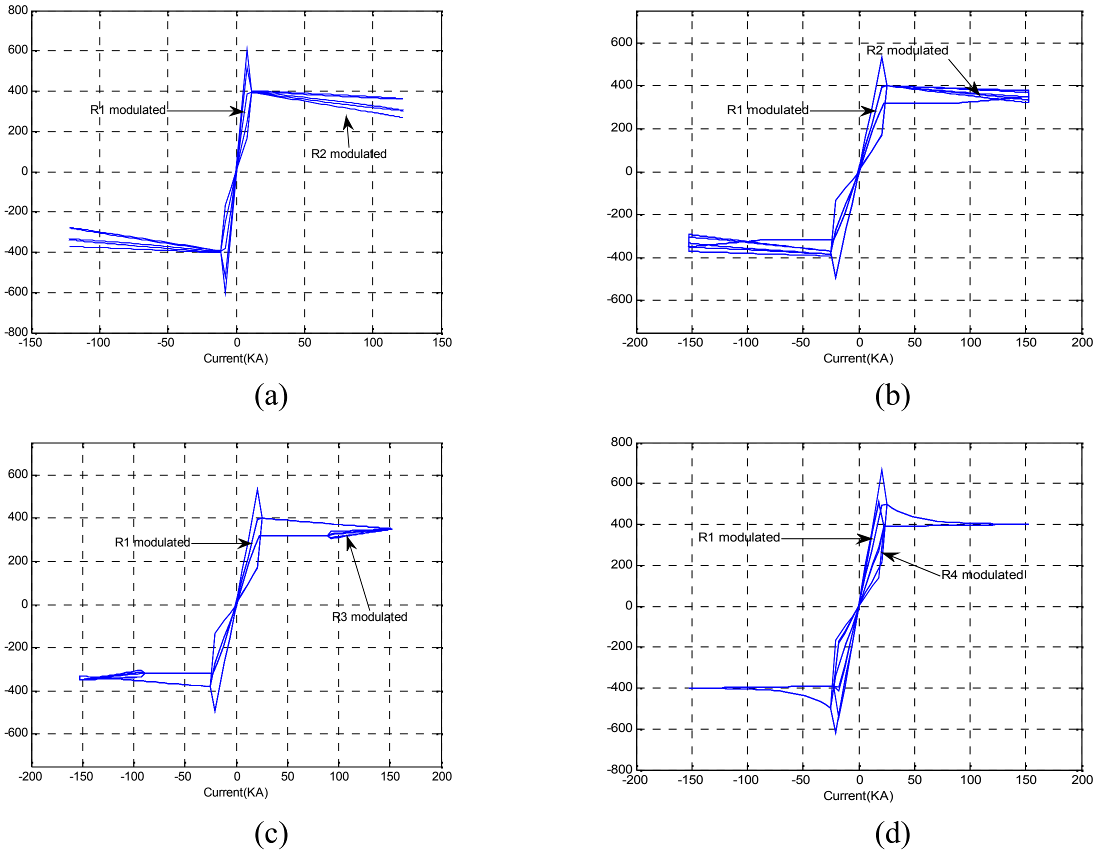

Figure 3.4 *V-I* Characteristics. with resistance modulation in different models as described in voltage source model of EAF (a) *model 1* with modulated R_1, R_2, (b) *model 2* with modulated R_1, R_2, (c) *model 2* with modulated R_1, R_2, (d) *model 3* with modulated R_1, R_4

Based on the resistace, EAF can be considered as static load or dynamic load. In static load model (as described in voltage source model), the arc resistance is approximated more or less constant for every cycle of arc furnace operation, where in dynamic load model the arc resistance is considered to vary sinusoidally or ramdomly around the static resistance. The sinusoidal variation of arc resistace may be equated as modulated resistance such as

$$R(t) = R(1 + m * \sin(\omega_f t)) \tag{3.9}$$

where '*m*' is the modulation index.The resistances in the different models of voltage source model are varied according to equation (3.9) and the simulated *V-I* characteristics are shown in figure 3.4.

3.2.1.7 Dynamic Model of Electric Arc

In the following section, the differential equation representing the dynamic behavior of electric arc is developed based on the principle of conservation of energy. Let the power balance equation for the arc is

$$P_1 + P_2 = P \tag{3.10}$$

where, P_1 = the power radiated in the form of heat to the external environment, P_2 = the power which increases the internal energy of the arc. The radius of the arc is directly related with this power. P = the total power. In equation (3.10), the cooling effect is assumed to be the function of the arc radius only. Therefore,

$$P_1 = C_1 r^n \tag{3.11}$$

where, C_1 is the proportionality constant, *r* is the arc radius. The power, P_1 is also the function of the arc temperature, but in order to make the model simple, the temperature effect is ignored. P_1 also does not depent on the arc radius if the environment around the arc is hot enough. In this case n = 0. If this is not the case and the arc is long, the heat radiation is from the lateral surface of the arc which make n = 1. For short arc, P_1 is proportional to its cross-section at the electrodes, so that n =2 [31]. The power, P_2 is proportional to the first derivative of the square of the arc radius, so

$$P_2 = C_2 r \frac{dr}{dt} \tag{3.12}$$

The arc resistivity can also be expressed as function of the arc radius, the hotter the arc, the larger the arc radius, the lesser the resistivity which can be expressed as,

$$\rho \propto \frac{1}{r^m} \tag{3.13}$$

where m = 0...2, to reflect the fact that the arc may be hotter in the interior if it has a larger radius. So the power supplied to the arc can be expressed as

$$P = vi = \frac{C_3 / r^m}{r^2} i^2 \tag{3.14}$$

Thus from equations (3.10), (3.11), (3.12) and (3.14), we get

$$C_1 r^n + C_2 r \frac{dr}{dt} = \frac{C_3}{r^{m+2}} i^2 \tag{3.15}$$

The arc voltage is given by

$$v = \frac{C_3}{r^{m+2}} i \tag{3.16}$$

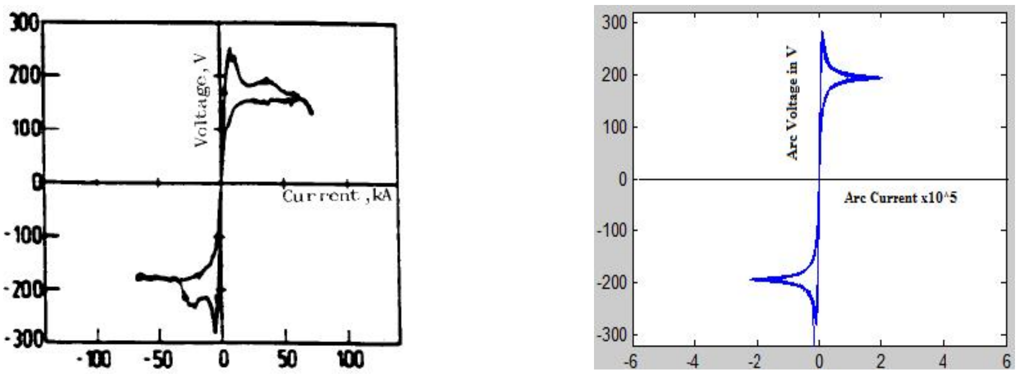

(a) (b)

Figure 3.5 Simulated characteristic (a) measured *V-I* characteristic, (b) simulated *V-I* characteristic

Figure 3.5(a) shows an actual dynamic *V-I* characteristics of a 500 V, 70 kA AC arc [31]. The characteristic of figure 3.5(b) has been obtained by MATLAB simulation of the test system described in chapter 5. The two characteristics compare well with each other: they follow the almost same basic pattern. The measured arc characteristic has a deterministic and a stochastic part, with the latter becoming less and less significant as the process of meltdown progresses. In this work only the deterministic part is modeled.

3.2.2 Frequency Domain Analysis Model

In this method, the arc voltage and current are represented by their frequency components with some presumptions to simplify the harmonic calculations. The arc voltage is considered to be a square wave with a particular magnitude, since the arc voltage changes its polarity very fast. Further the current is assumed to be zero when voltage changes its polarity. The approximate *V-I* characteristic of the EAF voltage is given by the following equation:

$$V_a = \begin{cases} V_l,\ i_a \geq 0 \\ V_l,\ i_a < 0 \end{cases} \tag{3.17}$$

where, V_l is the constant voltage which depends on arc length dynamics. In Fourier series analysis, V_a can be expressed as:

$$V_a = \sqrt{2}\sum_{n=1}^{N} V_{an} \sin(n\omega t + \phi_n) \tag{3.18}$$

V_{an} is the rms value of arc voltage of the n^{th} frequency component. The arc current can be expressed by the following equation which is obtained from the arc voltage.

$$i_a = \sqrt{2}\sum_{n=1}^{N} \frac{V_{an}}{Z_n} \sin(n\omega t + \phi_n + \theta_n) \tag{3.19}$$

where $\theta_n = \tan^{-1}(\frac{X_n}{R_n})$ and $Z_n = R_n + jX_n$

In this model, the equivalent circuit for the calculation of the different order harmonics consists of a harmonic voltage source and the system impedance for that harmonic frequency. The arc furnace load is assumed to draw the maximum power in the fundamental frequency, which is not always true for actual furnace operation. This model is suitable for steady-state iterative harmonic analysis [42] and it can not represent the stochastic characteristic.

3.2.3 Selection of EAF Model for Simulation

From the analysis of above models, it is seen that the *V-I* characteristic obtained from the dynamic model of electric arc closely match the actual *V-I* characteristic refered to figure 3.5. That is why, the dynamic model of the arc has been chosen for simulation to analyse the impact on turbine-generator shaft due to operation of EAFs.

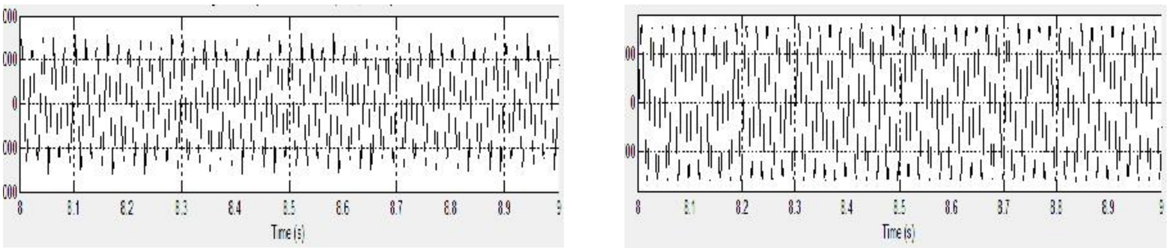

(a) (b)

Figure 3.6 Voltage and current at the primary side of furnace transformer (a) voltage waveform, (b) current waveform

Using the dynamic model of the arc for EAF, a test system has been simulated (described in chapter 5). From the simulation output, the voltage and current waveforms in phase-*a* at the primary side of the furnace transformer are presented in figure 3.6. In the simulation, 60% modulation is considered. The waveforms are modulated which can be expressed by the following equations.

The voltage waveform is

$$v_a(t) = \sqrt{2}V_{rms}[1 + \sum \Delta V_n \sin(2\pi f_n t + \phi_n)]\sin(2\pi f_s t) \quad (3.20)$$

The current waveform is

$$i_a(t) = \sqrt{2}I_{rms}[1 + \sum I_n \sin(2\pi f_n t + \phi_n)]\sin(2\pi f_s t + \beta) \quad (3.21)$$

Therefore, it is obvious that the furnace feeder becomes a source of harmonics, interharmonics and subsynchronous frequencies at time of EAF operation.

3.2.4 Analysis of Subsynchronous, Interharmonics and Harmonics

The EAF feeder current in phase-*a* is represented in equation (3.21). The feeder current in phase-*b* and phase-*c* can be represented by the following equations:

$$i_a(t) = \sqrt{2}I_{rms}[1 + \sum I_n \sin(2\pi f_n t + \phi_n)]\sin(2\pi f_s t + \beta) \quad (3.22)$$

$$i_b(t) = \sqrt{2}I_{rms}[1 + \sum I_n \sin(2\pi f_n t + \phi_n)]\sin(2\pi f_s t + \beta - 120^0) \quad (3.23)$$

$$i_c(t) = \sqrt{2}I_{rms}[1 + \sum I_n \sin(2\pi f_n t + \phi_n)]\sin(2\pi f_s t + \beta - 240^0) \quad (3.24)$$

where, f_s is the system fundamental frequency, I_n is the amplitude of modulating current, f_n is the frequency of the modulating current, β is the angle between EAF feeder voltage and current. The frequency f_n could randomly spread all over the subsynchronous range. The frequency spectrum of the modulating current gives f_s+f_n and f_s-f_n, which are defined as super and subsynchronous frequencies respectively. These frequencies spread all over the network. So, it is logical that the EAF can be considered as current source with frequencies in subsynchronous, harmonics and interharmonics range. This current may disturb the stator current which may cause perturbation in generator air-gap torque. In many studies, it is shown that the dominated torsional mode frequencies of turbine-generator shaft remain in the subsynchronous range [2,30]. If the subsynchronous frequencies generated from EAF match to torsional mode frequencies, the torsional torque will be amplified. The investigation of severity of torque amplification due to EAF operation is the main focus of this thesis.

3.3 Synchronous Machine Modeling

The principal source of electrical energy in power systems is the synchronous generators. Synchronous motors are used to drive many large loads. For reactive power compensation, synchronous condensers are used to control voltage level. All of these devices operate on the common principal and are collectively referred to as synchronous machines. The detailed machine modeling has been described in [30]. As this modeling is used in this thesis, the equations describing the performance of the synchronous generator are reviewed in this section.

It has already been dicussed, in section 3.2.5, that any change in the system current changes in the air-gap torque which changes the torsional torque in the turbine-generator shaft. The air-gap torque definitely depends on the electrical parameters of the synchronous generator so it is important to have an understanding of characteristics and accurate modelling of dynamic performance of the synchronous generator. The equations presented in this section are used to calculate different parameters in modeling synchronous generator using MATLAB power library. In this section, the steady-state performance of synchronous generator and the magnetic saturation effect on its different parameters are reviewed briefly. These are available in many standard text books.

3.3.1 Electrical Performance Equations of Synchronous Generator

The detailed performance equations of synchronous generator are developed in [30]. In this section, only the necessary equations are presented. Consider the figure 3.7 where the stator circuit is three phase Y-connected which carries AC currents and field windings are supplied from a DC source. It is assumed that the direction of stator currents is out of the machine and the direction of rotor circuit currents is into the machine.

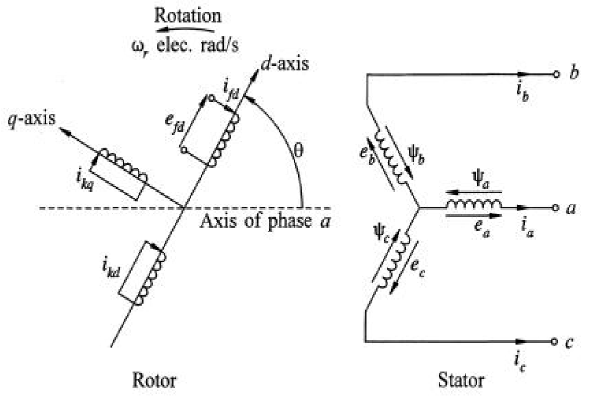

Figure 3.7 Stator and rotor circuits of a synchronous machine

The following notations are used.

Notations:

a, *b*, *c* – stator windings

fd – field winding

kd – *d*-axis damper winding

kq – *q*-axis damper winding

k – 1, 2, ... *n*, *n* = number of damper circuits

θ - angle between *d*- axis and phase-*a* winding magnetic axis in electrical radian.

ω_r - angular speed of rotor in electrical rad/sec.

e_a, e_b, e_c - instantaneous stator phase to neutral voltages

i_a, i_b, i_c - instantaneous stator currents in phases-*a, b, c*

i_{fd}, i_{kd}, i_{kq} - field and dapmer winding currents

e_{fd} - field voltage

R_a - armature resistance per phase

R_{fd}, R_{kd}, R_{kq} - rotor winding resistances

ψ_a, ψ_b, ψ_c – instantaneous flux linkages associated with phase-*a, b, c*

ψ_{fd}, ψ_{kd}, ψ_{kq} – instantaneous flux linkages associated with rotor circuit

l_{aa}, l_{bb}, l_{cc} - self inductances of stator windings

l_{ab}, l_{bc}, l_{ca} - mutual inductances between stator windings

l_{afd}, l_{akd}, l_{akq} - mutual inductances between stator and rotor windings

l_{ffd}, l_{kkd}, l_{kkq} - self inductances of rotor windings

For analysis purpose, currents in the damper windings are assumed to flow in two closed circuits of which one circuit is along the *d*-axis and the other is along *q*-axis

A. *Equations of Stator Windings*

The equations of voltage in each phase of synchronous generator can be formulated as follows:

$$e_a = \frac{d\psi_a}{dt} - R_a i_a \tag{3.25}$$

$$e_b = \frac{d\psi_b}{dt} - R_a i_b \tag{3.26}$$

$$e_c = \frac{d\psi_c}{dt} - R_a i_c \tag{3.27}$$

The instantaneous flux linkage associated with phase-*a* is

$$\psi_a = -l_{aa} i_a - l_{ab} i_b - l_{ac} i_c + l_{afd} i_{fd} + l_{akd} i_{kd} + l_{akq} i_{kq} \tag{3.28}$$

Similarly expression for flux linkages associated with phase-*b* and phase-*c* can be obtained, here units are webers, henrys and amperes. As the inductances depend on rotor position, they are time-varying. Expressoins for all inductances are available in [30]. The instantaneous flux linkages associated with stator windings can be expressed as follows:

$$\begin{aligned} \psi_a = & -i_a[L_{aa0} + L_{aa2}\cos 2\theta] + i_b[L_{ab0} + L_{aa2}\cos(2\theta + 60^0)] \\ & + i_c[L_{ab0} + L_{aa2}\cos(2\theta - 60^0)] \\ & + i_{fd} L_{afd}\cos\theta + i_{kd} L_{akd}\cos\theta - i_{kq} L_{akq}\sin\theta \end{aligned} \tag{3.29}$$

$$\begin{aligned}\psi_b = & \, i_a[L_{ab0} + L_{aa2}\cos(2\theta + 60^0)] - i_b[L_{aa0} + L_{aa2}\cos 2(\theta - 120^0)] \\ & + i_c[L_{ab0} + L_{aa2}\cos(2\theta - 180^0)] + i_{fd}L_{afd}\cos(\theta - 120^0) \\ & + i_{kd}L_{akd}\cos(\theta - 120^0) - i_{kq}L_{akq}\sin(\theta - 120^0)\end{aligned} \tag{3.30}$$

$$\begin{aligned}\psi_c = & \, i_a[L_{ab0} + L_{aa2}\cos(2\theta - 60^0)] + i_b[L_{aa0} + L_{aa2}\cos(2\theta - 180^0)] \\ & - i_c[L_{aa0} + L_{aa2}\cos 2(\theta - 240^0)] + i_{fd}L_{afd}\cos(\theta - 240^0) \\ & + i_{kd}L_{akd}\cos(\theta - 240^0) - i_{kq}L_{akq}\sin(\theta - 240^0)\end{aligned} \tag{3.31}$$

B. *Rotor Circuit Equations*

Rotor circuit voltage equations are

$$e_{fd} = \frac{d\psi_{fd}}{dt} + R_{fd}i_{fd} \tag{3.32}$$

$$0 = \frac{d\psi_{kd}}{dt} + R_{kd}i_{kd} \tag{3.33}$$

$$0 = \frac{d\psi_{kq}}{dt} + R_{kq}i_{kq} \tag{3.34}$$

As, rotor circuits see constant permeance due to cylindrical structure of stator, the self-inductances of rotor circuits and mutual inductances between each other do not vary with rotor position. Only the rotor-stator mutual inductances vary periodically.The rotor circuit flux linkages may be expressed as follows:

$$\psi_{fd} = L_{ffd}i_{fd} + L_{fkd}i_{kd} - L_{afd}[i_a\cos\theta + i_b\cos(\theta - 120^0) + i_c\cos(\theta - 240^0)] \tag{3.35}$$

$$\psi_{kd} = L_{fkd}i_{fd} + L_{kkd}i_{kd} - L_{akd}[i_a\cos\theta + i_b\cos(\theta - 120^0) + i_c\cos(\theta - 240^0)] \tag{3.36}$$

$$\psi_{kq} = L_{kkq}i_{kq} + L_{akq}[i_a\sin\theta + i_b\sin(\theta - 120^0) + i_c\sin(\theta - 240^0)] \tag{3.37}$$

Equations (3.25) to (3.31) associated with stator circuits together with equations (3.32) to (3.37) associated with rotor circuits completely describe electrical performance of a synchronous generator.

3.3.2 The dq0 Transformation

Those equations describing the electrical performance of a synchronous machine contain inductance terms which vary with θ which in turn varies with time, *t*. This introduces considerable complexity in solving machine and power system problems. It can be obtained a simpler form leading to a clear physical picture by appropriate transformation of stator variables. In equations (3.35) to (3.37) stator currents combine into convenient forms in each axis which suggests transformation of stator phase currents into new variables as follows:

$$i_d = k_d[i_a \cos\theta + i_b \cos(\theta - 120^0) + i_c \cos(\theta - 240^0)] \tag{3.38}$$

$$i_q = -k_q[i_a \sin\theta + i_b \sin(\theta - 120^0) + i_c \sin(\theta - 240^0)] \tag{3.39}$$

Constants k_d and k_q are arbitrary and their values may be chosen to simplify numerical coefficients in performance equations. In most of the literature on synchronous machine theory, k_d and k_q are taken as 2/3. For balanced sinusoidal conditions (with $k_d = k_q = 2/3$), peak values of i_d and i_q are equal to peak value of the stator current as shown below. For balanced condition, the phase currents can be expressed as

$$i_a = I_m \sin(\omega_s t + \phi) \tag{3.40}$$

$$i_b = I_m \sin(\omega_s t + \phi - 120^0) \tag{3.41}$$

$$i_c = I_m \sin(\omega_s t + \phi - 240^0) \tag{3.42}$$

Substituting in equation (3.38) gives

$$\begin{aligned} i_d &= k_d[I_m \sin(\omega_s t + \phi)\cos\theta + I_m \sin(\omega_s t + \phi - 120^0)\cos(\theta - 120^0) \\ &\quad + I_m \sin(\omega_s t + \phi - 240^0)\cos(\theta - 240^0)] \\ &= k_d \frac{3}{2} I_m \sin(\omega_s t + \phi - \theta) \end{aligned} \tag{3.43}$$

So, we see that for peak value of i_d to be equal to I_m, k_d should be equal to 2/3. Similarly from equation (3.39), for the balanced condition

$$i_q = -k_q \frac{3}{2} I_m \cos(\omega_s t + \phi - \theta) \tag{3.44}$$

The rotor speed should be equal to stator speed for synchronous operation. Hence, $\theta = \omega_r t = \omega_s t$. Therefore, from equation (3.43) and (3.44), we get $i_d = I_m \sin\phi$ = constant and $i_q = I_m \cos\phi$ = constant. This indicates that the currents in *abc* reference frame appear as direct currents in *dq0* reference frame.

To transform three-phase currents into three variables, a third component must be defined which will produce no field in the air-gap. Because i_d and i_q together produce a field identical to that produced by original set of phase currents. A convenient third variable is zero sequence current i_0, associated with symmetrical components:

$$i_0 = \frac{1}{3}(i_a + i_b + i_c) \tag{3.45}$$

Under balanced conditions $i_a+i_b+i_c = 0$ and, therefore, $i_0 = 0$.

The transformation from *abc* phase variables to *dq0* variables can be written in following matrix form:

$$\begin{bmatrix} i_d \\ i_q \\ i_0 \end{bmatrix} = \frac{2}{3}\begin{bmatrix} \cos\theta & \cos(\theta - 120^0) & \cos(\theta - 240^0) \\ -\sin\theta & -\sin(\theta - 120^0) & -\sin(\theta - 240^0) \\ \frac{1}{2} & \frac{1}{2} & \frac{1}{2} \end{bmatrix}\begin{bmatrix} i_a \\ i_b \\ i_c \end{bmatrix} \tag{3.46}$$

Inverse transformation is given by

$$\begin{bmatrix} i_a \\ i_b \\ i_c \end{bmatrix} = \begin{bmatrix} \cos\theta & -\sin\theta & 1 \\ \cos(\theta - 120^0) & -\sin(\theta - 120^0) & 1 \\ \cos(\theta - 240^0) & -\sin(\theta - 240^0) & 1 \end{bmatrix}\begin{bmatrix} i_d \\ i_q \\ i_0 \end{bmatrix} \tag{3.47}$$

Above transformations can also be applied to stator flux linkages and voltages. In this work, *dq0* reference frame is chosen because analysis of synchronous machine in *dq0* frame is simpler than in *abc* frame.

A. *Stator Flux Linkages in dq0 Components*

Using expressions for ψ_a, ψ_b and ψ_c (equations (3.29), (3.30) and (3.31)), transforming flux linkages and currents into *dq0* components using equation (3.46), we obtain following expressions:

$$\psi_d = -(L_{aa0} + L_{ab0} + \frac{3}{2}L_{aa2})i_d + L_{afd}i_{fd} + L_{akd}i_{kd}$$

$$\psi_q = -(L_{aa0} + L_{ab0} - \frac{3}{2}L_{aa2})i_q + L_{akq}i_{kq}$$

$$\psi_0 = -(L_{aa0} - 2L_{ab0})i_0$$

Defining following new inductances

$$L_d = L_{aa0} + L_{ab0} + \frac{3}{2} L_{aa2} \tag{3.48}$$

$$L_q = L_{aa0} + L_{ab0} - \frac{3}{2} L_{aa2} \tag{3.49}$$

$$L_0 = L_{aa0} - 2L_{ab0} \tag{3.50}$$

The flux linkage equations become

$$\psi_d = -L_d i_d + L_{afd} i_{fd} + L_{akd} i_{kd} \tag{3.51}$$

$$\psi_q = -L_q i_q + L_{akq} i_{kq} \tag{3.52}$$

$$\psi_0 = -L_0 i_0 \tag{3.53}$$

The *dq0* components of stator flux linkages are seen to be related to components of stator and rotor currents through constant inductances.

B. *Rotor Flux Linkages in dq0 Components*

Substituting expressions for i_d, i_q in equations (3.35) to (3.37) gives

$$\psi_{fd} = L_{ffd} i_{fd} + L_{fkd} i_{kd} - \frac{3}{2} L_{afd} i_d \tag{3.54}$$

$$\psi_{kd} = L_{fkd} i_{fd} + L_{kkd} i_{kd} - \frac{3}{2} L_{akd} i_d \tag{3.55}$$

$$\psi_{kq} = L_{kkq} i_{kq} - \frac{3}{2} L_{akq} i_q \tag{3.56}$$

Again, all inductances are seen to be constant, i.e., they are independent of rotor position. Note: saturation effects are not considered here. Zero sequence component of armature current, i_0 does not appear in rotor flux linkage equations, because it does not produce net mmf across air-gap.

C. *Stator Voltage Equations in dq0 Components*

Equations (3.25) to (3.27) are basic equations for phase voltages in terms of phase flux linkages and currents. By applying the *dq0* transformation of equation (3.46), following expressions in terms of transformed components of voltages, flux linkages and currents result:

$$e_d = \frac{d\psi_d}{dt} - \psi_q \frac{d\theta}{dt} - R_a i_d \quad (3.57)$$

$$e_q = \frac{d\psi_q}{dt} + \psi_d \frac{d\theta}{dt} - R_a i_q \quad (3.58)$$

$$e_0 = \frac{d\psi_0}{dt} - R_a i_0 \quad (3.59)$$

where, $d\theta/dt = p\theta$ is the angular velocity ω_r of the rotor.

D. ***Electrical Power and Torque***

The instantaneous three-phase power output of stator is

$$P_t = e_a i_a + e_b i_b + e_c i_c$$

In terms of *dq0* components,

$$P_t = \frac{3}{2}(e_d i_d + e_q i_q + 2e_0 i_0) \quad (3.60)$$

Under balanced operation, $e_0 = i_0 = 0$ and expression for power is given by

$$P_t = \frac{3}{2}(e_d i_d + e_q i_q)$$

Using equations (3.57) to (3.59) to express voltage components in terms of flux linkages and currents, by recognizing ω_r as the rotor speed $d\theta/dt$, and rearranging, we have

$$P_t = \frac{3}{2}[(i_d \frac{d\psi_d}{dt} + i_q \frac{d\psi_q}{dt} + 2i_0 \frac{d\psi_0}{dt}) + (\psi_d i_q - \psi_q i_d)\omega_r - (i_d^2 + i_q^2 + 2i_0^2)R_a]$$

=(rate of change of armature magnetic energy)+

(power transferred across the air gap)-armature resistance loss (3.61)

Air-gap torque T_e is obtained by dividing power transferred across air-gap (i.e., power corresponding to speed voltages) by rotor speed in mechanical radians per second.

$$T_e = \frac{3}{2}(\psi_d i_q - \psi_q i_d)\frac{\omega_r}{\omega_{mech}} = \frac{3}{2}(\psi_d i_q - \psi_q i_d)\frac{P_f}{2} \quad (3.62)$$

3.3.3 Complete Set of Electrical Equations in Per Unit

In view of the L_{ad}-base per unit system chosen [30], in per unit

$L_{afd} = L_{fda} = L_{akd} = L_{kda} = L_{ad}$

$L_{akq} = L_{kqa} = L_{aq}$

$L_{fkd} = L_{kdf}$

In the following equations, two *q*-axis amortisseur circuits are considered, and the subscripts *1q* and *2q* are used (in place of *kq*) to identify them. Only one *d*-axis amortisseur circuit is considered, and it is identified by the subscript *1d*.

A. ***Per Unit Stator Voltage Equations***

$$e_d = p\psi_d - \psi_q\omega_r - R_a i_d \tag{3.63}$$

$$e_q = p\psi_q - \psi_d\omega_r - R_a i_q \tag{3.64}$$

$$e_0 = p\psi_0 - R_a i_0 \tag{3.65}$$

B. ***Per Unit Rotor Voltage Equations***

$$e_{fd} = p\psi_{fd} + R_{fd} i_{fd} \tag{3.66}$$

$$0 = p\psi_{1d} + R_{1d} i_{1d} \tag{3.67}$$

$$0 = p\psi_{1q} + R_{1q} i_{1q} \tag{3.68}$$

$$0 = p\psi_{2q} + R_{2q} i_{2q} \tag{3.69}$$

C. ***Stator Flux Linkage Equations***

$$\psi_d = -(L_{ad} + L_l) i_d + L_{ad} i_{fd} + L_{ad} i_{1d} \tag{3.70}$$

$$\psi_q = -(L_{aq} + L_l) i_q + L_{aq} i_{1q} + L_{aq} i_{2q} \tag{3.71}$$

$$\psi_0 = -L_0 i_0 \tag{3.72}$$

D. ***Rotor Flux Linkage Equations***

$$\psi_{fd} = L_{ffd} i_{fd} + L_{f1d} i_{1d} - L_{ad} i_d \tag{3.73}$$

$$\psi_{1d} = L_{f1d} i_{fd} + L_{11d} i_{1d} - L_{ad} i_d \tag{3.74}$$

$$\psi_{1q} = L_{11q} i_{1q} + L_{aq} i_{2q} - L_{aq} i_q \tag{3.75}$$

$$\psi_{2q} = L_{aq} i_{1q} + L_{22q} i_{2q} - L_{aq} i_q \tag{3.76}$$

in writing equations (3.75) and (3.76), we have assumed that the per unit mutual inductance L_{12q} is equal to L_{aq}. This implies that the stator and rotor circuits in the q-axis all link a single mutual flux represented by L_{aq}. This is acceptable because the rotor circuits represent the overall rotor body effects, and actual windings with physical measurable voltages and currents do not exist.

E. *Per Unit Air-Gap Torque*

From equation (3.62), expressing the air-gap torque in pu, we get

$$T_e = \psi_d i_q - \psi_q i_d \tag{3.77}$$

So it is seen that the air-gap torque is function of dq-axis flux linkages and currents. So if there any change or disturbances in those parameters, air-gap torque will be disturbed which will result in perturbation in torsional oscillating torques. It has already been stated that if frequencies in air-gap torque are equal to frequencies in torsional oscillating torques, there forms resonance and the torsional oscillating torques are amplified/excited.

3.3.4 Steady-State Analysis

For stability analysis, it is necessary to find the initial steady-state values of machine variables as a function of specified terminal quantities. In this work, for calculating the synchronizing torque coefficient which is needed in eigenvalue analysis of power system (described in chapter 4), calculation of initial steady-state values of synchronous machines' parameters (detailed studies of it such as phasor representation of the machine, derivation of its rotor angle, evaluating its steady-state equivalent circuit) are necessary which are described in [30]. In this section, only the procedures of computing steady state values are followed. For this, it is assumed that all quantities are expressed in per unit.

(a) Using terminal active power P_t, reactive power Q_t, and magnitude of voltage E_t, the corresponding terminal current I_t and power factor angle ϕ are computed as follows:

$$I_t = \frac{\sqrt{P_t^2 + Q_t^2}}{E_t}, \text{ and } \quad \phi = \cos^{-1}\left(\frac{P_t}{E_t I_t}\right)$$

(b) The effective internal voltage, $\tilde{E}_q$ lies along the q-axis, as illustrated in figure 3.8. From this, the internal rotor angle δ_i can be calculated by the following equation.

$$\delta_i = \tan^{-1}\left(\frac{X_q I_t \cos\phi - R_a I_t \sin\phi}{E_t + R_a I_t \cos\phi + X_q I_t \sin\phi}\right)$$

(c) Then, the *dq* components of stator voltage and current can be expressed in term of δ_i as follows:

$$e_d = E_t \sin\delta_i, \quad e_q = E_t \cos\delta_i, \; i_d = I_t \sin(\delta_i + \phi), \; i_q = I_t \cos(\delta_i + \phi)$$

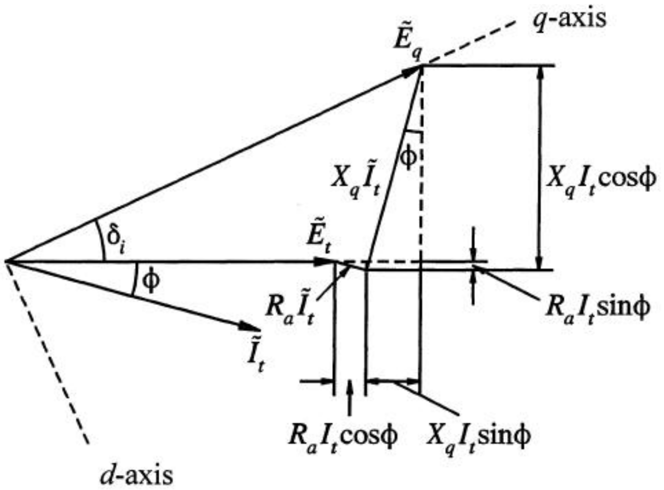

Figure 3.8 Steady-state phasor diagram [30]

(d) The remaining steady-state *dq*-axis machine quantities are computed as follows [30]

$$_{d} = e_q + R_a i_q$$

$$_{q} = -e_d - R_a i_d$$

$$= \frac{e_q + R_a i_q + X_d i_d}{X_{ad}}$$

$$e_{fd} = R_{fd} i_{fd}$$

$$_{fd} = (L_{ad} + L_{fd}) i_{fd} - L_{ad} i_d$$

$$_{d} = L_{ad}(i_{fd} - i_d)$$

$$_{q} = \psi_{2q} = -L_{aq} i_q$$

$$= P_t + R_a I_t^2$$

In the calculation of the steady-state quantities, the magnetic saturation has not yet considered. It is very important to mention here that the inductances L_{ad}, L_{aq}, L_d, L_q and the corresponding reactances vary with saturation. The method of accounting for saturation is discussed in next section.

3.3.5 Magnetic Saturation

To make the analysis simple, the effects of stator and rotor magnetic saturation were ignored in developing performance equations of synchronous generator. In this section, saturation effect is considered. Before discussing saturation effect, it is useful to review the characteristics of synchronous machines with stator terminals open and shorted, because magnetic circuit data essential to the treatment of saturation are given by the open-circuit characteristic. The open and short circuit characteristics of machines are described elaborately in [30]. Only the represenation of saturatoin in stabilty studies is paraphrased.

For stability studies, magnetic saturation is considered with the folloiwng assumptions:

(a) The leakage inductances are considered independent of saturation. Only the mutual inductances L_{ad} and L_{aq} are influenced by saturation effect.

(b) The magnetic saturation is independent of leakage fluxes. Only the air-gap flux linkage contributes to mangnetic saturation.

(c) Under both loaded and no-load conditions, the saturation relationship between the resultant air-gap flux and the mmf is same which allows the saturation to be represented by the OCC curve. It is important because the only saturation data are available from OCC.

(d) *d*-and *q*-axis are free from magnetic coupling due to nonlinearities introduced by saturation.

Considering the above assumptions, the saturation effects may be represented by

$$L_{ad} = K_{sd} L_{adu} \tag{3.78}$$

$$L_{aq} = K_{sq} L_{aqu} \tag{3.79}$$

where L_{adu} and L_{aqu} are the unsaturated values of L_{ad} and L_{aq}. K_{sd} and K_{sq} are saturation factors which indicate degrees of saturation in the *d*- and *q*- axis, respectively. We first discuss how *d*-axis saturation is represented and then consider saturation of the *q*-axis.

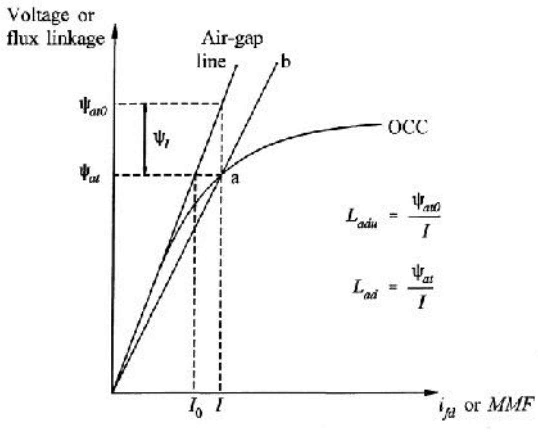

Figure 3.9 Open-circuit characteristic showing effects of saturation

According to assumption (c), the OCC curve can be used to determine the degree of *d*-axis saturation as shown in figure 3.9. For an operating point 'a' on the OCC, the factor K_{sd} can be expressed by

$$K_{sd} = \frac{\psi_{at}}{\psi_{at0}} \tag{3.80}$$

which gives the degree of saturation for any specified value of air-gap flux linkage or voltage. The mathematical expression which represents the deviation of OCC from the air-gap line is necessary to measure the degree of saturation and it is discussed in the following.

Let us define in figure 3.9

$$\psi_I = \psi_{at0} - \psi_{at} \tag{3.81}$$

Putting this in equation (3.80), we get

$$K_{sd} = \frac{\psi_{at}}{\psi_{at} + \psi_I} \tag{3.82}$$

The OCC curve can be segmented as unsaturated segment I, nonlinear segment II, and fully saturated linear segment III which are bounded by thresold values ψ_{T1} and ψ_{T2} shown in figure 3.10.

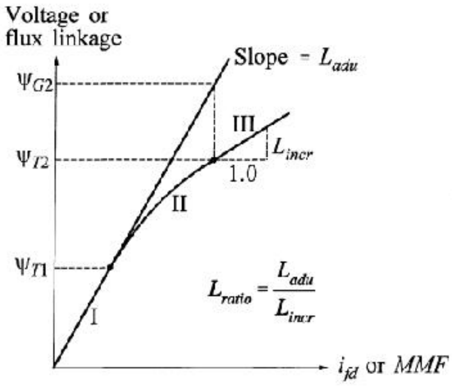

Figure 3.10 Representation of saturation characteristic

For segment I bounded by $\psi_{at} \leq \psi_{T1}$

$$\psi_I = 0 \tag{3.83}$$

For segment II bounded by $\psi_{T1} \leq \psi_{at} \leq \psi_{T2}$, ψ_I can be expressed by an exponential function:

$$\psi_I = A_{sat} e^{B_{sat}(\psi_{at} - \psi_{T1})} \tag{3.84}$$

where A_{sat} and B_{sat} are constants characterized by saturation in the segement II. When $\psi_{at} = \psi_{T1}$, from equation (3.84), $\psi_I = A_{sat}$ which results in a small discontinuity at the junction of segements I and II. However, A_{sat} is normally very small and the discontinuity is unimportant.

For segment III bounded by $\psi_{at} > \psi_{T2}$,

$$\psi_I = \psi_{G2} + L_{ratio}(\psi_{at} - \psi_{T2}) - \psi_{at} \tag{3.85}$$

where L_{ratio} is defined in figure 3.10. So we see that the saturation behaviour for any given machine is specified by ψ_{T1} , ψ_{T2}, ψ_{G2}, A_{sat}, B_{sat} and L_{ratio}.

For any operating condition, the value of K_{sd} is computed as a function of the corresponding air-gap flux linkage given by

$$\psi_{at} = \sqrt{\psi_{ad}^{\ 2} + \psi_{aq}^{\ 2}} \tag{3.86}$$

where ψ_{ad} and ψ_{aq} are the *d*- and *q*-axis components of air gap or mutual flux linkages shown in figure 3.11.

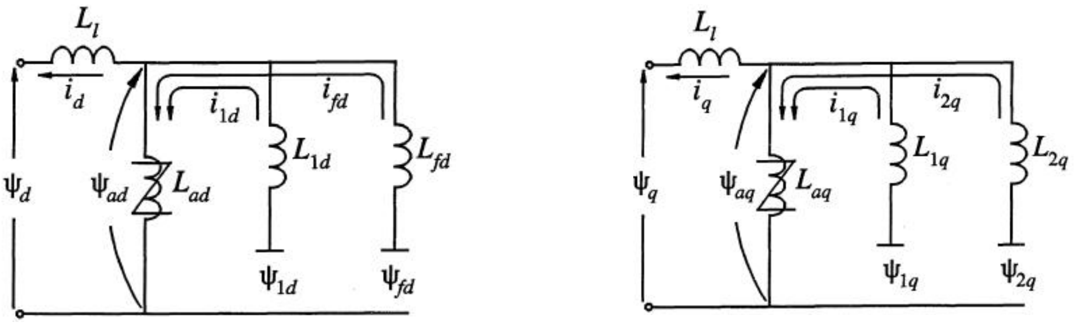

(a) (b)

Figure 3.11 Equivalent circuits identifying nonlinear elements and air-gap flux linkages (a) *d*-axis, (b) *q*-axis

The *d*-and *q*- axis ari-gap flux linkages are given by

$$\psi_{ad} = \psi_d + L_l i_d = (e_q + R_a i_q) + L_l i_d \tag{3.87}$$

$$\psi_{aq} = \psi_q + L_l i_q = (-e_d - R_a i_d) + L_l i_q \tag{3.88}$$

Therefore, ψ_{at} in per unit is equal to the air-gap voltage

$$\tilde{E}_a = \tilde{E}_t + (R_a + jX_l)\tilde{I}_t \tag{3.89}$$

Therefore, for any given values of terminal voltage and current, K_{sd} can be determined by first computing $\tilde{E}_a$ and then using equations (3.82) and (3.83), (3.84) or (3.85). In salient pole machine, the path for *q*-axis flux is largely in air, hence L_{aq} does not vary significantly with saturation of the iron. Therefore, K_{sq} is considered to be equal to 1.0 for all loading conditions. For round rotor machines, there occurs magnetic saturation in both *d*-and *q*-axes. Using no-load saturation characteristic of *q*-axis, K_{sq} can be calculated. But *q*-axis saturation data is usually unavailable; hence, K_{sq} is considered to be equal to K_{sd}.

3.4 Synchronous Machine Parameters

The inductances and resistances of the stator and rotor circuits are referred to as basic parameters shown in figure 3.12 [30]. These basic parameters can not be determined from measured responses of the machine. So, these parameters are expressed in terms of derived parameters which are used as machine data. In this section, these derived paramters are defined in terms of basic parameter.

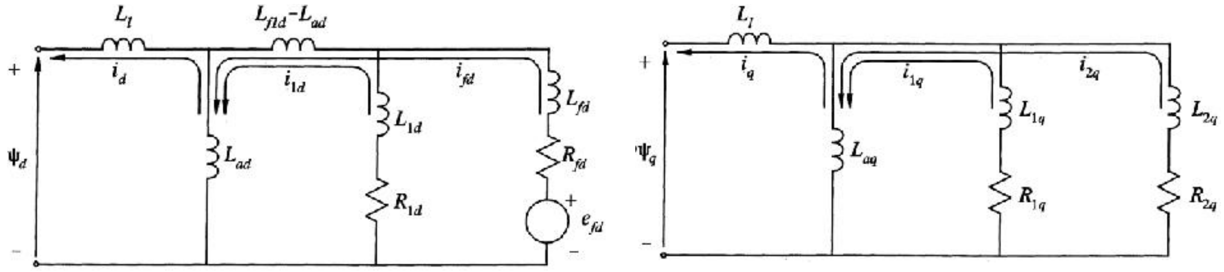

Figure 3.12 Complete *d*-and *q*-axis equivalent circuits (a) *d*-axis, (b) *q*-axis

3.4.1 Operational Parameters

A convenient way of identifying the machine electrical characteristics is in terms of operational parameters relating the armature and field terminal. The expressions for the *d*-axis operational parameters [30] are given by

$$L_d(s) = L_d \frac{1+(T_4+T_5)s+T_4T_6s^2}{1+(T_1+T_2)s+T_1T_3s^2} \tag{3.90}$$

$$G(s) = G_0 \frac{1+sT_{kd}}{1+(T_1+T_2)s+T_1T_3s^2} \tag{3.91}$$

G(s) is the stator to field transfer function, and $L_d(s)$ is the *d*-axis operational inductance.

where

$$\begin{aligned}
G_0 &= \frac{L_{ad}}{R_{fd}} & T_{kd} &= \frac{L_{1d}}{R_{1d}} \\
T_1 &= \frac{L_{ad}+L_{fd}}{R_{fd}} & T_2 &= \frac{L_{ad}+L_{1d}}{R_{1d}} \\
T_3 &= \frac{1}{R_{1d}}\left(L_{1d}+\frac{L_{ad}L_{fd}}{L_{ad}+L_{fd}}\right) & T_4 &= \frac{1}{R_{fd}}\left(L_{fd}+\frac{L_{ad}L_l}{L_{ad}+L_l}\right) \\
T_5 &= \frac{1}{R_{1d}}\left(L_{1d}+\frac{L_{ad}L_l}{L_{ad}+L_l}\right) & T_6 &= \frac{1}{R_{1d}}\left(L_{1d}+\frac{L_{ad}L_{fd}L_l}{L_{ad}L_l+L_{ad}L_{fd}+L_{fd}L_l}\right)
\end{aligned} \tag{3.92}$$

Equations (3.90) and (3.91) can be expressed in the factored form:

$$L_d(s) = L_d \frac{(1+sT_d')(1+sT_d'')}{(1+sT_{d0}')(1+sT_{d0}'')} \tag{3.93}$$

$$G(s) = G_0 \frac{1 + sT_{kd}}{(1 + sT'_{d0})(1 + sT''_{d0})} \tag{3.94}$$

Similarly the q-axis operational inductane can be expressed in the factored form:

$$L_q(s) = L_q \frac{(1 + sT'_q)(1 + sT''_q)}{(1 + sT'_{q0})(1 + sT''_{q0})} \tag{3.95}$$

The time constants in equations (3.93) to (3.95) represent important machine parameters wihich are discussed in the following section.

3.4.2 Standard Parameters

Following a disturbance, currents are induced in the machine rotor circuits. As shown in [30] for a short-circuit, some of these induced rotor currents decay more rapidly than others. Machine parameters that influence rapidly decaying components are called the subtransient parameters, while those influencing the slowly decaying components are called the transient parameters and those influencing sustained components are the synchronous parameters.

The time constants which determine the rate of decay of currents and voltages during subtransient, transient and sustained conditions form the standard parameters are used in specifying synchronous machine electrical characteristics. These standard parameters can be calculated from the operational parameters *$L_d(s)$, $G(s)$,*and *$L_q(s)$*. The constants T'_{d0}, T''_{d0}, T'_d, T''_d are the four main d-axis time constants of the machine. Their relationships to the basic parameters are obtained by equating the respective numerators and denominators of equations (3.90) and (3.93). Thus,

$$(1 + sT'_{d0})(1 + sT''_{d0}) = 1 + (T_1 + T_2)s + T_1T_3s^2 \tag{3.96}$$

$$(1 + sT'_d)(1 + sT''_d) = 1 + (T_4 + T_5)s + T_4T_6s^2 \tag{3.97}$$

Solving the above equations, the four time constants can be obtined which would be very complex expressions. With some resonable approximation, two types of generator models such as classical model and accurate model are available in different text books. Unless otherwise specified, the classical model is used generally. Hence, only the standard parameters' expressoins based on classical model are reviewed here.

***Parameter Based on Classical Definitions*:**

From equation (3.92), it is seen that if the value of R_{1d} is very much larger than R_{fd}, then T_2 and T_3 become very much smaller than T_1, and T_5 and T_6 become very much smaller than T_4. Hence

$$(1+sT'_{d0})(1+sT''_{d0}) \approx (1+sT_1)(1+sT_3) \tag{3.98}$$

$$(1+sT'_d)(1+sT''_d) \approx (1+sT_4)(1+sT_6) \tag{3.99}$$

So from equations (3.98) and (3.99), we have the following approximate relationships

$$T'_{d0} \approx T_1, \qquad T''_{d0} \approx T_3, \qquad T'_d \approx T_4, \qquad T''_d \approx T_6 \tag{3.100}$$

The expressions for T_1 to T_6 in equation (3.92) are in per unit (radians). They have to be divided by rated angular frequency to be converted to seconds. If the stator terminals are open (i.e., $\Delta i_d = 0$) then the incremental *d*-axis flux linkage can be expressed as

$$\Delta\psi_d(s) = G_0 \frac{1+sT_{kd}}{(1+sT'_{d0})(1+sT''_{d0})} \Delta e_{fd} \tag{3.101}$$

The equation (3.101) indicates that, for open-circuit conditions, the *d*-axis stator flux and hence the terminal voltage respond to a change in field voltage with time constants T'_{d0}, T''_{d0}. As $T_1 >> T_3$, from approximation equation (3.100), $T'_{d0} >> T''_{d0}$. Hence, T''_{d0} is associated with the initial change and is referred to as the *d*-axis open-circuit subtransient time constant. T'_{d0} represents a slow change corresponding to the transient period and is referred to as the *d*-axis open-circuit transient time constant. The time constant T'_d and T''_d represent the transient and subtransient short-circuit time constants, respectively.

Let the effective values of $L_d(s)$ be examined here under steady-state, transient, and subtransient conditions. Under steady-state conditions, putting s = 0 in equation (3.93), we get

$$L_d(0) = L_d \tag{3.102}$$

which represents the *d*-axis synchronous inductance. During a rapid transient, putting s--> ∞ in equation (3.93), the limiting value of $L_d(s)$ is given by

$$L''_d = L_d(\infty) = L_d\left(\frac{T'_d T''_d}{T'_{d0} T''_{d0}}\right) \tag{3.103}$$

which represents the effective inductance $\Delta\psi_d/\Delta i_d$ immediately following a sudden change and is called the *d*-axis subtransient inductance. In the absence of the damper winding and putting s--> ∞ in equation (3.93), the limiting value of inductance is given by

$$L'_d = L_d(\infty) = L_d\left(\frac{T'_d}{T'_{d0}}\right) \tag{3.104}$$

which is referred to as the *d*-axis transient inductane. Putting the expressions of time constants from equations (3.92) and(3.100) in equations(3.103) and (3.104) , we get,

$$L''_d = L_l + \frac{L_{ad}L_{fd}L_{1d}}{L_{ad}L_{fd} + L_{ad}L_{1d} + L_{fd}L_{1d}} \tag{3.105}$$

$$L'_d = L_l + \frac{L_{ad}L_{fd}}{L_{ad} + L_{fd}} \tag{3.106}$$

The principle of constant flux linkage states that the flux linking an inductive circuit with a finite resistance and emf cannot change instantly. So the rotor flux linkages do not change instantly following a disturbance. Using this principle the expressions in equations (3.100) and (3.106) can also be derived. Figure 3.13 shows the reduced equivalent circuit just after following a disturbance and with incremental rotor flux linkages ($\Delta\psi_{fd}$, $\Delta\psi_{1d}$) set to zero.

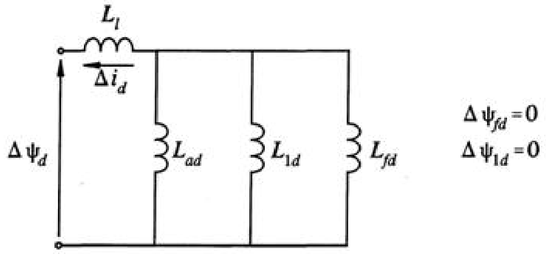

Figure 3.13 Equivalent circuit for incremental values, immediately following a disturbance

Similarly, using the corresponding equations related to *q*-axis, the *q*-axis open-circuit transient and subtransient time constants can be calulated as follows:

$$T'_{q0} = \frac{L_{aq} + L_{1q}}{R_{1q}} \tag{3.107}$$

$$T''_{q0} = \frac{1}{R_{2q}}\left(L_{2q} + \frac{L_{aq}L_{1q}}{L_{aq} + L_{1q}}\right) \tag{3.108}$$

and the subtransient and transient inductances are given by

$$L_q'' = L_l + \frac{L_{aq} L_{1q} L_{2q}}{L_{aq} L_{1q} + L_{aq} L_{2q} + L_{1q} L_{2q}} \tag{3.109}$$

$$L_q' = L_l + \frac{L_{aq} L_{1q}}{L_{aq} + L_{1q}} \tag{3.110}$$

Under steady-state, the synchronous inductance of $L_q(s)$ (equation (3.95)) is equal to L_q. The above expressions of standard parameters are derived based on the assumptions that during subtransient period $R_{fd} = R_{1q} = 0$ and that during transient period $R_{1d} = R_{2q} = \infty$.These assumptions have been used in the classical theroy on synchronous machine. Table 3.1 summerizes the accurate and classical expressions for the standard parameters of synchronous machine model which considers two rotor circuits in each axis with equal mutual inductances.

Table 3.1 Expressions for standard parameters of synchronous machine

Parameters	Classical Expresson	Accurate Expression [30]
T'_{d0}	T_1	T_1+T_2
T'_d	T_4	T_4+T_5
T''_{d0}	T_3	$T_3[T_1/(T_1+T_2)]$
T''_d	T_6	$T_6[T_4/(T_4+T_5)]$
L'_d	$L_d(T_4/T_1)$	$L_d(T_4+T_5)/(T_1+T_2)$
L''_d	$L_d(T_4T_6)/(T_1T_3)$	$L_d(T_4T_6)/(T_1T_3)$

Notes: (1) Similar expressions apply to q-axis parameters (2) All parameters are in pu
(3) Time constants in seconds are obtained by dividing the pu values by $\omega_0 = 2\pi f$
All mutual inductances in *d*-axis assumed equal.

3.4.3 Parameters of Salient Pole Machines

For a laminated salient pole machine, there is only one damper winding in the *q*-axis which represents rapidly decaying subtransient effects. Here, no distinction is made between transient and synchronous (steady state) conditions. Hence, the expressions for the *q*-axis parameters of a salient pole machine are as follows:

$$\begin{aligned} L_q &= L_l + L_{aq} \\ L_q'' &= L_l + \frac{L_{aq} L_{1q}}{L_{aq} + L_{1q}} \\ T_{q0}'' &= \frac{L_{aq} + L_{1q}}{R_{1q}} \end{aligned} \tag{3.111}$$

3.4.4 Reactances

In pu, the synchronous, transient and subtransient reactances are equal to the corresponding inductances. Hence, common practice is to identify synchronous machine parameters in terms of the reactances, instead of the inductances.

3.4.5 Typical Values of Standard Parameters

From the expressions for machine parameters summarized in equation (3.92) and Table 3.1, it is readily apparent that

$$X_d \geq X_q > X'_q \geq X'_d > X''_q \geq X''_d \tag{3.112}$$

$$T'_{d0} > T'_d > T''_{d0} > T''_d > T_{kd} \tag{3.113}$$

$$T'_{q0} > T'_q > T''_{q0} > T''_q \tag{3.114}$$

Table 3.2 gives ranges within which generator parameters normally lie.

Table 3.2 Typical values of standard parameters

Parameter		Hydraulic Units	Thermal Units
nchronous Reactance	X_d	0.6-1.5	1.0-2.3
	X_q	0.4-1.0	1.0-2.3
nsient Reactance	X'_d	0.2-0.5	0.15-0.4
	X'_q	-	0.3-1.0
btransient Reactance	X''_d	0.15-0.35	0.12-0.25
	X''_q	0.2-0.45	0.12-0.25
nsient OC Time Constant	T'_{d0}	1.5-9.0 s	3.0-10.0 s
	T'_{q0}	-	0.5-2.0 s
btransient OC Time Constant	T''_{d0}	0.01-0.05 s	0.02-0.05 s
	T''_{q0}	0.01-0.09 s	0.02-0.05 s
tor Leakage Inductance	X_l	0.1-0.2	0.1-0.2
tor Resistance	R_a	0.002-0.02	0.0015-0.005

Notes: (1). Reactance values are in per unit with stator base values equal to the corresponding machine rated values. (2) Time constants are in seconds.

CHAPTER 4

TORSIONAL OSCILLATION OF TURBINE-GENERATOR SHAFT

4.1 Introduction

A steam turbine-generator rotor consists of mass sections such as rotor of turbine sections, generator rotor, couplings and exciter rotor. If the generator is perturbed, torsional oscillations result in between different sections of the turbine generator rotor. The torsional oscillations could interact with the electrical system in an adverse manner. Some problems related to torsional oscillation are;

- Torsional oscillation with power system control
- Subsynchronous resonance with series-copensated trasnmission lines
- Torsional fatigue duty due to network switching

The effect of torsional oscillations on power system is a big concern now-a-days. This effect becomes bigger when the torsional oscillations are excited because it may damage completely not only the turbine-generator rotor but also all the rotating machines in power system. The torsional oscillations get advarsely excited if any frequency produced in the power system becomes equal or closely match to the oscillation frquencies of the transmitted torque between mass sections of turbine-generator shaft. The torsional excitation due to operation of multiple number of EAFs at the same PCC is the prime concern of this thesis. To do that, the torsional characteristic of turbine-generator shaft is studied in this chapter. For calculating the torsional modes of the turbine-generator shaft, eigenvalue analysis technique is used.

4.2 Eigenvalue Analysis Technique

Eigenvlaue analysis technique is a useful tool to investigate whether a power system is stable or not. This technique is applicable to linear system. But, a power system consists of many dynamic and static components, most of them are nonlinear in nature. A set of nonlinear differential and algebraic equations can be used to describe the synchronous machine, exciter, and any other control mechanisms. The algebraic equations couple the generator state variables and the generator's steady-state operating point power injection into the system. Again, there are the power system network equations i.e., the Kirchhoff's law circuit equations that the steady-state operating point must satisfy.

All thsese equations, like the set of differential equations, the algebraic equations, and the network equations can be linearized (termed as state-space representation) at the steady-state operating point. The set of linear differential and algebraic equations describe the power system dynamic response for small deviations from the steady operating point. To analyse the dynamic response of the power system, the eigenvaule analysis technique is applied to those state-space equations. Because, eigenvalues of power systems give a good picture of the stability in the current operating point.

Consider a square matrix, $\boldsymbol{A}$ which can be the coefficent matrix of the state-space equations describing power system. This matrix is also called as plant matrix or state matrix. Eigenvalues of $\boldsymbol{A}$ are given by values of scalar parameter λ for which there exist a non-zero vector $\boldsymbol{X}$ such that $\boldsymbol{AX} = \lambda\boldsymbol{X}$. This equation can be rearranged in the following ways:

$$\boldsymbol{AX} = \lambda\boldsymbol{X}$$
$$\Rightarrow \boldsymbol{AX} - \lambda\boldsymbol{X} = 0$$
$$\Rightarrow \boldsymbol{AX} - \lambda\boldsymbol{IX} = 0$$
$$\Rightarrow (\boldsymbol{A} - \lambda\boldsymbol{I})\boldsymbol{X} = 0$$

If non-zero solutions are desired, the determinant of the coefficient matrix $(\boldsymbol{A} - \lambda\boldsymbol{I})$ must be zero. If $(\boldsymbol{A} - \lambda\boldsymbol{I})$ is not zero, then the system possesses only the trivial solution $\boldsymbol{X} = 0$. But, by definition, eigenvectors are non-zero. So, in order for $\boldsymbol{X}$ to be an eigenvector of matrix $\boldsymbol{A}$, λ must be chosen so that

$$det(\boldsymbol{A} - \lambda\boldsymbol{I}) = 0$$

Expansion of determinant gives characteristic equation. The n solutions of $\lambda = \lambda_1, \lambda_2, ..., \lambda_n$ are eigenvalues of $\boldsymbol{A}$. Eigenvalues may be real or complex. If $\boldsymbol{A}$ is real, complex eigenvalues always occur in conjugate pairs.

Eigenvalue and Stability:

Stability of the system is determined by the eigenvalues as follows:

(a) *A real eigenvalue* corresponds to a non-oscillatory mode. A negative real eigenvalue represents a decaying mode. The larger its magnitude, the faster is the decay. A positive real eigenvalue represents aperiodic instability.

(b) *Complex eigenvalues* occur in conjugate pairs, and each pair corresponds to an oscillatory mode. Real component of eigenvalues gives damping, and imaginary component gives frequency of oscillation. A negative real part represents a damped oscillation whereas a positive real part represents oscillation of increasing amplitude.

Thus, for a complex pair of eigenvalues

$$\lambda = \sigma \pm \boldsymbol{j}\omega \tag{4.1}$$

Frequency of oscillation in Hz is given by

$$f = \frac{\omega}{2\pi} \tag{4.2}$$

This represents actual or damped frequency. The damping ratio is given by

$$\xi = \frac{-\sigma}{\sqrt{\sigma^2 + \omega^2}} \tag{4.3}$$

Damping ratio ζ determines rate of decay of amplitude of oscillation. In this thesis work, eigenvalue analysis technique is used to find frequencies of torsional oscillating torques of the turbine-generator shaft system.

4.3 Turbine-Generator Torsional Characteristics

A rotor system has a large number of torsional vibrational modes both in super and subsynchronous range with respect to rated frequency of the system. The problem due to interaction between the rotor mechanical and electrical systems is in the subsynchronous frequency range. For investigating this interaction, the rotor system can be represented by a simple lumped-mass model of the turbine-generator shaft [30].

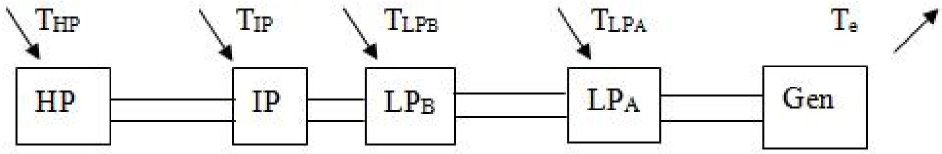

Figure 4.1 Structure of a typical lumped-mass shaft system

Figure 4.1 shows five torsional masses; HP, IP, 2 LP sections, Generator, assuming the generator unit has a static exciter. This system is used to investigate the excitation of torsional oscillations.

3.4.6 Physical Parameters Related to Rotor Mass Sections

***PU intertia constant, H*:**

$$H = J\frac{1}{2}\frac{\omega_{0m}{}^{2}}{VA_{base}} = J\frac{1}{2}\frac{(2\pi(r/\min)/60)^{2}}{VA_{base}}$$

ω_{0m} = rated speed in mechanical rad/s = $(2/P_f)\omega_0$, J is moment of inertia of rotor mass in kgm^2.

***Torsional stiffness K*:**

We know that

$$T = K\theta$$

where T = torque, N-m, θ = twist, rad, K = N-m/rad. The torsional stiffness difines the relationship between the torque transmitted and angular twist between two ends of the shaft. The base torque and the torsional stiffness in pu are expressed by the following two equations:

$$T_{base} = \frac{VA_{base}}{\omega_{0m}} = VA_{base}\frac{p_f}{2\omega_0}$$

$$K \text{ pu torque/elect.rad} = \frac{K}{p_f/2}\frac{N-m/mech.rad}{T_{base}} = \frac{K, N-m/mech.rad}{VA_{base}}(\frac{4\omega_0}{p_f{}^{2}})$$

Damping Factor D_m:

There are a number of sources which contribute to damp torsional oscillations. The sources are electrical (generator, exciter, transmission network), steam forces on turbine blades and shaft material hysteresis [30].

The damping levels associated with torsional oscillations are very small and are a function of the turbine-generator output. Here, we assume that all sources of damping may be expressed by damping torques which are proportional to speed deviations of individual masses. For this work, damping factors of different masses are chosen very small.

3.4.7 Mathematical Model of Shaft System

The equations of motion of each section of the turbine-generator shaft system are formulated here. Let us consider the rotor of generator and LP_A of turbine as shown in figure 4.2. The torque components associated with the generator rotor are as follows:

Input torque = $T_{12} = K_{12} (\delta_2\text{-}\delta_1)$
Output torque = T_e
Damping torque = $D_1(\Delta\omega_1)$
Accelerating torque = $T_a = T_{12}\text{-}T_e\text{-}\ D_1(\Delta\omega_1)$

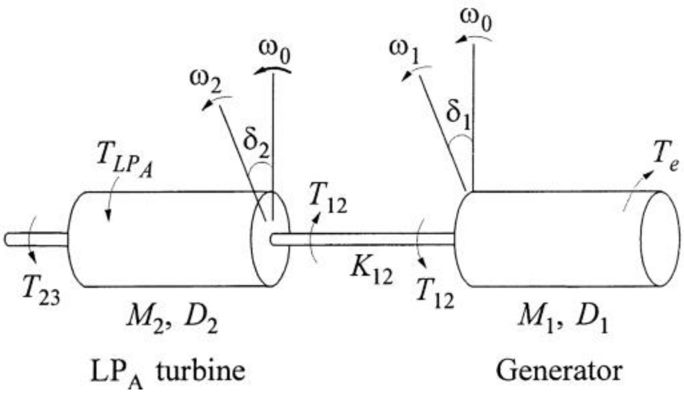

Figure 4.2 Rotor of generator and LP_A section of turbine

The equations of rotating motion of the generator rotor are

$$2H_1 \frac{d\Delta\omega_1}{dt} = T_a = K_{12}(\delta_2 - \delta_1) - T_e - D_1(\Delta\omega_1) \tag{4.4}$$

$$\frac{d\delta_1}{dt} = \omega_0 \Delta\omega_1 \tag{4.5}$$

The torque components associated with the LP_A section of turbine are derived in the following:

Input torque = T_{LPA}+T_{23} = T_{LPA}+$K_{23}(\delta_3$-$\delta_2)$

Output torque = T_{12} = K_{12} $(\delta_2$-$\delta_1)$

Damping torque = $D_2(\Delta\omega_2)$

The equations of rotating motion of the LP_A section of the shaft are:

$$2H_2 \frac{d\Delta\omega_2}{dt} = T_a = T_{LPA} + K_{23}(\delta_3 - \delta_2) - K_{12}(\delta_2 - \delta_1) - D_2(\Delta\omega_2) \tag{4.6}$$

$$\frac{d\delta_2}{dt} = \omega_0 \Delta\omega_2 \tag{4.7}$$

Similarly, the equations of rotating motion of the LP_B section of the shaft are:

$$2H_3 \frac{d\Delta\omega_3}{dt} = T_{LPB} + K_{34}(\delta_4 - \delta_3) - K_{23}(\delta_3 - \delta_2) - D_3(\Delta\omega_3) \tag{4.8}$$

$$\frac{d\delta_3}{dt} = \omega_0 \Delta\omega_3 \tag{4.9}$$

The equations of rotating motion of the IP section of the shaft are:

$$2H_4 \frac{d\Delta\omega_4}{dt} = T_{IP} + K_{45}(\delta_5 - \delta_4) - K_{34}(\delta_4 - \delta_3) - D_4(\Delta\omega_4) \tag{4.10}$$

$$\frac{d\delta_4}{dt} = \omega_0 \Delta\omega_4 \tag{4.11}$$

The equations of rotating motion of the HP section of the shaft are:

$$2H_5 \frac{d\Delta\omega_5}{dt} = T_{HP} - K_{45}(\delta_5 - \delta_4) - D_5(\Delta\omega_5) \tag{4.12}$$

$$\frac{d\delta_5}{dt} = \omega_0 \Delta\omega_5 \tag{4.13}$$

The generator electromagnetic torque, during transient condition, is determined by the dynamics of the generator and the power system. The torsional torques associated with each section of turbine shaft depend on the dynamics of the turbine and its governing system.

3.4.8 Calculation of Torsional Modes and Its Frequencies

The torsional frequencies and its mode shapes can be derived by using eigenvalue analysis technique. For this, the equations of complete shaft system have to be expressed in state-space form as follows:

$$\dot{x} = Ax + Bu$$
$$y = Cx + Du$$

where, *x* is the state vector, *y* is the output vector, *u* is the input vector, *A* is the state matrix, *B* is the control matrix, *C* is the output matrix, *D* is the feedforward matrix.

For small disturbance, the change in electromagnetic torque can be expressed as

$$\Delta T_e = K_s \Delta\delta_1$$

where K_s is the synchronizing torqe coefficient. Its value for the test system is calculated using MATLAB programming, as shown in Appendix A. Here, the mechanical torques developed by the turbine section are assumed to be constant.

The equations (4.4) to (4.13) have to be expressed in the form of state-space representatoin. The linearized equations of the shaft system can be written in state-space as follows:

Generator:

$$\frac{d\Delta\omega_1}{dt} = -\frac{D_1}{2H_1}(\Delta\omega_1) - \frac{K_{12}+K_S}{2H_1}(\Delta\delta_1) + \frac{K_{12}}{2H_1}(\Delta\delta_2) \tag{4.14}$$

$$\frac{d\Delta\delta_1}{dt} = \omega_0 \Delta\omega \tag{4.15}$$

LP_A:

$$\frac{d\Delta\omega_2}{dt} = \frac{K_{12}}{2H_2}(\Delta\delta_1) - \frac{D_2}{2H_2}(\Delta\omega_2) - \frac{K_{12}+K_{23}}{2H_1}(\Delta\delta_2) + \frac{K_{23}}{2H_2}(\Delta\delta_3) \tag{4.16}$$

$$\frac{d\Delta\delta_2}{dt} = \omega_0 \Delta\omega_2 \tag{4.17}$$

LP

LP_B:

$$\frac{d\Delta\omega_3}{dt} = \frac{K_{23}}{2H_3}(\Delta\delta_2) - \frac{D_3}{2H_3}(\Delta\omega_3) - \frac{K_{23}+K_{34}}{2H_3}(\Delta\delta_3) + \frac{K_{34}}{2H_3}(\Delta\delta_4) \tag{4.18}$$

$$\frac{d\Delta\delta_3}{dt} = \omega_0\Delta\omega_3 \tag{4.19}$$

IP:

$$\frac{d\Delta\omega_4}{dt} = \frac{K_{34}}{2H_4}(\Delta\delta_3) - \frac{D_4}{2H_4}(\Delta\omega_4) - \frac{K_{34}+K_{45}}{2H_4}(\Delta\delta_4) + \frac{K_{45}}{2H_4}(\Delta\delta_5) \tag{4.20}$$

$$\frac{d\Delta\delta_4}{dt} = \omega_0\Delta\omega_4 \tag{4.21}$$

HP:

$$\frac{d\Delta\omega_5}{dt} = \frac{K_{45}}{2H_5}(\Delta\delta_4) - \frac{D_5}{2H_5}(\Delta\omega_5) - \frac{K_{45}}{2H_5}(\Delta\delta_5) \tag{4.22}$$

$$\frac{d\Delta\delta_5}{dt} = \omega_0\Delta\omega_5 \tag{4.23}$$

where the state variables are the speed deviations $\Delta\omega_i$ and the rotor angle deviation $\Delta\delta_i$, with $i = 1$ to 5. The equations (4.14) to (4.23) can be written in matrix form as follows:

$$\begin{bmatrix} \Delta\dot{\omega}_1 \\ \Delta\dot{\delta}_1 \\ \Delta\dot{\omega}_2 \\ \Delta\dot{\delta}_2 \\ \Delta\dot{\omega}_3 \\ \Delta\dot{\delta}_3 \\ \Delta\dot{\omega}_4 \\ \Delta\dot{\delta}_4 \\ \Delta\dot{\omega}_5 \\ \Delta\dot{\delta}_5 \end{bmatrix} = \begin{bmatrix} -\frac{D_1}{2H_1} & -\frac{K_{12}+K_s}{2H_1} & 0 & \frac{K_{12}}{2H_1} & 0 & 0 & 0 & 0 & 0 & 0 \\ \omega_0 & 0 & 0 & 0 & 0 & 0 & 0 & 0 & 0 & 0 \\ 0 & \frac{K_{12}}{2H_2} & -\frac{D_2}{2H_2} & -\frac{K_{12}+K_{23}}{2H_2} & 0 & \frac{K_{23}}{2H_2} & 0 & 0 & 0 & 0 \\ 0 & 0 & \omega_0 & 0 & 0 & 0 & 0 & 0 & 0 & 0 \\ 0 & 0 & 0 & \frac{K_{23}}{2H_3} & -\frac{D_3}{2H_3} & -\frac{K_{23}+K_{34}}{2H_3} & 0 & \frac{K_{34}}{2H_3} & 0 & 0 \\ 0 & 0 & 0 & 0 & \omega_0 & 0 & 0 & 0 & 0 & 0 \\ 0 & 0 & 0 & 0 & 0 & \frac{K_{34}}{2H_4} & -\frac{D_4}{2H_4} & -\frac{K_{34}+K_{45}}{2H_4} & 0 & \frac{K_{45}}{2H_4} \\ 0 & 0 & 0 & 0 & 0 & 0 & \omega_0 & 0 & 0 & 0 \\ 0 & 0 & 0 & 0 & 0 & 0 & 0 & \frac{K_{45}}{2H_5} & -\frac{D_5}{2H_5} & -\frac{K_{45}}{2H_5} \\ 0 & 0 & 0 & 0 & 0 & 0 & 0 & 0 & \omega_0 & 0 \end{bmatrix} \begin{bmatrix} \Delta\omega_1 \\ \Delta\delta_1 \\ \Delta\omega_2 \\ \Delta\delta_2 \\ \Delta\omega_3 \\ \Delta\delta_3 \\ \Delta\omega_4 \\ \Delta\delta_4 \\ \Delta\omega_5 \\ \Delta\delta_5 \end{bmatrix}$$

in short form

$$\begin{bmatrix} \Delta\dot{\omega}_i \\ \Delta\dot{\delta}_i \end{bmatrix} = \boldsymbol{A} \begin{bmatrix} \Delta\omega_i \\ \Delta\delta_i \end{bmatrix} \tag{4.24}$$

Where ***A*** is the state matrix.

From the equation, we see that ***A*** depends on the torsional stiffness coefficient, the inertia constants, damping factors and the synchronizing torque coefficient. Now, using the eigenvalue analysis technique, the eigenvalues of matrix ***A*** can be found. MATLAB simulation tool has been used to calculate the eigenvalues of the state matrix, ***A***. From the eigenvalues, the torsional modes and its frquencies can be obtained using equations (4.1) to (4.2). To find out the eigenvalues of ***A***, the physical parameters of turbine-generator shaft, in Table 4.1, are used.

Table 4.1: Physical parameters of turbine-generator shaft

Element	***D*** **(pu torque/pu speed deviation)**	***K*** **(pu torque/electr.rad.)**	***H*** **(MW-s/MVA)**
nerator	0.16	--	0.556
A	2.4832	51.92	0.775
B	0.40	63	0.751
	0.40	40.33	0.151
	0.32	18.17	0.081

3.4.9 Torsional Modes and Their Frequencies from MATLAB Simulation

A test system (described in chapter 5) is simulated using MATLAB. The MATLAB simulation for finding the eigenvalues of a test system has been shown in Appendix A. From the simulation, the eigenvalues of the plant matrix ***A***, are derived. The torsional modes and their frequencies are derived form the eigenvalues using equations (4.1) to (4.2) and presented in Table 4.2.

Table 4.2: Eigenvalues of state matrix ***A***, torsional modes and their frequencies.

Eigenvalues λ		**Mode frequency (Hz)**	**Torsional Mode**
λ_1	-0.6931651492505 + 285.4484238317879i	45.4	4
λ_2	-0.6931651492505 - 285.4484238317879i		
λ_3	-0.5566807095606 + 196.7330425025057i	31.3	3
λ_4	-0.5566807095606 – 196.7330425025057i		
λ_5	-0.6441084939733 + 156.2125676838909i	24.9	2
λ_6	-0.6441084939733 - 156.2125676838909i		
λ_7	-0.3551595225466 + 105.4251804554375i	16.8	1
λ_8	-0.3551595225466 - 105.4251804554375i		
λ_9	-0.4069225976704 + 3.4898816348349i	0.55	0 (system mode)
λ_{10}	-0.4069225976704 - 3.4898816348349i		

As the turbine-generator shaft has five masses, there are five modes of torsional oscillation. The mode frequencies are calculated from imaginary part of eiginevalues using equation (4.2). The relative rotational displacements (right eigenvectors associated to either speed deviations or the angle deviations) of individual masses for each mode of oscillation are shown in figure 4.3.

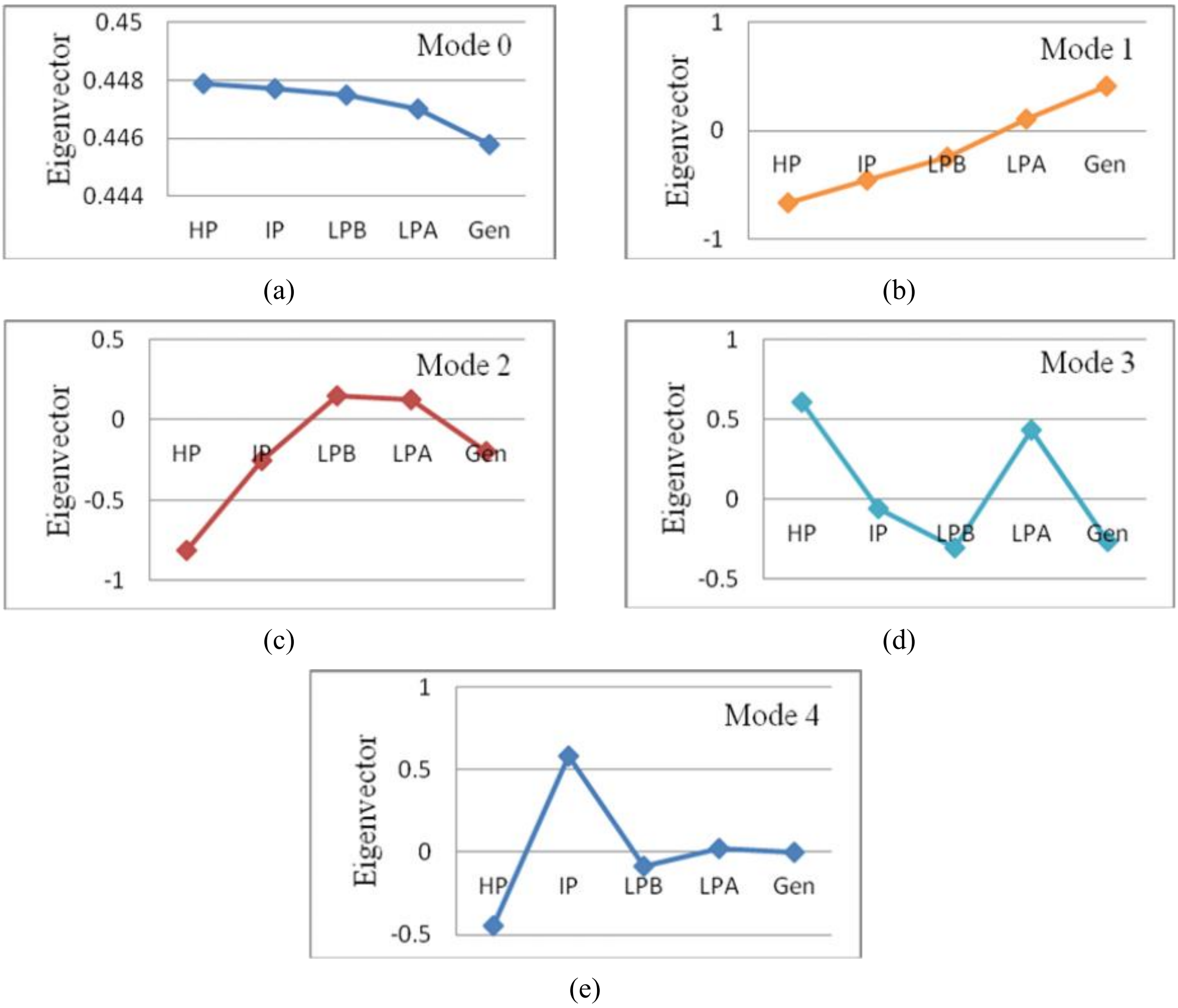

Figure 4.3 Rotor mode shapes of a 555 MVA, 3000 rpm, 2-pole, steam turbine-generator (a) mode 0, (b) mode 1, (c) mode 2, (d) mode 3, (e) mode 4

The mode 0 represents the oscillation of the entire rotor against the power system. It depends on the total inertia constant of all rotor masses and synchronizing torque coefficient K_s. From figure 4.3, it is seen that all masses take part nearly equally in mode 0. Modes 1 to 4 represent the torsional mode of oscillation. Mode 1 hase one polarity reversal where polarities of eigenvector associated with generator and LP_A are opposite to those assiciated to LP_B, IP and HP sections. This indicates that if mode 1 is excited, generator and LP_A oscillate against other three masses. Mode 2 has two polarity reversals, Mode 3 has three polarity reversals and Mode 4 has four polarity reversals. In Mode 4, there is very low relative amplitudes of rotational displacement between generator and LP_A. This indicates this mode can not be easily excited.

4.4 Torsional Interaction with Power System Control

Normally torsional oscillations are not affected by the generating unit or network controls. However, there have been several instances of torsional mode instability due to interactions with the generating unit excitation and prime mover controls.

4.5 Torsional Interaction Resulting in SSR

Any frequency, produced from EAF operation, close to torsional frequencies, excite torsional oscillations. This condition is termed as subsynchronous resonance. At this condition, a large subsynchronous current may result from a small voltage induced by rotor oscillations. A rotor torque corresponding to this current is in such phase that it enhances the rotor oscillation. If this torque become larger than mechanical damping, the coupled electromechanical system will experience increasing oscillations.

4.6 Consequences of SSR

The torsional excitation may result in dangerous situation. The turbine-generator shaft may break with disastrous consequences if the torsional excitation occurs and sustain for long duration. Even if the torsional excitation does not sustain for long duration, it may cause loss of fatigue life of the turbine-generator shaft.

CHAPTER 5

TORSIONAL MODE AMPLIFICATION IN TEST SYSTEM

5.1 Introduction

The torsional modes of the turbine-generator system has been evaluated using eigenvalue analysis technique in chapter 4. If any of the frequencies of torsional mode is generated in the power system, the turbine-generator shaft realizes torsional resonance which amplify the torsional oscillating torques. EAF in the power system can be the potential source of those frequencies termed as subsynchornous frequencies. Actually, the torsional mode amplification occurs due to disturbance in air-gap torque of synchronous generator. In chapter 3, the air-gap torque has been expressed as function of the *dq*-components of stator currents and flux linkages. In chapter 3, it has been shown that the stator currents are the subsynchronous frequency carrier. So any frequency equal to torsional mode frequency in stator currents affect the electromagnetic torque resulting in torsional oscillating torques amplification. For assessing the torsional oscillating torques amplification, a test system having a synchronous generator supplying power to an EAF and infinite bus, is considered.

5.2 Description of the Test System

The electromechanical system shown in figure 5.1 is used to analyse torsional resonance in turbine-generator shaft due to operation of EAF. The steam turbine unit has 4 stages such as a high-pressure (HP) stage, an intermediate-pressure (IP) and two low-pressure (LP_A and LP_B) stages. In the simulation, the speed governing system is used which is not shown in the figure 5.1. The speed governing system includes a speed relay, a proportional regulator, and a servomotor which controls the gate opening. Turbine power is distributed in fractions to various shaft stages.The turbine shaft is coupled to the masses including the synchronous generator resulting in total five masses. The turbine-generator shaft is characterized by mass inertias H, rigidity coefficients K and damping factors D which values are shown in Table 4.1.

The synchronous generator is rated as 3000rpm/2-pole, 24kV, 555 MVA. A static exciter is used with the generator. The electrical paramerters in pu, based on rated value of the synchronous generator, are given in Table 5.1. The generator is supplying power to the network via a step-up transformer (24kV/132kV, 555 MVA) through a transmission line of length 50 km. The 132 kV bus also supplies power to an steel industry through a 132kV/24kV transformer.

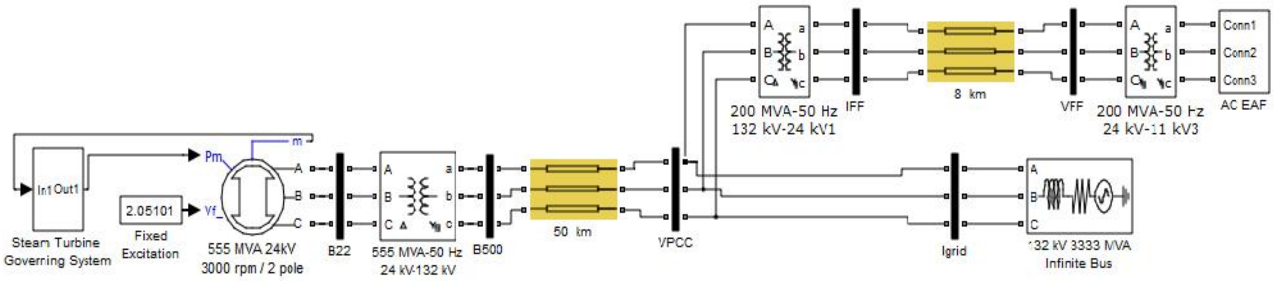

Figure 5.1 Simulated test system

The steel industry is located at 8 km distance from PCC (at 132 kV bus) and using EAF to pruduce steel. Other transformers, one rated as 24kV/11kV, 200MVA, 3-φ and anothers rated as 11KV/.5KV, 50MVA, 3 single phase are also installed in the furnace feeder line to step down voltage to furnace operating value. The EAF is designed as single phase furnace and three single phase furnaces, behaving as three phase EAF, are connected to three phases of 24kV/11kV, 200MVA, 3-ϕ transformer through single phase transformers. The impedances of the three-phase transformers are chosen as 0.008+j0.13 pu and for the single phase transformers as 0.0006+j0.13 pu. The parameters considered for the transmission lines are given in Table 5.2.

Table 5.1: Generator data of the test system

Parameters	Value (PU)	Parameters	Value
Xd	1.51	*Xl*	0.13 pu
Xd'	0.257	R_a	0.003 pu
Xd''	0.203	*Tdo'*	8.1 s
Xq	1.47	*Tdo''*	0.0335 s
Xq'	0.6	*Tqo'*	1.06 s
Xq''	0.229	*Tqo''*	0.08 s

Table 5.2: Positive and zero sequence components of line impedance

Sequences	Resistance (Ohm/km)	Inductance (H/km)	Capacitance (F/km)
Positive	0.01165	0.8679e-3	13.41e-9
Zero	0.2676	3.008e-3	8.57e-9

5.3 Determination of Torsional Mode Frequencies

The torsional mode frequencies were determined by eigenvalue analysis technique in chapter 4. The mode frequencies were 0.55, 16.8, 24.9, 31.3 and 45.4 Hz. The mode frequencies can also be obtained from the FFT analysis of torsional oscillating torque signals. Figures 5.2 and 5.3 show the FFT of torsional oscillating torque signals between generator-LP_A section and IP-HP section respectively. It is seen from the figures 5.2 and 5.3 that the torsional mode frequencies are 1.2, 16.8, 24.9, 31.3, 45.4 Hz which are almost the same as obtained from eigenvalue analysis technique. The only error is in mode 0 where frequencies from eigenvalue analysis and FFT analysis are different. This error arises, may be, becuase of different assumptions in deriving performance equations of generator which were used in eigenvalue analysis.

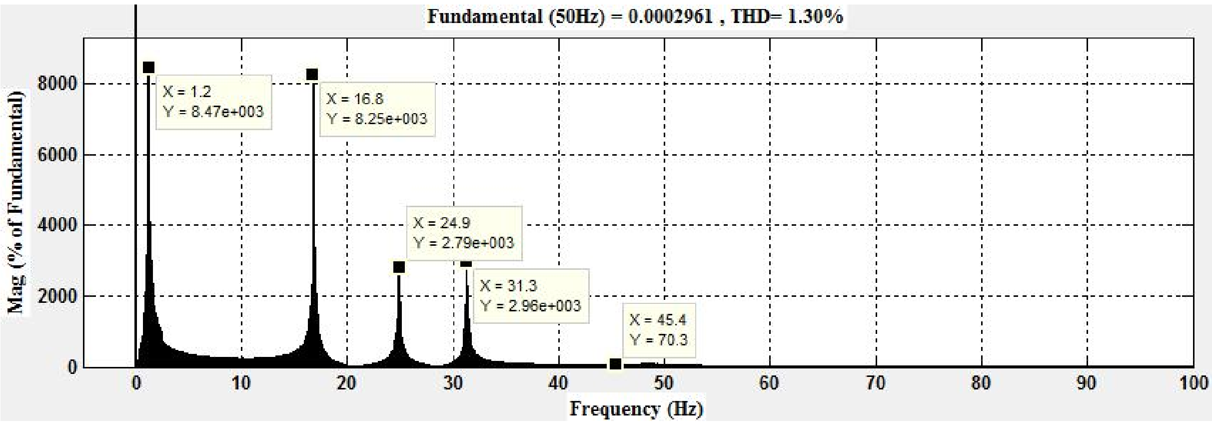

Figure 5.2 FFT of torsional torque between generator and LP_A section

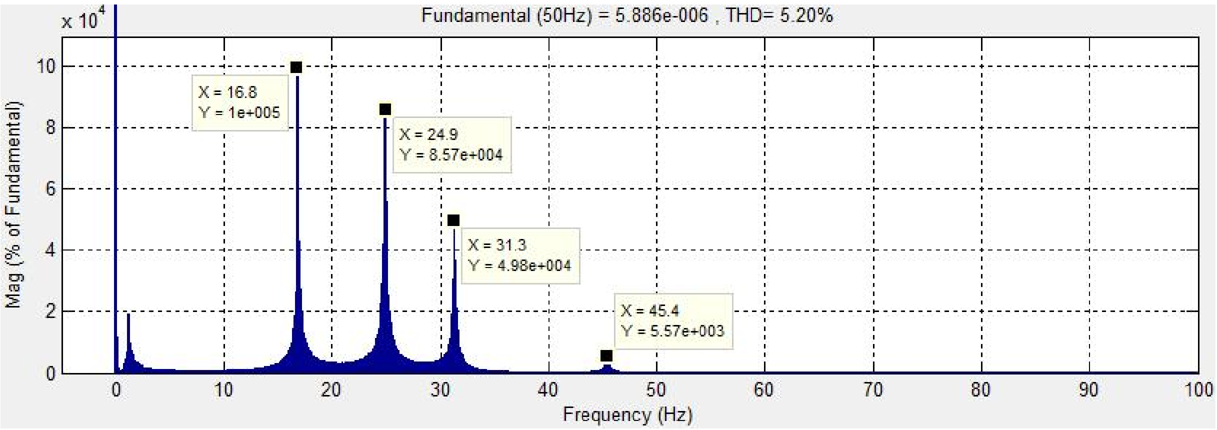

Figure 5.3 FFT of torsional torque between HP and IP section

5.4 Analysis of Simulation Output

The dynamic behavior of electric arc was chosen for modeling EAF, because this model captures changes in the *V-I* characteristics if the operation conditions alter in the power supply system. The differential equations of electric arc, explained in chapter 3, were developed based on the principle of energy conservation. Using those equations, the electric arc was modeled. Then among the two models of EAF such as deterministic and stocastic model, the former one was considered. In this deterministic model, the electric arc resistance was modified sinusoidally so that the characteristics of the modeled EAF closely match to behaviors of the actual 3-phase AC EAF. Having this deterministic model of EAF in the power system as shown in figure 5.1, the test system is simulated using MATLAB power library and the necessary output of the simulation is explained in the following section.

5.4.1 Feeder Voltage and Current

Due to movement of the electrodes and melting of the scraps, the arc length changes which cause change in arc resistance. Figure 5.4 shows the variation of arc resistance and arc voltage. From the figure 5.4, it is seen that when the arc voltage increases from its zero crossing point to arc ignition voltage, the equivalent circuit of EAF becomes an open circuit. Although it becomes an open circuit, a small leakage current may flow through the foamy slag which may be assumed to have a constant high resistance. The impulses in figure 5.4(a) can be assumed as the constant high resistance. When the arc is established, a transient process appears at the voltage waveform at the beginning of the arc melting process. The arc voltage drops exponentially from ignition voltage to a constant value. During arc established period, the electrodes and scraps are assumed to be short circuited which results in almost zero resistance. After melting the scraps, the arc need to be extinguished which results in drop of arc voltage to arc extinction voltage.

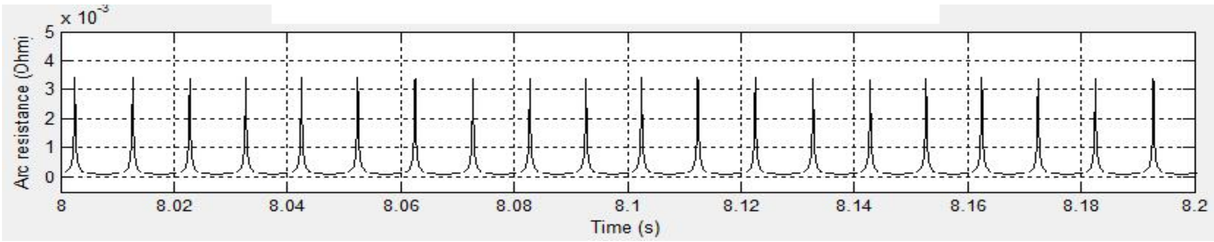

(a)

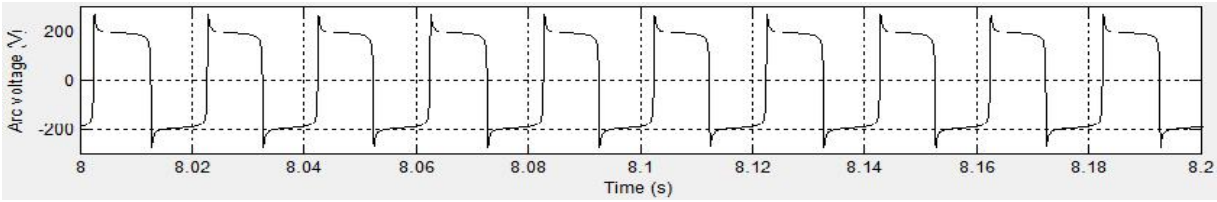

(b)

Figure 5.4 (a) Arc resistance in ohm, (b) arc voltage in volts

A deterministic model approach is used to obtain the actual characteristic of the EAF load. In this model, the arc resistance is varied sinusoidally as shown in figure 5.5. Figure 5.5(a) shows the modulated arc resistance and figure 5.5(b) shows the modulated arc voltage. During modulation of the arc resistance a 60% modulation index is chosen in simulation. The frequency of the modulating signal is 10 Hz.

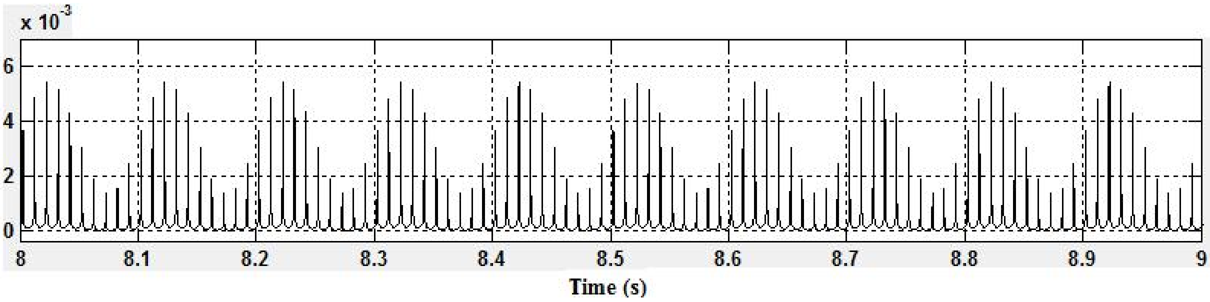

(a)

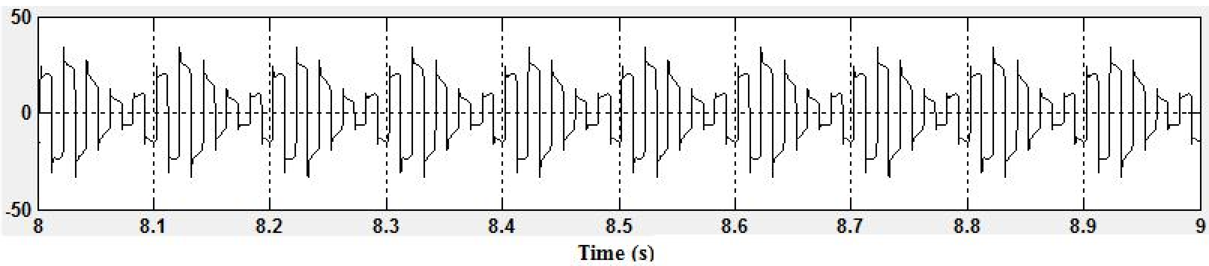

(b)

Figure 5.5(a) Modulated arc resistance in ohm, (b) modulated arc voltage in volts

Figure 5.6 shows the voltage (pu) and current (pu) of feeder which is supplying power to the EAF. From figure 5.6(a), It is seen that the waveform is a modulated signal which cause voltage flicker. Figure 5.6(b) shows the feeder current waveform. The FFT, in figure 5.7, shows that the two frequencies 40 Hz and 60 Hz are present in the feeder current waveforms. These frequencies are present because 10 Hz signal was impregnated during resistance modulation. For this reason, the furnace feeder is considered as the source of super and subsynchronous frequencies and the EAF can be considered as the source current which disturbs the air-gap torque in the synchronous generator.

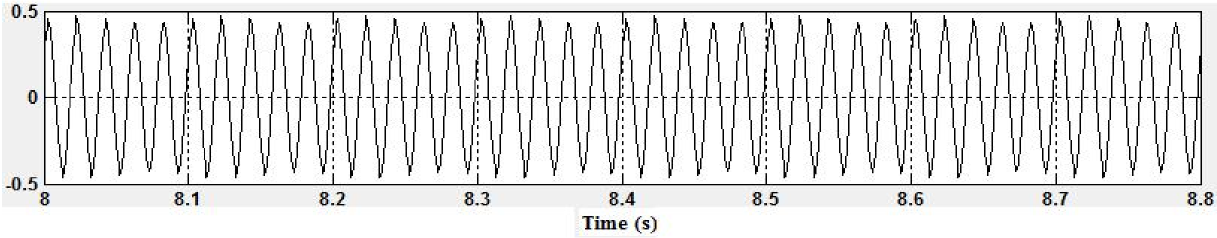

(a)

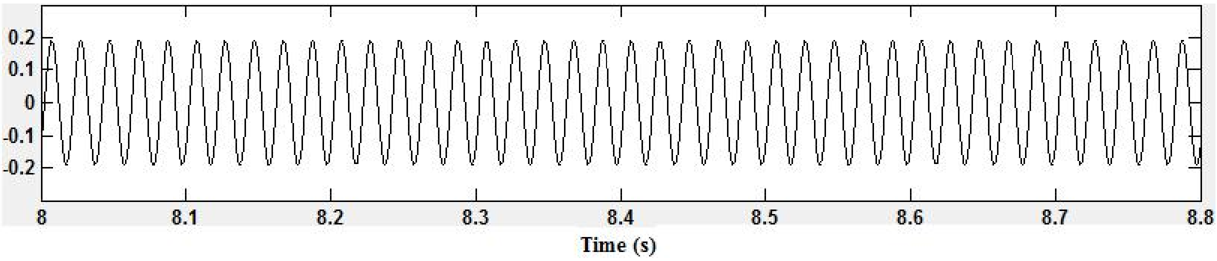

(b)

Figure 5.6 Furnace feeder voltage and current of phase-*a* (a) voltage (pu), (b) current (pu)

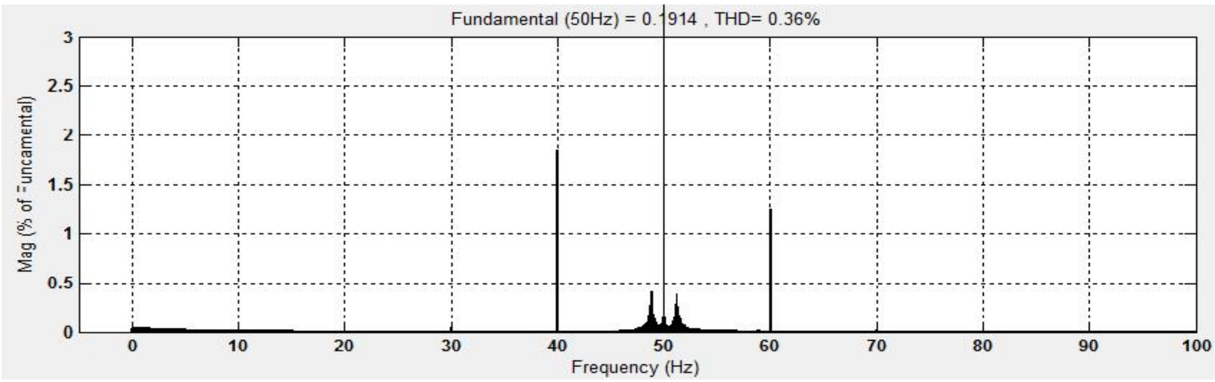

(a)

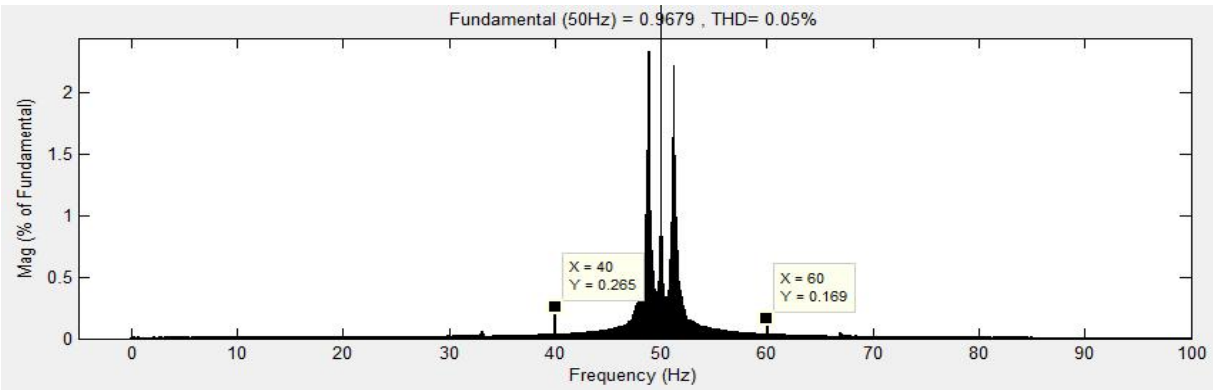

(b)

Figure 5.7 (a) FFT of feeder current in phase-*a* near furnace transformer, (b) FFT of current in phase-*a* at PCC

5.4.2 FFT Analysis of Stator Current

Figure 5.8 shows the FFT of stator current where (a) represents the FFT of stator current (A) when there is no EAF in the system and (b) represents the FFT of stator current (pu) when thare is an EAF in the system. From figure 5.8(a), it is seen that only the 50 Hz (Fundamental frequency of the system) component is present because there is no source of subsynchronous frequencies in the power system. From figure 5.8(b), it is seen that not only the 50 Hz component but also 16.8 Hz (50-16.8 = 33.2Hz) component is present. The signal with 16.8 Hz was used to modulate the arc resistance. It is also seen that 33.2 Hz signal has greater magnitude than magnitude of 66.8 Hz (50+16.8 Hz) signal. It can prove the hypothesis that torsional oscillations are more prone to be affected by subsynchronous frequencies in the system.

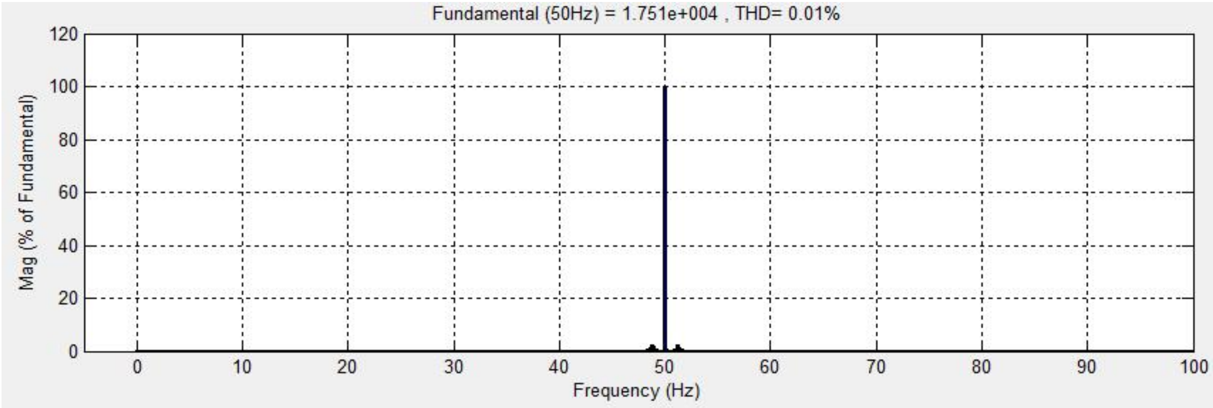

(a)

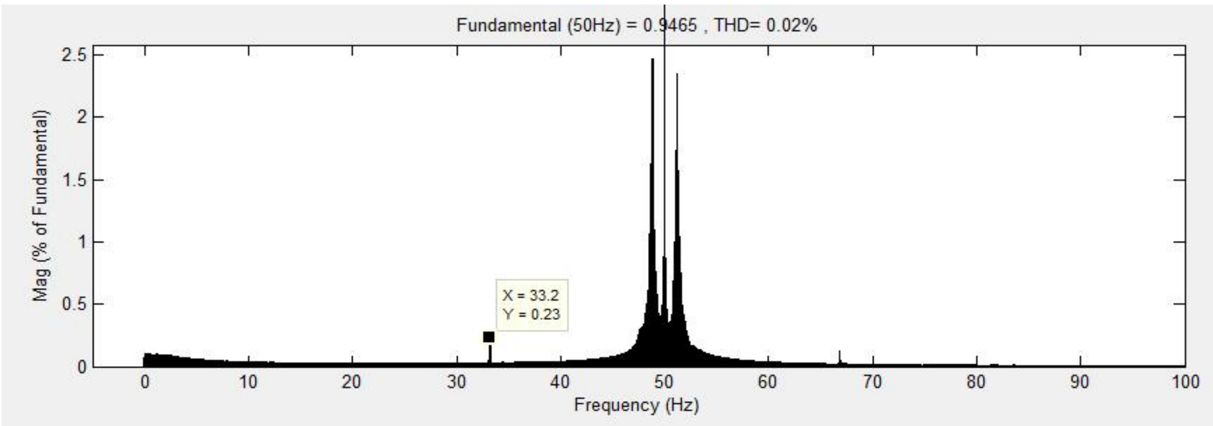

(b)

Figure 5.8 FFT of stator currents (a) without EAF in the system, (b) with EAF producing 16.8 Hz in the system

5.4.3 FFT Analysis of dq0 Current Components

It was shown in chapter 3 that in balanced steady-state condition the *dq0* component, i.e., i_d and i_q become constant. This indicate that the alternating stator currents in the *abc* reference frame appear as direct current in the *dq0* reference frame. The figures 5.9 and 5.10 show the *d*-and *q*-axis current component and their FFT respectively. These *d*-and *q*-axis current components are obtained from the simulation when there are no EAFs in the system. From figures 5.9(a) and 5.10(a), it is seen that *d*-and *q*-axis current appear constant after 5 seconds of starting of synchronous generator. Figures 5.9(b) and 5.10(b) show the magnified graph, in time range 8-10 second at steady state, of figure 5.9(a) and 5.10(a) respectively. The magnified figures prove the *d*-and *q*-axis current as constant with negligible variation around the constant DC value.

From FFT of *d*-and *q*-axis current as shown in figure 5.9(c) and 5.10(c), it is seen that there are no dominant frequency components other than DC component. It proves that the system is running in steady-state condition and stator currnents contain no super/subsynchronous frequencies.

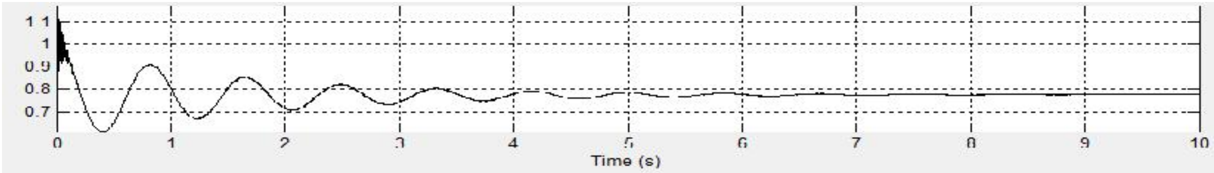

(a)

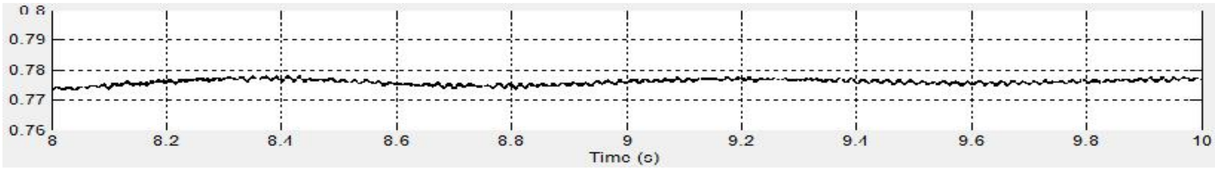

(b)

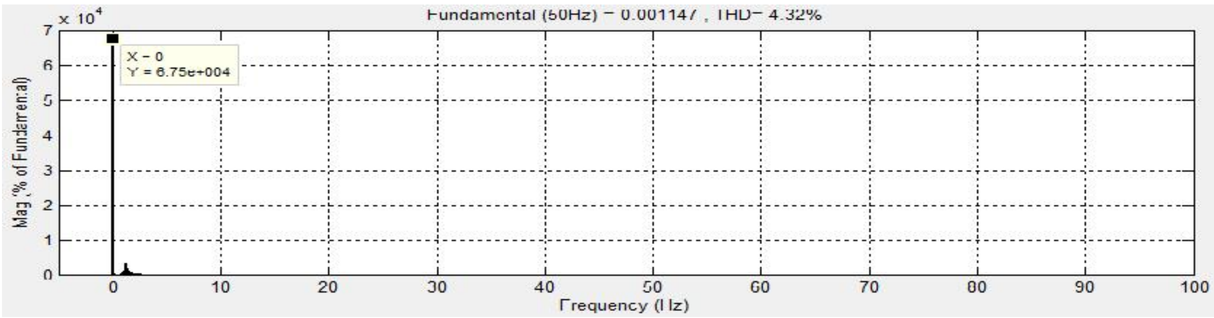

(c)

Figure 5.9 *d*-axis current without EAF in the system (a) *d*-axis current component i_d, (b) scaled current i_d , (c) FFT of current i_d

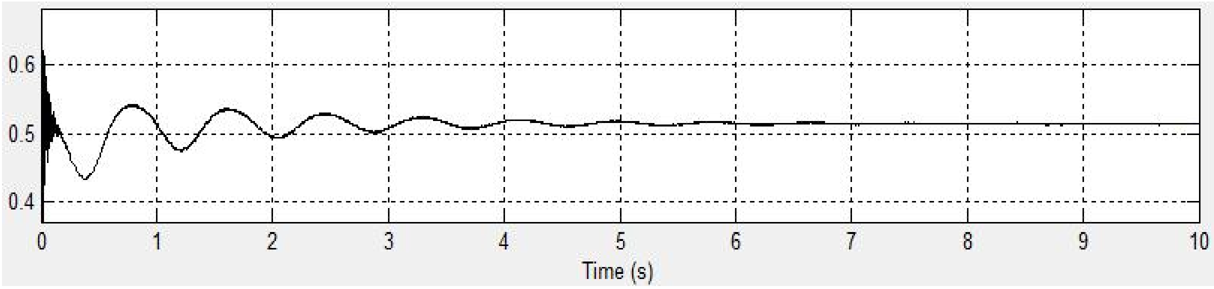

(a)

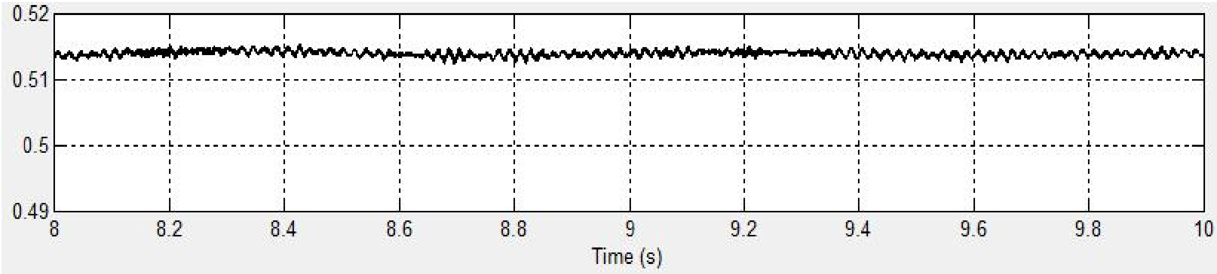

(b)

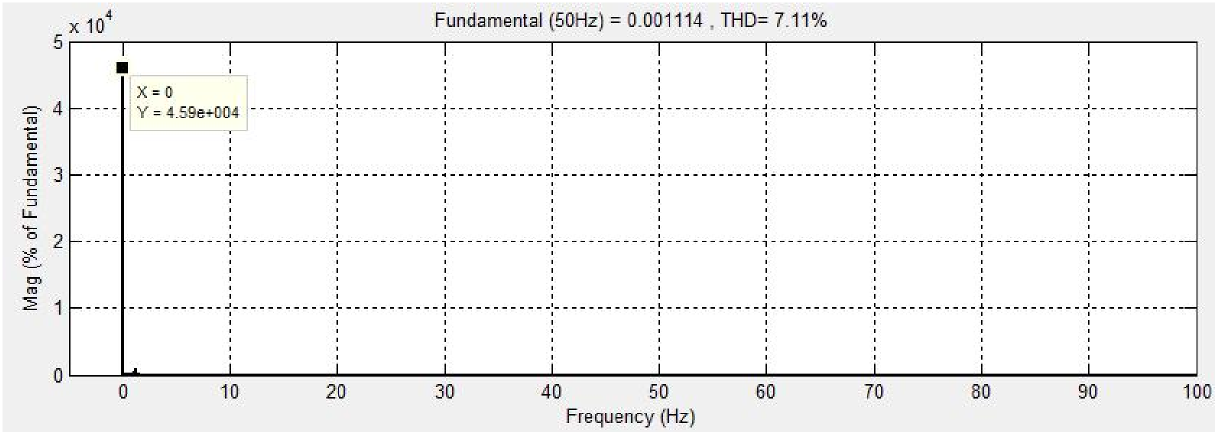

(c)

Figure 5.10 q-axis current component without EAF in the system (a) q-axis current component i_q, (b) scaled current i_q , (c) FFT of current i_q

The figures 5.11 and 5.12 explain the *d*-and *q*-axis current component with EAF in the system. Since the frequency of the modulating signal is 16.8 Hz, it is also seen in figure 5.11(c) and 5.12(c). The FFTs also prove of having 16.8 Hz frequency component as dominant in the *d*-and *q*-axis current waveforms. Comparing *dq*-axis current components in figures 5.9(b) and 5.10(b) with *dq*-axis current components in figures 5.11(b) and 5.12(b), it is deducible that, due to presence of 16.8 Hz signal in the stator currents, the amplitude of oscillation of dq-axis current components is little bit larger when the system is running with EAF.

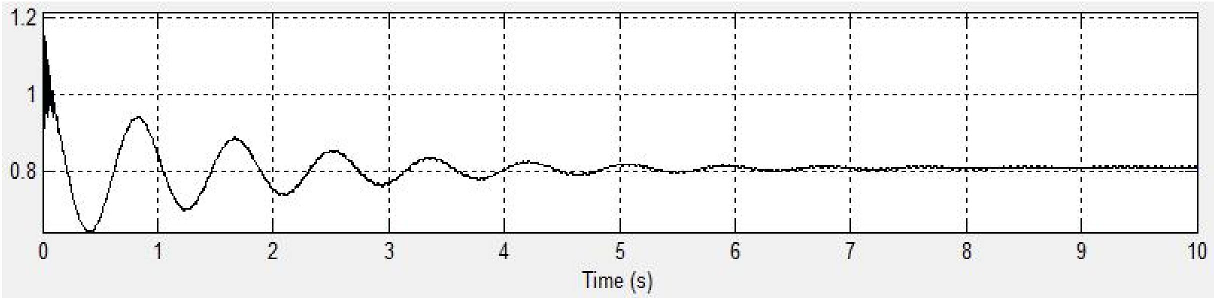

(a)

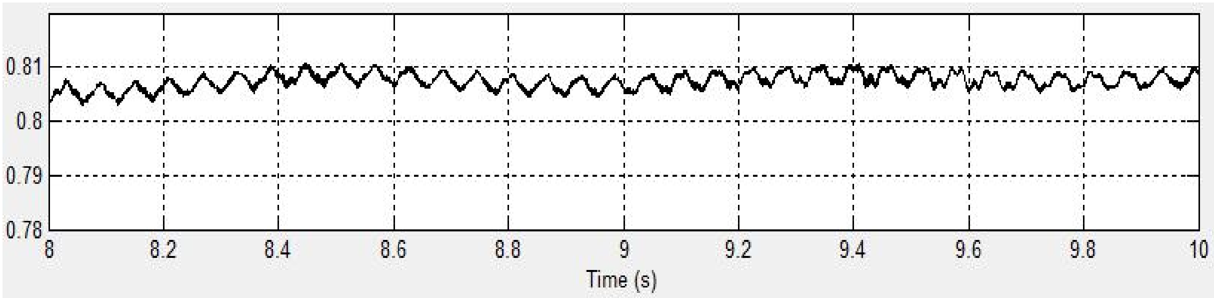

(b)

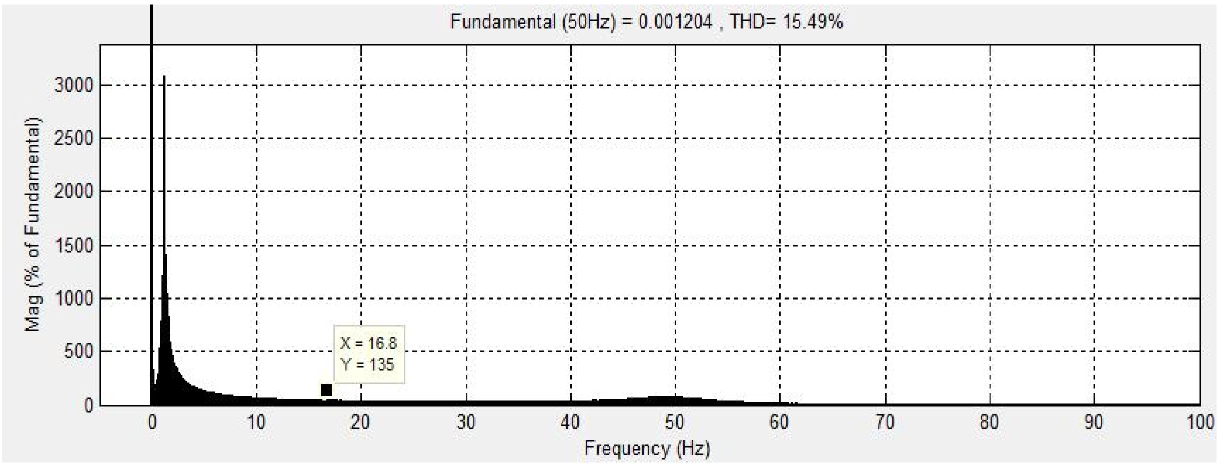

(c)

Figure 5.11 d-axis current component with EAF in the system (a) d-axis current component i_d, (b) scaled current i_d, (c) FFT of current i_d

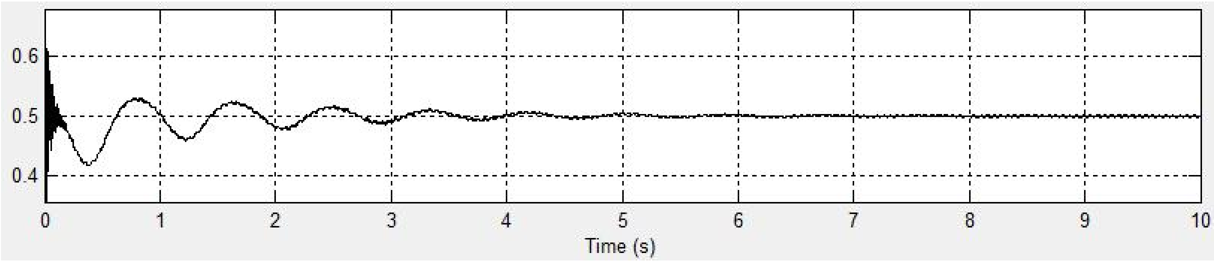

(a)

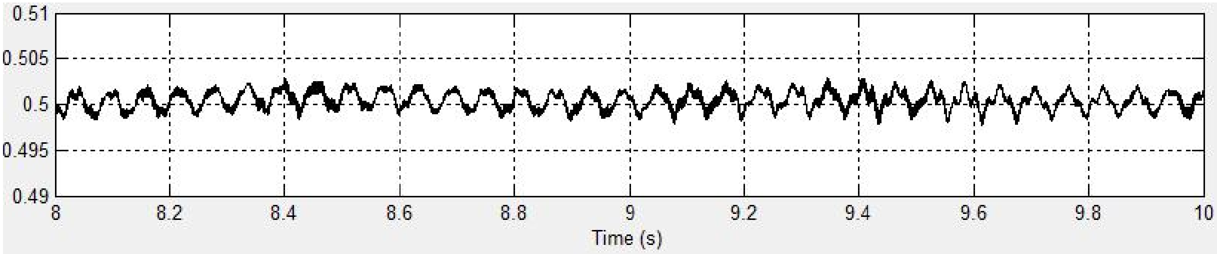

(b)

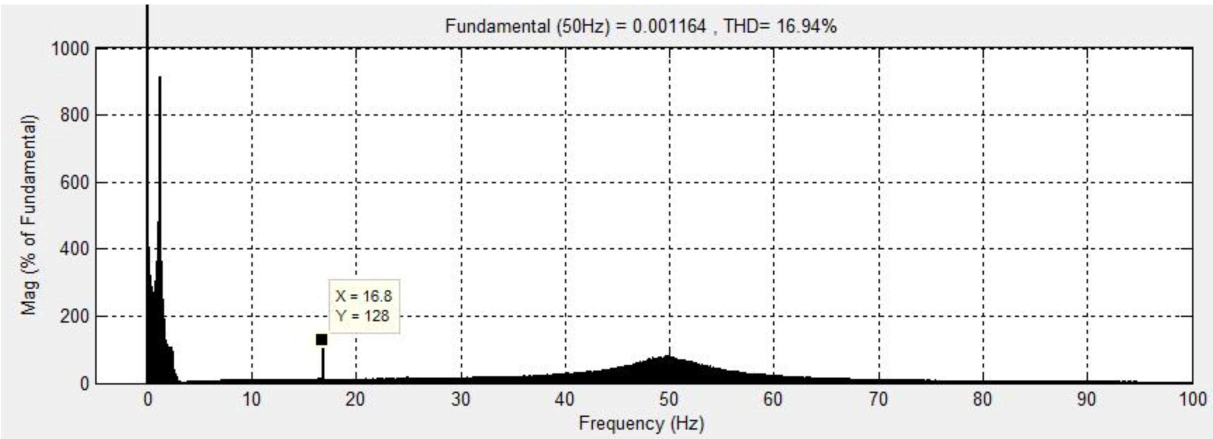

(c)

Figure 5.12 q-axis current component with EAF in the system (a) q-axis current component i_q, (b) scaled current i_q, (c) FFT of current i_q

5.4.4 Analysis of Electromagnetic Torque

In chapter 3, it was shown that the air-gap torque is the function of d-and q-axis current and flux linkages. So, if the stator current is perturbed, d-and q-axis current components are perturbed and correspondingly the air-gap torque is perturbed. In the previous discussion, we have seen that the EAF feeder is a source of harmonic currents. These harmonic currents, in super and sub-harmonic range, are spread throughout the network. As a result, the generator air-gap torque is disturbed by those harmonics. Figure 5.13 shows the air gap torque when there is no EAF in the system. It is seen that after 5 seconds of starting the generator, the torque become constant. It is also seen from FFT of air-gap torque in figure 5.13(c) that there is no other frquency component as dominant.

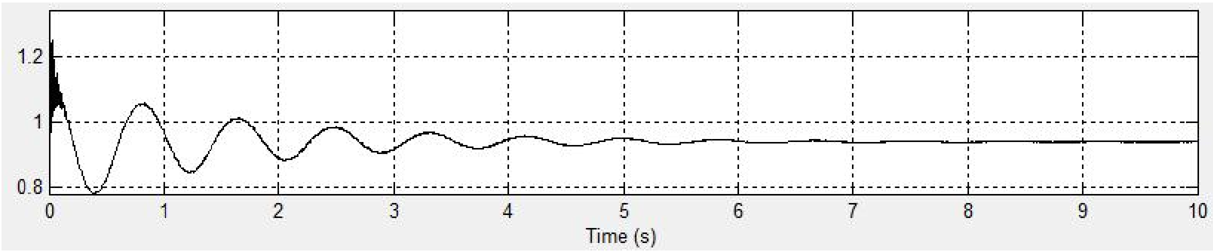

(a)

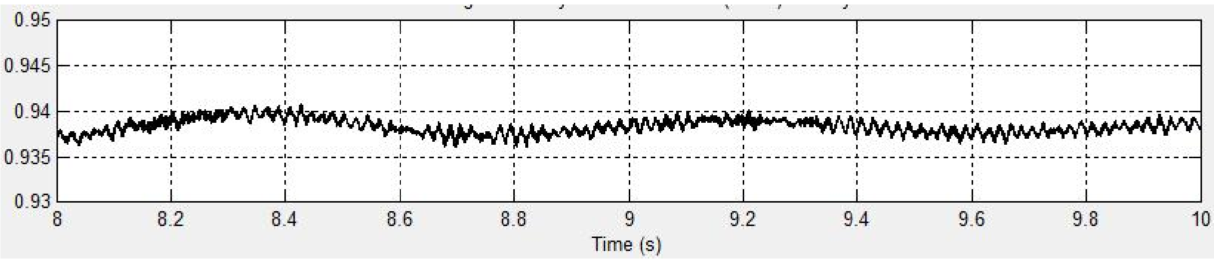

(b)

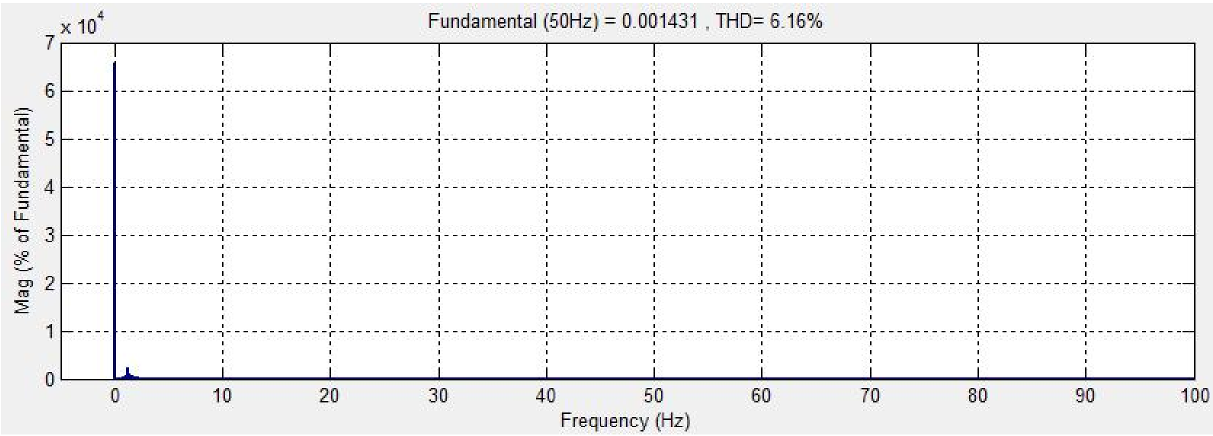

(c)

Figure 5.13 Air-gap torque without EAF in the system (a) electromagnetic torque T_e, (b) scaled T_e, (c) FFT of T_e

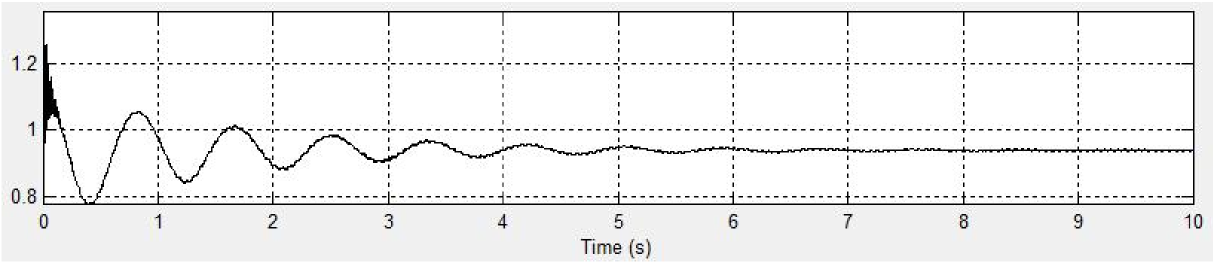

(a)

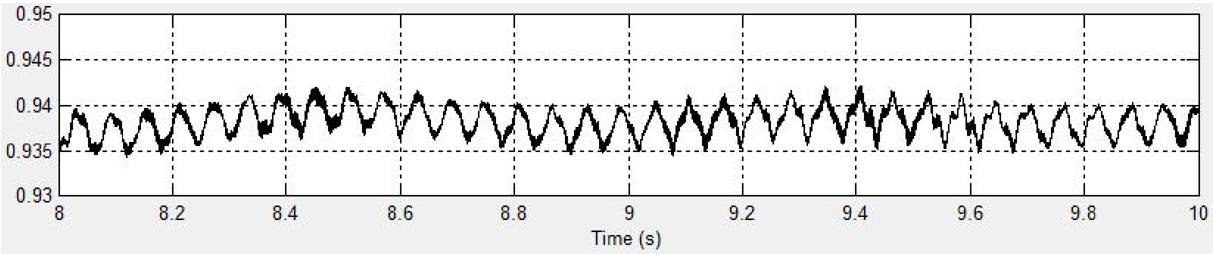

(b)

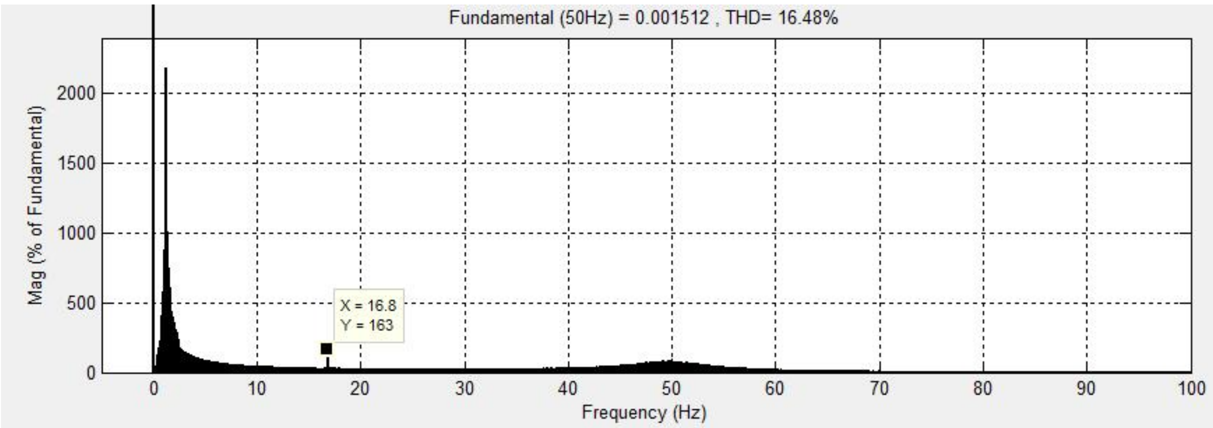

(c)

Figure 5.14 Air-gap torque with EAF in the system (a) electromagnetic torque T_e, (b) scaled T_e, (c) FFT of T_e

When there is an EAF in the system, the air gap torque is perturbed as shown in figure 5.14(b). In figure 5.13(b), we see that there is small variation of air-gap torque around its constant value. This may be the result due to small pulsation in mechanical input power. But from figure 5.14(b), we see that the variatoin of air-gap torque around its constant value is amplified. This amplification is the result of perturbation of *d*-and *q*-axis current component due to operation of EAF in the system. The EAF produces a sub-harmonic current of frequency 16.8 Hz which perturb the air-gap torque. The presence of 16.8 Hz signal component in the air-gap toruqe is shown in the FFT, figure 5.14(c).

5.4.5 Analysis of Torsional Torque Amplification

The perturbation of generator air-gap torque disturbs the generator rotor, and through which farther disturbs the turbine-generator-exciter mechanism. From the eigenvalue analysis in chapter 4, it is seen that the turbine-generator-exciter system usually has torsional modes in the subsynchronous frequency range. Thus, there is a possibility that the EAF-induced air-gap torque disturbance invades those torsional modes and lead to resonant excitations.

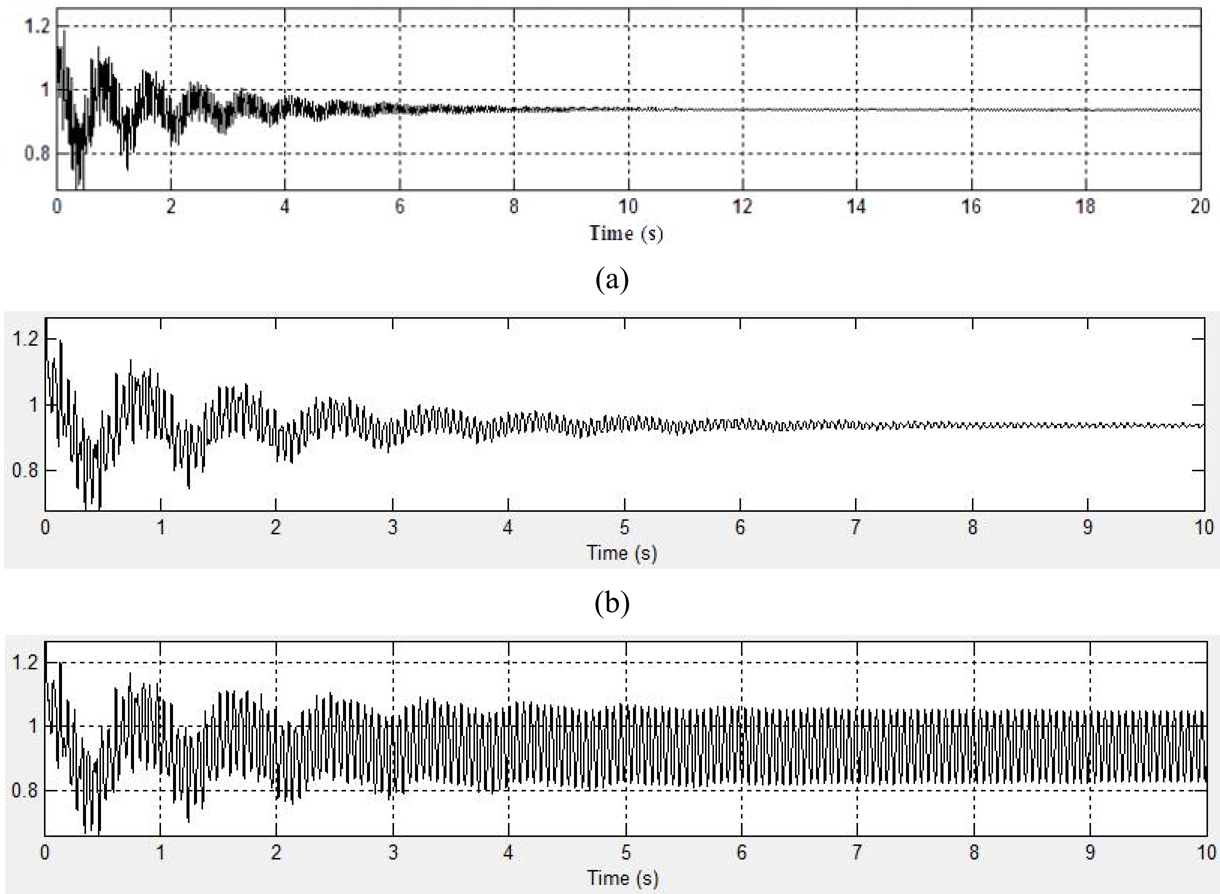

Figure 5.15 Torsional torque transmission between generator - LP_A section of turbine (a) without EAF, (b) with EAF but without resonance, (c) resonance with EAF

Figure 5.15 shows the torsional torque transmission between generator and LP_A section of the turbine where 5.15(a) represents the transmitted torque when there is no EAF in the system, 5.15(b) represents the transmitted torque when there is a EAF in the power system and 5.15(c) represents the resonant excitation of the transmitted torque. From figure 5.15(a), it is seen that the torsional torque reach to a steady value after 8 seconds of starting generator. When there is an EAF in the system, we see from figure 5.15(b), the transmitted torque reach to its steady value after 8 seconds. But if the EAF produce any frequency equal to torsional mode frequency or frequency close to torsional mode frequency, the torsional torques between generator and LP_A mass are amplified as shown in figure 5.15(c).

5.4.6 Quantification of Torsional Torque

The amplified torsional torques are quantified in Table 5.3. To quantify the torsional torque, the FFT of each torsional torque signal is performed. From the FFT, the torsional torques are measured. For comparison, a 16.8 Hz resonant condition is simulated. From the Table 5.3, it is seen that when the resonant excitation occurs, the torsional torque between generator and LP_A section of turbine is amplified by 4.57 times which is quite a big value.

Table 5.3:Excitation of torsional modes

Torque without EAF at 16.8 Hz modes	**Torque with EAF, without resonance at 16.8 Hz modes**	**Torque with EAF, with resonance at 16.8 Hz modes**	**Torque amplification**
0.02443	a = 0.02533	b = 0.11569	b/a = 4.57

The steady and torsional torques transmitted between different sections of turbine-generator masses are quantified from the FFT analysis of the the torque signals. Actually the torsional modes are variations of torsional torques around its steady value. Here $T_{(LPA\text{-}Gen)}$ represents torsional torque transmitted between generator and LP_A section of turbine section, $T_{(LPB\text{-}LPA)}$ represents torque transmitted between LP_A and LP_B of turbine section, $T_{(IP\text{-}LPB)}$ represents torque transmitted between LP_B an IP section, and $T_{(HP\text{-}IP)}$ represents torque transmitted between IP and HP section of turbine. Table 5.4 summerizes the torsional torques at the torsional mode frequencies when there is no EAF in the simulated network. Table 5.5 summerizes the torsional torques at the torsional mode frequencies when there is one EAF in the simulated network. The

EAF is assumed not to produce any frequency equal or closely equal to the torsional mode frequencies. Table 5.6 summerizes the torsional torques at resonant condition. In this case, the EAF is assumed to produce frequency 16.8 Hz which is equal to one torsional mode frquency.

Table 5.4: Torsional torque without EAF connected in the grid (single frequency test)

f(Hz) / Torque(pu)	0	1.2	16.8	24.9	31.3	45.4	50	THD%
$T_{(HP-IP)}$	0.26311	0.00115	0.00589	0.00504	0.00293	0.00033	$5.886x10^{-6}$	5.20
$T_{(IP-LPB)}$	0.48773	0.00333	0.01337	0.00792	0.00239	0.00047	$1.615x10^{-5}$	5.69
$T_{(LPB-LPA)}$	0.71418	0.01397	0.03299	0.00089	0.01126	0.00012	$5.213x10^{-5}$	4.35
$T_{(LPA-Gen)}$	0.93864	0.02508	0.02443	0.00826	0.00877	0.00021	$2.961x10^{-4}$	1.30

Table 5.5: Torsional torque with one EAF at PCC without resonance (single frequency test)

f(Hz) / Torque(pu)	0	1.2	16.8	24.9	31.3	45.4	50	THD%
$T_{(HP-IP)}$	0.26261	0.001156	0.006099	0.005215	0.003083	0.0003547	$6.179x10^{-6}$	5.60
$T_{(IP-LPB)}$	0.48931	0.003354	0.013867	0.008195	0.002524	0.0005083	$1.729x10^{-5}$	6.08
$T_{(LPB-LPA)}$	0.71382	0.014004	0.034165	0.000921	0.011824	0.0001248	$5.449x10^{-5}$	5.19
$T_{(LPA-Gen)}$	0.93856	0.025206	0.025332	0.008538	0.009197	0.0002226	$3.139x10^{-4}$	0.99

Table 5.6: Torsional torque with one EAF at PCC with resonance at 16.8 Hz

f(Hz) / Torque(pu)	0	1.2	16.8	24.9	31.3	45.4	50	THD%
$T_{(HP-IP)}$	0.2621	0.001129	0.027815	0.0052777	0.0031203	0.000342	$1.783x10^{-5}$	50.04
$T_{(IP-LPB)}$	0.48906	0.003260	0.063726	0.0083239	0.0018056	0.000504	$2.47x10^{-5}$	80.27
$T_{(LPB-LPA)}$	0.71374	0.013825	0.156236	0.0007003	0.0119144	0.000164	$1.124x10^{-4}$	42.17
$T_{(LPA-Gen)}$	0.93823	0.02501	0.115696	0.0085189	0.0093247	0.000158	$2.878x10^{-4}$	11.72

Torsional torques at resonant excitation (Table 5.6) is compared to torsional torques at non-resonant condition (Table 5.5) and summerized in Table 5.7. From Table 5.7, it is seen that as the 16.8 Hz torsional mode is excited, the torsional torques are amplified relating to this mode only. Others modes are not amplified. We see that the 16.8 Hz mode is amplifed on an average 4.57 times with respect to modes at non-resonant condition.

Table 5.7: Torsional torque amplification with one EAF at PCC and resonance at 16.8 Hz

Torque ratio between sections \ f (Hz)	0	1.2	16.8	24.9	31.3	45.4
HP-IP	0.998069	0.97672	4.560775	1.012004	1.011984	0.965235
IP-LP_B	0.999495	0.972006	4.595647	1.015667	0.715247	0.991246
LP_B-LP_A	0.999889	0.987232	4.572984	0.760369	1.007617	1.314936
LP_A-Gen	0.999645	0.992208	4.567172	0.997749	1.013857	0.711093

5.5 Torque due to Multiple Number of Frequencies Produced in EAF

As EAF produces subsynchronous frequencies in the range of 0-30 Hz, in this part of simulation, frequencies, as for example 10, 12, 18, 27, 35 and 40 Hz, are used to modulate the furnace arc resistance. The different conditions of resonant excitation are simulated, as for example 24.9 Hz frequency is used to modulate arc resistance, then the torsional torques are measured using the FFT technique. The combination of mode 0, mode 0 and 1, mode 0, 1 and 2, etc. are chosen for torsional resonance to simulate the network and their effects are observed. The measured values of torsional torques are summerized on Table 5.8 to Table 5.14.

Table 5.8: Torsional torques without EAF connected in the grid (multiple frequency test)

Torque(pu) \ f(Hz)	0	1.2	16.8	24.9	31.3	45.4	50	THD%
$T_{(HP-IP)}$	0.262665	0.001144	0.005837	0.0051015	0.002977	0.000325	5.837×10^{-6}	4.70
$T_{(IP-LPB)}$	0.48856	0.003325	0.013286	0.0080061	0.002427	0.000171	1.576×10^{-5}	6.20
$T_{(LPB-LPA)}$	0.711648	0.013936	0.032716	0.0009044	0.011416	0.000115	4.942×10^{-5}	5.88
$T_{(LPA-Gen)}$	0.940048	0.025077	0.024246	0.0083687	0.008885	0.000207	2.866×10^{-4}	1.25

Table 5.9: Torsional torque with one EAF at PCC without resonance (multiple frequency test)

f(Hz) / Torque(pu)	0	1.2	16.8	24.9	31.3	45.4	50	THD%
$T_{(HP-IP)}$	0.263203	0.0011607	0.00582	0.004926	0.00318	0.000368	9.139×10^{-6}	4.34
$T_{(IP-LPB)}$	0.488228	0.0033472	0.01324	0.007739	0.00260	0.000529	2.132×10^{-5}	3.22
$T_{(LPB-LPA)}$	0.714083	0.0140774	0.03260	0.000868	0.01226	0.000124	7.294×10^{-5}	2.19
$T_{(LPA-Gen)}$	0.940296	0.0252502	0.02419	0.008106	0.01025	0.000221	4.053×10^{-4}	1.05

Table 5.10: Torsional torque with one EAF at PCC and with resonance at 1.2 Hz

f(Hz) / Torque(pu)	0	1.2	16.8	24.9	31.3	45.4	50	THD%
$T_{(HP-IP)}$	0.263171	0.0014451	0.006695	0.005177	0.003076	0.000355	6.629×10^{-6}	3.98
$T_{(IP-LPB)}$	0.488376	0.0041861	0.015202	0.008115	0.002515	0.000509	1.836×10^{-5}	5.59
$T_{(LPB-LPA)}$	0.714	0.017593	0.037471	0.000903	0.011824	0.000125	5.712×10^{-5}	5.10
$T_{(LPA-Gen)}$	0.9403	0.031487	0.02774	0.008422	0.010145	0.000221	3.853×10^{-4}	2.56

Table 5.11: Torsional torque with one EAF at PCC and with resonance at 1.2 and 16.8 Hz

f(Hz) / Torque(pu)	0	1.2	16.8	24.9	31.3	45.4	50	THD%
$T_{(HP-IP)}$	0.26319	0.0014195	0.027338	0.005229	0.003006	0.000345	1.698×10^{-5}	49.25
$T_{(IP-LPB)}$	0.488565	0.0041102	0.062298	0.008220	0.002461	0.000496	2.585×10^{-5}	71.43
$T_{(LPB-LPA)}$	0.71355	0.0173595	0.15336	0.006879	0.011502	0.000172	1.065×10^{-4}	41.05
$T_{(LPA-Gen)}$	0.938499	0.0314871	0.113720	0.008407	0.008957	0.000165	3.057×10^{-4}	10.30

Table 5.12: Torsional torque with one EAF at PCC and with resonance at 1.2, 16.8 and 24.9 Hz

f(Hz) / Torque(pu)	0	1.2	16.8	24.9	31.3	45.4	50	THD%
$T_{(HP-IP)}$	0.262877	0.0014637	0.024307	0.034006	0.003519	0.000393	2.957×10^{-5}	77.04
$T_{(IP-LPB)}$	0.48813	0.0041737	0.055253	0.053345	0.002846	0.000582	7.95×10^{-5}	53.34
$T_{(LPB-LPA)}$	0.714322	0.0173754	0.136383	0.005861	0.013721	0.000199	1.379×10^{-5}	357.58
$T_{(LPA-Gen)}$	0.941127	0.0313709	0.101261	0.055197	0.010523	0.000227	3.971×10^{-4}	4.19

Table 5.13: Torsional torque with one EAF at PCC and with resonance at 1.2, 16.8, 24.9 and 31.3 Hz

f(Hz) / Torque(pu)	0	1.2	16.8	24.9	31.3	45.4	50	THD%
$T_{(HP\text{-}IP)}$	0.262275	0.0014122	0.027438	0.033894	0.023941	0.000353	1.345×10^{-5}	24.45
$T_{(IP\text{-}LPB)}$	0.489372	0.0041095	0.062426	0.053329	0.019544	0.000465	3.137×10^{-5}	13.06
$T_{(LPB\text{-}LPA)}$	0.711461	0.0173792	0.153697	0.005703	0.092327	0.000108	5.431×10^{-5}	6.31
$T_{(LPA\text{-}Gen)}$	0.94013	0.031461	0.11411	0.056017	0.077413	0.000211	3.241×10^{-4}	3.58

Table 5.14: Torsional torque with one EAF at PCC and with resonance at 1.2, 16.8, 24.9, 31.3 and 45.4 Hz

f(Hz) / Torque(pu)	0	1.2	16.8	24.9	31.3	45.4	50	THD%
$T_{(HP\text{-}IP)}$	0.262653	0.0014136	0.027125	0.033619	0.023782	0.005702	9.551×10^{-6}	26.63
$T_{(IP\text{-}LPB)}$	0.486794	0.0040953	0.061631	0.052699	0.019383	0.008173	4.466×10^{-5}	14.53
$T_{(LPB\text{-}LPA)}$	0.713376	0.0173885	0.151592	0.005648	0.091154	0.002041	4.954×10^{-5}	5.57
$T_{(LPA\text{-}Gen)}$	0.940102	.0312547	0.112222	0.055126	0.071123	0.003913	2.461×10^{-4}	37.14

Table 5.15: Torsional torque with one EAF at PCC (multiple frequency test)

Resonance Condition	f(Hz) / Torque ratio	0	1.2	16.8	24.9	31.3	45.4
Resonant at 1.2 Hz	**HP-IP**	0.999879	1.245094	1.150089	1.051022	0.967137	0.962937
	IP-LP_B	1.000303	1.250606	1.148218	1.048579	0.967044	0.961864
	LP_B-LP_A	0.999884	1.249729	1.149261	1.039759	0.964903	1.008829
	LP_A-Gen	1.000004	1.247004	1.146451	1.038983	0.989361	1.000028
Resonant at 1.2 and 16.8 Hz	**HP-IP**	0.99995	1.223043	4.695971	1.061698	0.945003	0.935901
	IP-LP_B	1.00069	1.227922	4.705424	1.06217	0.946129	0.938692
	LP_B-LP_A	0.999254	1.233145	4.703691	7.92628	0.938638	1.382805
	LP_A-Gen	0.998089	1.247004	4.699887	1.037102	0.873506	0.744586
Resonant at 1.2, 16.8 and 24.9 Hz	**HP-IP**	0.998762	1.261113	4.175274	6.903379	1.106421	1.067823
	IP-LP_B	0.999799	1.246923	4.173238	6.892802	1.094216	1.100625
	LP_B-LP_A	1.000335	1.234274	4.182994	6.752125	1.119727	1.612566
	LP_A-Gen	1.000884	1.242403	4.184939	6.809388	1.026239	1.026424

Resonance Condition	f(Hz) / Torque ratio	0	1.2	16.8	24.9	31.3	45.4
Resonant at 1.2, 16.8, 24.9 and 31.3 Hz	**HP-IP**	0.996473	1.216772	4.713183	6.880744	7.527736	0.956797
	IP-LP$_B$	1.002343	1.227719	4.715077	6.8908	7.513729	0.878087
	LP$_B$-LP$_A$	0.996329	1.234544	4.714037	6.569864	7.534487	0.867224
	LP$_A$-Gen	0.999823	1.245971	4.715989	6.91056	7.549475	0.950772
Resonant at 1.2, 16.8, 24.9, 31.3 and 45.4 Hz	**HP-IP**	0.997908	1.21789	4.65939	6.825022	7.477738	15.48173
	IP-LP$_B$	0.997063	1.223492	4.654993	6.809369	7.451804	15.4572
	LP$_B$-LP$_A$	0.99901	1.235208	4.649477	6.50651	7.43873	16.46033
	LP$_A$-Gen	0.999794	1.237801	4.637944	6.800691	6.936052	17.68233

Table 5.15 explain the torsional torque amplification due to resonant excitation of different modes. It is seen that if a mode is excited, the torques of the corresponding mode are amplified. It does not affect the torques corresponding to other modes. For example, if mode 2 is excited due to resonance, only the torques corresponding to mode 2 are amplified. The average torque due to resonant excitation of mode 1 is 4.55 times of its non-resonant torque, and that due to resonant excitation of mode 2 is 6.8 times of its non-resonant torque. The average torque due to resonant excitation of mode 3 is 7.4 times of its non-resonant torque, and that due to resonant excitation of mode 4 is 16.3 times of its non-resonant torque. So, it is deducible that if the higher mode is excited the torque amplification becomes higher.

5.6 Torque due to Operation of Two EAFs at PCC

The two EAFs are connected at the same PCC. The capacities and characteristics of the two EAFs are considered similar. Multiple number of modulating signals with frequencies 10, 12, 18, 27, 35 and 40 Hz are chosen to modualte the arc resistances for both the EAFs, i.e. the worst case condition is considered. In the simulation, to excite mode 1, 16.8 Hz frequency is used to vary arc resistances for both EAFs. To excite other modes, corresponding frequencies are produced in the furnaces. The different combinations of mode excitation and the measured torsional torques are summerized on Table 5.16 to Table 5.21.

Table 5.16: Torsional torque with two EAFs at PCC without resonance

f(Hz) / Torque(pu)	0	1.2	16.8	24.9	31.3	45.4	50	THD%
$T_{(HP-IP)}$	0.26334	0.001154	0.005702	0.0049104	0.003089	0.000391	1.98×10^{-5}	2.76
$T_{(IP-LPB)}$	0.486529	0.003324	0.012959	0.0077299	0.002528	0.000559	4.547×10^{-5}	1.17
$T_{(LPB-LPA)}$	0.714204	0.013911	0.032054	0.0008714	0.011872	0.000126	1.556×10^{-4}	3.55
$T_{(LPA-Gen)}$	0.941328	0.024928	0.023707	0.0080885	0.009239	0.000223	8.716×10^{-4}	1.23

Table 5.17: Torsional torque with two EAFs at PCC with resonance at 1.2 Hz

f(Hz) / Torque(pu)	0	1.2	16.8	24.9	31.3	45.4	50	THD%
$T_{(HP-IP)}$	0.262432	0.001690	0.003269	0.0013233	0.0026243	0.000044	1.112×10^{-5}	2.44
$T_{(IP-LPB)}$	0.489456	0.004923	0.007453	0.002083	0.0021442	0.000063	2.781×10^{-5}	1.73
$T_{(LPB-LPA)}$	0.713046	0.020701	0.018454	0.0002414	0.0101232	0.000112	1.756×10^{-4}	1.52
$T_{(LPA-Gen)}$	0.94004	0.037072	0.014630	0.0021118	0.006951	0.000243	3.31×10^{-4}	0.63

Table 5.18: Torsional torque with two EAFs at PCC with resonance at 1.2 and 16.8 Hz

f(Hz) / Torque(pu)	0	1.2	16.8	24.9	31.3	45.4	50	THD%
$T_{(HP-IP)}$	0.262876	0.001662	0.049151	0.0055175	0.0031266	0.000374	3.171×10^{-5}	59.05
$T_{(IP-LPB)}$	0.488432	0.004785	0.112036	0.0087200	0.0025829	0.000552	5.519×10^{-5}	75.31
$T_{(LPB-LPA)}$	0.712746	0.020261	0.276777	0.0006295	0.0118851	0.000241	1.809×10^{-4}	54.39
$T_{(LPA-Gen)}$	0.94024	0.036792	0.2044	0.0088476	0.009344	0.000112	2.92×10^{-4}	24.38

Table 5.19: Torsional torque with two EAFs at PCC with resonance at 1.2, 16.8 and 24.9 Hz

f(Hz) / Torque(pu)	0	1.2	16.8	24.9	31.3	45.4	50	THD%
$T_{(HP-IP)}$	0.26373	0.001676	0.049393	0.061239	0.0029726	0.000369	2.235×10^{-5}	66.89
$T_{(IP-LPB)}$	0.4859	0.004806	0.112243	0.0962082	0.0023761	0.000468	4.859×10^{-5}	25.28
$T_{(LPB-LPA)}$	0.713912	0.020131	0.277736	0.0106062	0.0117246	0.000252	1.864×10^{-4}	54.96
$T_{(LPA-Gen)}$	0.939676	0.036829	0.205266	0.100196	0.0093968	0.000013	2.708×10^{-4}	46.63

Table 5.20: Torsional torque with two EAFs at PCC with resonance at 1.2, 16.8, 24.9 and 31.3 Hz

f(Hz) / Torque(pu)	0	1.2	16.8	24.9	31.3	45.4	50	THD%
$T_{(HP-IP)}$	0.26381	0.001647	0.049329	0.061335	0.04959	0.000386	2.61×10^{-5}	28.23
$T_{(IP-LPB)}$	0.486512	0.004772	0.112272	0.0963668	0.0361142	0.000477	4.678×10^{-5}	17.93
$T_{(LPB-LPA)}$	0.715155	0.020365	0.275845	0.0102165	0.170275	0.000101	6.811×10^{-5}	24.67
$T_{(LPA-Gen)}$	0.939675	0.036562	0.204678	0.1004598	0.1322379	0.000155	3.417×10^{-4}	54.45

Table 5.21: Torsional torque with two EAFs at PCC with resonance at 1.2, 16.8, 24.9, 31.3 and 45.4 Hz

f(Hz) / Torque(pu)	0	1.2	16.8	24.9	31.3	45.4	50	THD%
$T_{(HP-IP)}$	0.26304	0.001642	0.049101	0.0611568	0.04384	0.010763	2.192×10^{-5}	20.58
$T_{(IP-LPB)}$	0.488074	0.004749	0.111887	0.096029	0.0357686	0.015418	8.81×10^{-5}	17.32
$T_{(LPB-LPA)}$	0.711833	0.020249	0.274367	0.0101592	0.1686284	0.003856	6.911×10^{-5}	22.78
$T_{(LPA-Gen)}$	0.938304	0.036489	0.203625	0.100021	0.1312974	0.007396	3.258×10^{-4}	57.10

Table 5.22: Torsional torque with two EAFs at PCC (multiple frequency test)

Resonance Condition	f(Hz) / Torque ratio	0	1.2	16.8	24.9	31.3	45.4
Resonant at 1.2 Hz	HP-IP	0.996552	1.464248	0.57332	0.269485	0.849624	0.111752
	$IP-LP_B$	1.006016	1.480921	0.575131	0.269469	0.848116	0.112875
	LP_B-LP_A	0.998379	1.488149	0.575723	0.277038	0.852678	0.893772
	LP_A-Gen	0.998632	1.487177	0.617112	0.261086	0.752357	1.090129
Resonant at 1.2 and 16.8 Hz	HP-IP	0.998238	1.439441	8.619266	1.123644	1.01224	0.959286
	$IP-LP_B$	1.00391	1.439584	8.64543	1.12809	1.02166	0.986803
	LP_B-LP_A	0.997959	1.456497	8.634818	0.722471	1.001082	1.916054
	LP_A-Gen	0.998844	1.475945	8.621737	1.093856	1.011369	0.503176
Resonant at 1.2, 16.8 and 24.9 Hz	HP-IP	1.001481	1.452128	8.661879	12.47129	0.962364	0.945431
	$IP-LP_B$	0.998707	1.445775	8.661419	12.44624	0.939845	0.837517
	LP_B-LP_A	0.999591	1.44718	8.664737	12.17196	0.987558	2.003998
	LP_A-Gen	0.998245	1.477421	8.658282	12.38754	1.01708	0.05606

Resonance Condition	f(Hz) / Torque ratio	0	1.2	16.8	24.9	31.3	45.4
Resonant at 1.2, 16.8, 24.9 and 31.3 Hz	**HP-IP**	1.001785	1.426711	8.650568	12.49084	16.05478	0.990309
	IP-LP_B	0.999965	1.435549	8.663665	12.46676	14.28492	0.85316
	LP_B-LP_A	1.001332	1.463979	8.605757	11.72478	14.34223	0.804339
	LP_A-Gen	0.998244	1.466714	8.633476	12.42015	14.31307	0.694898
Resonant at 1.2, 16.8, 24.9, 31.3 and 45.4 Hz	**HP-IP**	0.998861	1.422293	8.610585	12.45455	14.19321	27.59247
	IP-LP_B	1.003176	1.428638	8.633956	12.42306	14.14823	27.56664
	LP_B-LP_A	0.99668	1.455665	8.559622	11.65898	14.20354	30.71091
	LP_A-Gen	0.996788	1.463814	8.589047	12.3659	14.21127	33.27481

From Table 5.22, it is seen that the average torsional torque due to resonant excitation of mode 1 is 8.63 times of its non-resonant torsional torques. The average torsional torque due to resonant excitation of mode 2 is 12.3 times of its non-resonant torsional torques. For mode 3 it is 14.5 and for mode 4 it is 29.8. The torque amplifications due one EAF at PCC are compared with torque amplifications due to operation of multiple EAFs at the same PCC in the Table 5.23.

Table 5.23: Comparison of torque amplification

Mode	One EAF	Two EAFs	Three EAFs	Four EAFs	Five EAFs
0	1.24	1.46	1.64	1.83	2.01
1	4.55	8.63	12.42	15.86	19.48
2	6.8	12.3	17.04	22.1	26.71
3	7.4	14.5	19.65	24.61	29.82
4	16.3	29.8	41.46	50.08	58.98

From the Table 5.23, it is seen that the torsional torque amplification, due to resonant excitation of two EAFs at same PCC, is almost double to that due to resonant excitation of one EAF at the PCC. As the number of EAFs increase at the PCC there cause increased amplification of torsional oscillating torques at turbine-generator shaft.

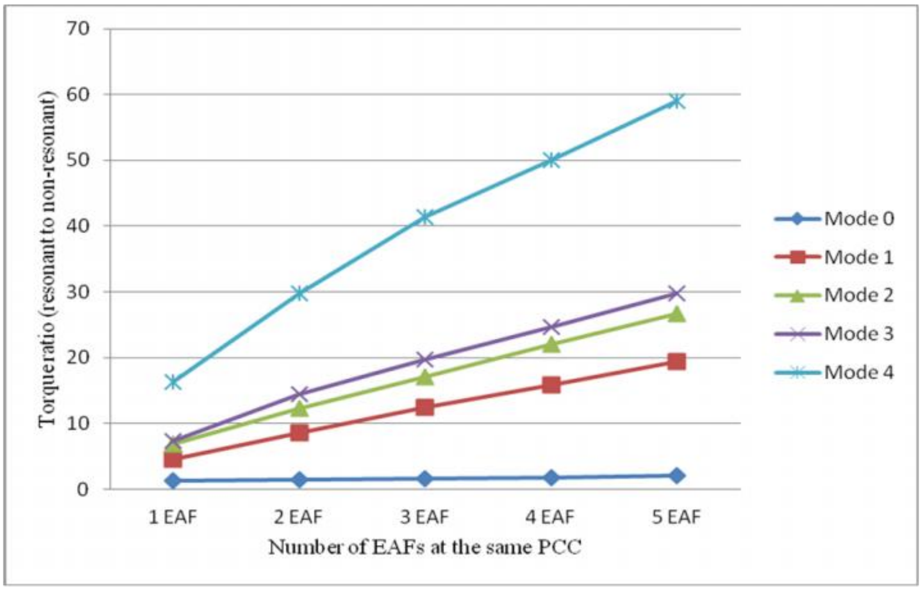

Figure 5.16 Torque ratio (resonant to nonresonant) due to multiple EAFs at the same PCC

From the graphs shown in figure 5.16, a set of polynomial equations can be obtained. The equations correlate between torque ratio and number of EAFs. The equations for different modes are as follows:

$$T_{ratio(m4)} = 0.1767N^3_{eaf} - 2.4643N^2_{eaf} + 19.979N_{eaf} - 1.456 \quad (5.1)$$

$$T_{ratio(m3)} = 0.1833N^3_{eaf} - 1.9336N^2_{eaf} + 11.523N_{eaf} - 2.354 \quad (5.2)$$

$$T_{ratio(m2)} = 0.0258N^3_{eaf} - 0.3368N^2_{eaf} + 6.1974N_{eaf} + 0.94 \quad (5.3)$$

$$T_{ratio(m1)} = 0.039N^3_{eaf} - 0.4432N^2_{eaf} + 5.1776N_{eaf} - 0.232 \quad (5.4)$$

$$T_{ratio(m0)} = 0.0025N^3_{eaf} - 0.0275N^2_{eaf} + 0.28N_{eaf} + 0.986 \quad (5.5)$$

where $T_{ratio(mk)} = b/a$; b = torque per unit in resonant condition and a = torque per unit in non-resonant condition. k = 0 to 4 for different modes. N_{eaf} = number of EAFs connected to the same PCC. These equations are developed using the torque ratio data from Table 5.23 therefore, the constant coefficients in the equations may become different for different system because the physical parameters for different network components are different. From the trends of the graph in figure 5.16, the torque ratio of a torsional mode due to operation of any number of EAF at the same PCC can be approximated. For example, if N_{eaf} = 8, then the torque ratio corresponding to mode 3 can be calculated using equation (5.2) as follows:

$$
\begin{aligned}
T_{ratio(m3)} &= 0.1833N^3{}_{eaf} - 1.9336N^2{}_{eaf} + 11.523N_{eaf} - 2.354 \\
&= 0.1833 \times 8^3 - 1.9336 \times 8^2 + 11.523 \times 8 - 2.354 \\
&= 59.97
\end{aligned}
$$

This value indicates that mode 3 will be amplified by 59.97 times of its non-resonant torsional oscillating torque if 8 EAFs are connected to the same PCC and mode 3 is excited.

From the analysis, it is deducible that the more the EAFs added to the same PCC and if resonant excitation occurs, the larger the amplitude of oscillation of torsional torque occurs.

5.7 Torque due to Change in Location of EAF

A simulation is performed to check the impact of EAF on generator shaft due to variation of location of EAF in the power grid. In this case, the distances between generator to PCC and PCC to infinite bus are considered 10 km, and 70 km which are kept fixed. The distances between PCC to EAF are chosen as 8, 24, 48, 72 km etc. The physical parameters of the component in the network and network structure are considered same as before. The same subsynchronous frequencies 10, 12, 18, 27, 35, 40 Hz are considered to be produced from EAF and non-resonant torsional torques between mass sections of the turbine-generator shaft are measured. Then the torsional mode frequencies 1.2, 16.8, 24.9, 31.3 and 45.4 Hz are produced from the EAF, the amplified torsional torques are measured and compared to its non-resonant torsional torques. The measured torsional torques at different conditions are given in Table 5.24 to 5.28. Table 5.29 shows the amplified torsional torques at different conditions.

Table 5.24: Non-resonant torsional torques at 8 km distance between PCC to EAF

f (Hz) / Torque (pu)	**0**	**1.2**	**16.8**	**24.9**	**31.3**	**45.4**
$T_{(HP\text{-}IP)}$	2.63E-01	5.38E-04	7.85E-03	5.25E-03	2.87E-03	3.72E-04
$T_{(IP\text{-}LPB)}$	4.89E-01	1.48E-03	1.79E-02	8.27E-03	2.34E-03	5.31E-04
$T_{(LPB\text{-}LPA)}$	7.15E-01	6.07E-03	4.39E-02	8.97E-04	1.10E-02	1.21E-04
$T_{(LPA\text{-}Gen)}$	9.41E-01	1.09E-02	3.27E-02	8.68E-03	8.60E-03	2.15E-04

Table 5.25: Resonant torsional torques at 8 km distance between PCC to EAF

f (Hz) / Torque (pu)	**0**	**1.2**	**16.8**	**24.9**	**31.3**	**45.4**
$T_{(HP-IP)}$	2.63E-01	1.10E-03	1.08E-01	1.17E-01	8.30E-02	1.36E-02
$T_{(IP-LPB)}$	4.90E-01	3.08E-03	2.46E-01	1.84E-01	6.79E-02	1.94E-02
$T_{(LPB-LPA)}$	7.14E-01	1.29E-02	6.07E-01	1.92E-02	3.21E-01	4.96E-03
$T_{(LPA-Gen)}$	9.39E-01	2.32E-02	4.50E-01	1.92E-01	2.49E-01	8.88E-03

Table 5.26: Resonant torsional torques at 24 km distance between PCC to EAF

f (Hz) / Torque (pu)	**0**	**1.2**	**16.8**	**24.9**	**31.3**	**45.4**
$T_{(HP-IP)}$	2.63E-01	8.30E-04	6.17E-02	6.62E-02	4.65E-02	7.46E-03
$T_{(IP-LPB)}$	4.89E-01	2.32E-03	1.40E-01	1.04E-01	3.80E-02	1.07E-02
$T_{(LPB-LPA)}$	7.15E-01	9.66E-03	3.47E-01	1.09E-02	1.80E-01	2.72E-03
$T_{(LPA-Gen)}$	9.41E-01	1.74E-02	2.57E-01	1.08E-01	1.39E-01	4.86E-03

Table 5.27: Resonant torsional torques at 48 km distance between PCC to EAF

f (Hz) / Torque (pu)	**0**	**1.2**	**16.8**	**24.9**	**31.3**	**45.4**
$T_{(HP-IP)}$	2.64E-01	6.94E-04	3.93E-02	4.13E-02	2.86E-02	4.54E-03
$T_{(IP-LPB)}$	4.89E-01	1.94E-03	8.93E-02	6.46E-02	2.35E-02	6.46E-03
$T_{(LPB-LPA)}$	7.14E-01	8.02E-03	2.20E-01	6.80E-03	1.11E-01	1.65E-03
$T_{(LPA-Gen)}$	9.39E-01	1.44E-02	1.64E-01	6.76E-02	8.58E-02	2.94E-03

Table 5.28: Resonant torsional torques at 72 km distance between PCC to EAF

f (Hz) / Torque (pu)	**0**	**1.2**	**16.8**	**24.9**	**31.3**	**45.4**
$T_{(HP-IP)}$	2.63E-01	6.36E-04	2.97E-02	3.07E-02	2.11E-02	3.31E-03
$T_{(IP-LPB)}$	4.88E-01	1.78E-03	6.75E-02	4.79E-02	1.73E-02	4.75E-03
$T_{(LPB-LPA)}$	7.14E-01	7.34E-03	1.67E-01	5.04E-03	8.13E-02	1.20E-03
$T_{(LPA-Gen)}$	9.41E-01	1.32E-02	1.24E-01	5.00E-02	6.32E-02	2.15E-03

Table 5.29: Torsional torque at resonance with distance variation between EAF and PCC

Distance between PCC and EAF	f(Hz) / Torque ratio	0	1.2	16.8	24.9	31.3	45.4
8 km	HP-IP	1.003207	2.043296	13.79139	22.30513	28.96957	36.5161
	IP-LP_B	1.002827	2.078284	13.78231	22.29229	29.06974	36.55865
	LP_B-LP_A	0.998912	2.121402	13.81866	21.41836	29.19436	41.10653
	LP_A-Gen	0.998613	2.138518	13.78242	22.16457	28.93984	41.23327
24 km	HP-IP	1.002609	1.542244	7.854058	12.6095	16.22731	20.05941
	IP-LP_B	1.000033	1.569416	7.854871	12.57379	16.28118	20.07923
	LP_B-LP_A	0.999673	1.592115	7.892308	12.10952	16.35976	22.57272
	LP_A-Gen	1.000191	1.60165	7.85463	12.47738	16.18795	22.57228
48 km	HP-IP	1.00585	1.288447	5.004761	7.870201	9.98758	12.19486
	IP-LP_B	1.00022	1.308948	4.999737	7.809067	10.05841	12.16279
	LP_B-LP_A	0.999147	1.321524	5.013974	7.578154	10.07374	13.67278
	LP_A-Gen	0.998835	1.328446	5.00531	7.785756	9.976864	13.66486
72 km	HP-IP	1.001988	1.181455	3.780764	5.839808	7.3766	8.895311
	IP-LP_B	0.99766	1.199303	3.780605	5.794487	7.40494	8.946564
	LP_B-LP_A	0.999372	1.209276	3.798639	5.6208	7.405259	9.956417
	LP_A-Gen	1.000686	1.213721	3.783822	5.767311	7.347778	10.0024

Table 5.30: Average torque due to distance variation between EAF and PCC

Distance / Torsional Modes	8 km	24 km	48 km	72 km
Mode 0	2.1	1.58	1.31	1.2
Mode 1	13.79	7.86	5.01	3.79
Mode 2	22.05	12.44	7.76	5.76
Mode 3	29.04	16.26	10.02	7.38
Mode 4	38.85	21.32	12.92	9.45

The amplified torsional torques at different modes at different distances between EAF and PCC are compared in Table 5.30. From Table 5.30, it is seen that as the distance between EAF and PCC is increasing, the torsional torques are decreasing.

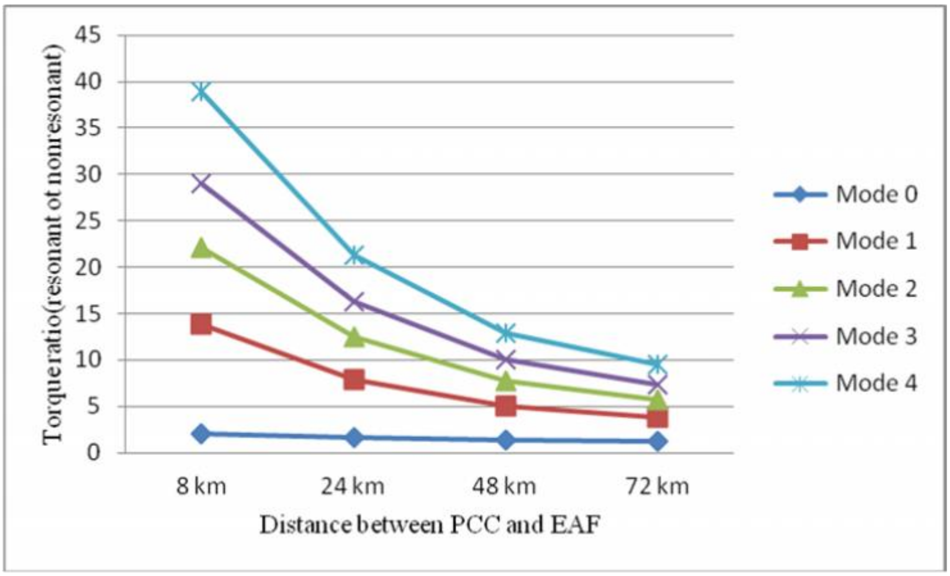

Figure 5.17 Torque ratio (resonant to non-resonant condition) due to different distances between PCC and EAF

Figure 5.17 shows the trend of decreasing torsional torques of different modes. It is seen that the rates of decrease of torque ratio are different for different modes. The higher modes of oscillation decreases at a higher rate upto 48 km distance then the decreasing rates become almost similar for the modes 1 to 4. There is very insignificant change in torsional torque ratio of system mode (mode 0) which also proves that system mode is almost undisturbed by the frequencies produced in the electrical network.

From the analysis, it is assessed that greater the distance between generator and EAF, lesser the impact of EAF operation on the turbine-generator shaft. Placing EAF at larger distance from generator do not eliminate the impact but it may be less harmful for the fatigue life of the turbine-generator shaft. It requires metallurgical test of the shaft whether the existing amplified torsional torques are harmful for it or not.

CHAPTER 6

TORSIONAL MODE AMPLIFICATION IN BPS

6.1 Introduction

The impact of steel mills loads on power generating unit was analysed for a test system in chapter 5. In the simulation of the test system, an worse case condition was considered, that is, if a torsional resonance occurred, it sustained for 10 seconds and all the simulations were performed for 10 seconds. But the resonance may not sustain for 10 seconds, it may be longer or lesser. The duration of resonance is totally unpredictable, it depends on characteristics of the EAF, its control systems and perhaps on duration of scraps melting cycle. However, perhaps the amplification of Torsional oscillating torques between mass sections of turbine-generator shaft do not depend on duratoin of resonance, it depends on occurance of resonance. When I am going to assess the impact of steel mills loads on generating units in Bangladesh Power System (BPS)-Chittagong region, the 10 second duration of resonance is considered. Because it helps to compare the results obtained from simulation of BPS-Chittagong region to the results obtained from the simulation of the test system. There are many steel industries in Chittagong region and many of them are using EAFs to produce good quality and large quantity of steel. But impact of steel mills loads on generating units in BPS has not yet been investigated which is the main focus of this thesis.

In this work, the Chittagong region of the BPS with a number of steel mills using EAFs is modeled and simulated. The Chattagong region of BPS is modeled with all the large power plants in the region included and the national grid as an equivalent generation at the Comilla-North bus. Impact of simultaneous operation of multiple EAFs on all the large power plants in the region is investigated.

6.2 Steel Mills in Chittagong

There are many steel mills in Chittagong region listed in Table 6.1 with their electrical load capacity and type of furnace. All these mills are not using EAFs. From the Table 6.1, it is seen that four steel mills are using EAFs and three of them are in chittagong region. Among the steel mills in Chittagong region, BSRM and MKSBSL are using AC EAFs where Abul Khair is using DC EAF. To see the impacts on turbine-generator shaft due to operation of EAFs, two AC EAFs in Chittagong region are modeled in the simulation.

Table 6.1: List of steel mills in Chittagong region.

Name	Bus	Bus	oltage level at PCC (kV)	Furnace type	Furnace load (MW)
steel	aulia	bir Steel	132	uction + ladle	33
alpur	aulia		132	uction	10
him steel	ripur		132	uction + Arc	22+24
RM	milla- N	hazari	230	F + Ladle	87+19
SBSL	ulia	ulshi	132	F + Ladle	13.6
ul Khair	milla- N	hazari	230	EAF + Ladle	140 + 24
dern	ulia	ulshi	132	uction	30
en circle	orashal		132	uction + Ladle	30

6.3 Description of Application Area of BPS

Figure 6.1 shows the 230kV (Red solid line) and 132kV (Blue solid line) power grid of BPS at Chittagong region. In this region, there are three large power stations named Kaptai Hydro Power Plants, Raozan Steam Turbine Power Plants and Sikalbaha Steam and Gas Turbine Power Plants. There are two generating units at Raozan with total power capacaity of 420 MW, two generating units at Sikalbaha of capacity 88 MW, and five generating units at Kaptai with total capacity of 230 MW. There are three voltage regulating transformers which connect 230 kV and 132 kV buses at Hathazari substation. The rating of each transformer is 100 MVA, 230 kV-Y/Y-132 kV, and its positve sequence impedance is 0.0015+j0.0644 (pu). The voltage regulating transformer at Comilla North has the same rating as of Hathazari, and its positive sequence impedance is 0.001+j0.043 (pu). The rating of the fixed tapped step-up transformers at Kaptai is 100 MVA, 11 kV-D/Y-132 kV each, and its impedance is 0.0002+j0.1505 pu each. The rating of the fixed tapped step-up transformers at Sikalbaha is 100 MVA, 11 kV-Yg/D-132 kV each, and its impedance is 0.0001+j0.1429 pu each. The rating of the fixed tapped step-up transformers at Raozan is 100 MVA, 15.75 kV-D/Yg-230 kV each, and its impedance is $7e^{-5}$+j0.0667 pu each. The other transformers are fixed tapped step-down of rating 100 MVA 132 kV-D/Yg-33 kV with different impedance rating obtained from data provided by PGCB.

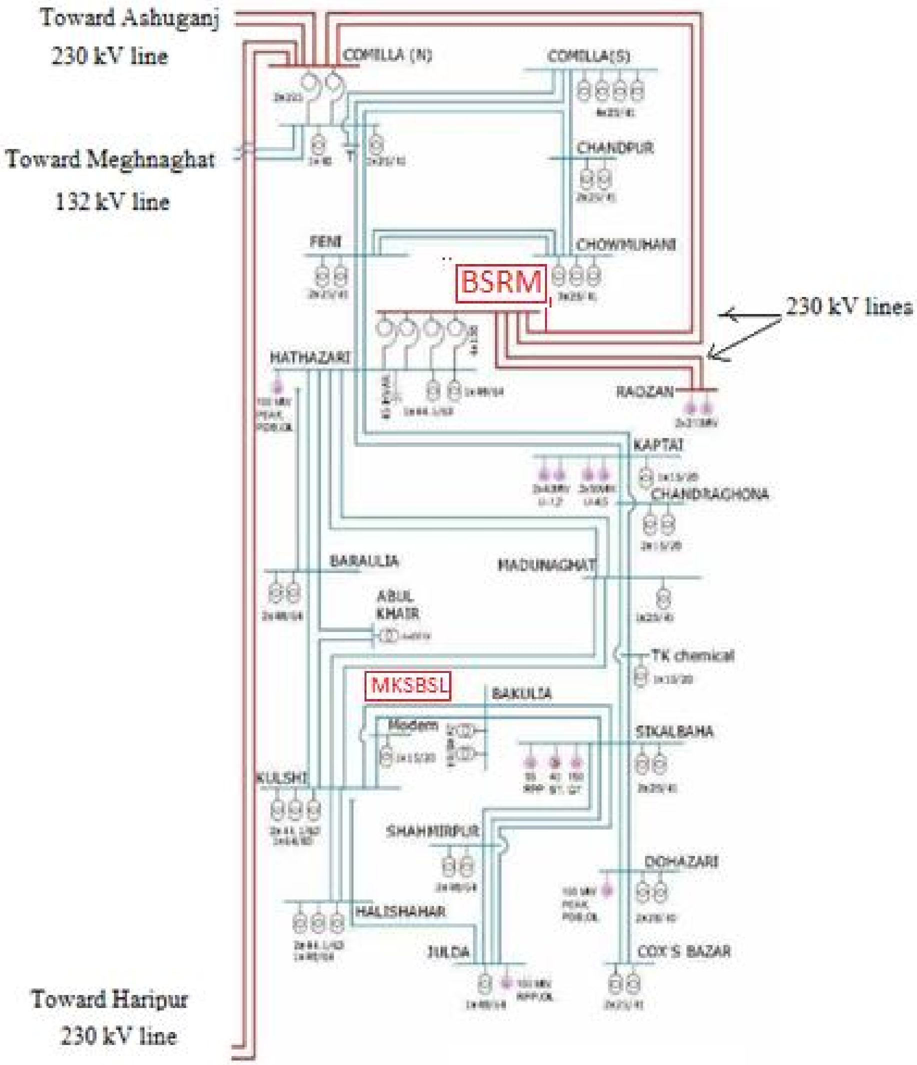

Figure 6.1 230 kV and 132 kV power grid of BPS in the Chittagong region [45]

For simulating the power system (BPS-Chittagong region), the following assumptions /simplification are used.

- Generating units at Raozan plant have been considered as a single unit with a total capacity of 420 MW.
- Two units at Sikalbaha, one is steam turbine and another one is gas turbine generating unit, have been considered as a steam turbine generating unit of power capacity 88 MW.
- Five units at Kaptai Hydro power plant have also been considered as one equivalent unit of electrical power capacity of 230 MW.

- The physical parameters such as *H*, *K* and *D* of the turbine-generating units are not available. These values are used from different sources and IEEE(R) benchmark for subsynchronous resonance study [43-44]. The parameters *H*, *K*, and *D* for steam-turbine generating units at Raozan and Sikalbaha are given in Table 6.2.
- Some constants are also used directly from research journal and IEEE(R) benchmark for subsynchronous resonance study [43-44]. The constants are given in Table B-1 to B-3, Appendix B.
- Five stages such as HP, IP, LP_B, LP_A and generator, are considered for generating units at Raozan and Sikalbaha.
- Fixed excitation is considered for steam turbine generating units and controlled excitation is considered for hydro-turbine generating units.

Table 6.2: Mechanical Data for Raozan and Sikalbaha generating units

Mass	***H*** **(MW.s/MVA)**	***K*** **(pu torque/elect.rad)**	***D*** **pu torque/pu speed deviation)**
neraotor	0.8	-	-
A	1.116	51.92	2.4832
B	1.081	63	0.40
	0.217	40.33	0.40
	0.117	18.17	0.32

The generator electrical parameters are given in Tables 6.3 to 6.5. The transmission line data are given in Table 6.6. These data are provided by BPDB and PGCB.

Table 6.3: Generator Data for Raozan Plant

Parameters	**Value (PU)**	**Parameters**	**Value**
Xd	1.83	*Xl*	0.1 pu
Xd'	0.219	R_a	0.003 pu
Xd''	0.133	*Tdo'*	5.5 s
Xq	1.65	*Tdo''*	0.163 s
Xq'	0.197	*Tqo'*	0.849 s
Xq''	0.12	*Tqo''*	0.016 s
Rotor type	round rotor	No. of Pole	2

Table 6.4: Generator Data for Sikalbaha Plant

Parameters	Value (PU)	Parameters	Value
Xd	1.94	*Xl*	0.1 pu
Xd'	0.219	R_a	0.003 pu
Xd''	0.128	*Tdo'*	4.5 s
Xq	1.94	*Tdo''*	0.05 s
Xq'	0.27	*Tqo'*	1.041 s
Xq''	0.128	*Tqo''*	0.03 s
Rotor type	round rotor	No. of Pole	2

Table 6.5: Generator Data for Kaptai Plant

Parameters	Value (PU)	Parameters	Value
Xd	1.25	*Xl*	0.1 pu
Xd'	0.35	R_a	0.0045 pu
Xd''	0.26	*Td'*	1.33 s
Xq	0.535	*Td''*	0.03 s
Xq'		*Tqo'*	
Xq''	0.21	*Tqo''*	0.3 s
Rotor	salient pole	No. of pole	44
Inertia constant H(MW-s/MVA)		3.86	

Table 6.6: Line impedance data

Line	Positive sequence components			Zero sequence components		
	***R*(Ω/km)**	***L*(H/km)**	***C*(F/km)**	***R*(Ω/km)**	***L*(H/km)**	***C*(F/km)**
230 kV	milla-North to Hathazari substation					
	0.01917	0.000422	3.669e-8	0.04356	0.000821	2.175e-7
	ɔzan power plant to Hathazari substation					
	0.01742	0.000316	3.683e-8	0.10977	0.00115975	1.947e-8
132 kV	0.10106	0.00131	1.333e-8	0.3781	0.00393427	8.964e-9

6.4 Torsional Mode Frequencies of Turbine-Generator Shaft

The simulated power system at Chittagong region has three equivalent generators as described before. So, calculation of torsional mode frequencies of the turbine-generator shaft using eigenvalue analysis becomes cumbersome. To ease the calculation complexity, FFT analysis of the torsional torque signal is used. Figures 6.2 to 6.3 show the FFTs of torsional torque signals between generator-LP_A and LP_B-IP sections, respectively. From both the figures, it is seen that the torsional mode frequencies are 14, 20.7, 26.1 and 37.9 Hz.

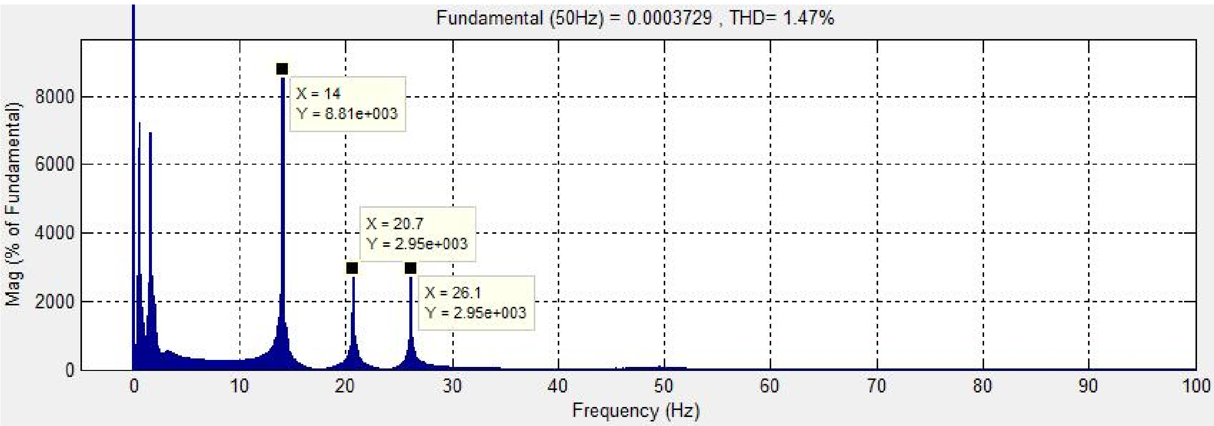

Figure 6.2 FFT of torsional torque between generator and LP_A section in Raozan plant

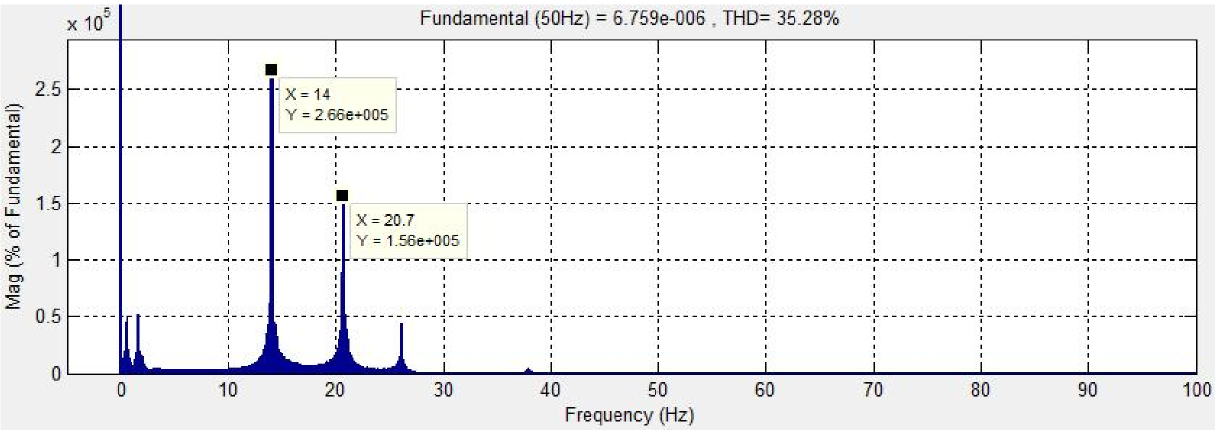

Figure 6.3 FFT of torsional torque between LP_B and IP section in Raozan plant

6.5 Analysis of Simulation Output

Among the two steel mills using AC EAFs, BSRM is connected near Hathazari electric grid sub-station and MKSBSL is connected at modern as shown in BPS-Chittagong region power grid. BSRM is near Raozan Power Plant and MKSBSL is near Sikalbaha Power Plant. The electric load capacity of BSRM is 87 MW and of MKSBSL is aprroximately 13.6 MW. The modelings of EAFs are similar to EAFs in test system. As the torsional mode frequencies are 14, 20.7, 26.1 and 37.9 Hz, the EAFs are considered to produce frequencies equal to frquencies of torsional modes other than 37.9 Hz. The worst case condition of torsional resonance is considered by producing all frequencies from EAFs equal to frquencies of transmitted oscillating torque between different mass sections of the turbine-generator shaft. Then, the impact of those steel mills loads on generating units at Raozan power plant and Sikalbaha power plant is investigated.

There are only two masses in hydro-turbine-generator shaft, one is turbine and another is generator. So torque oscillation occur only between them. This torsional torque is not investigated derectly but the change in air-gap torque is investigated.

6.5.1 Analysis of dq0 Current Components

Figure 6.4 shows the d-and q-axis current waveforms of generating unit at Raozan power plant. From figure 6.4(b) and (d), it is seen that when there are no EAFs connencted in the power grid, there are no dominating frequency other than zero frequency. It was expected as dq-axis current components become constant if there is no super/sub-harmonic or super/subsynchronous frequency signals in the stator currents.

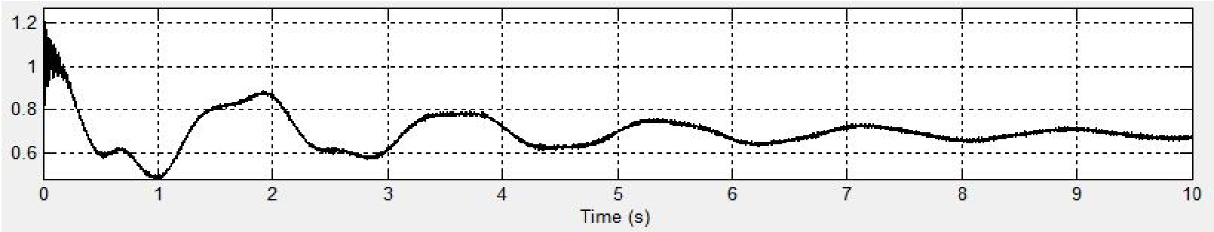

(a)

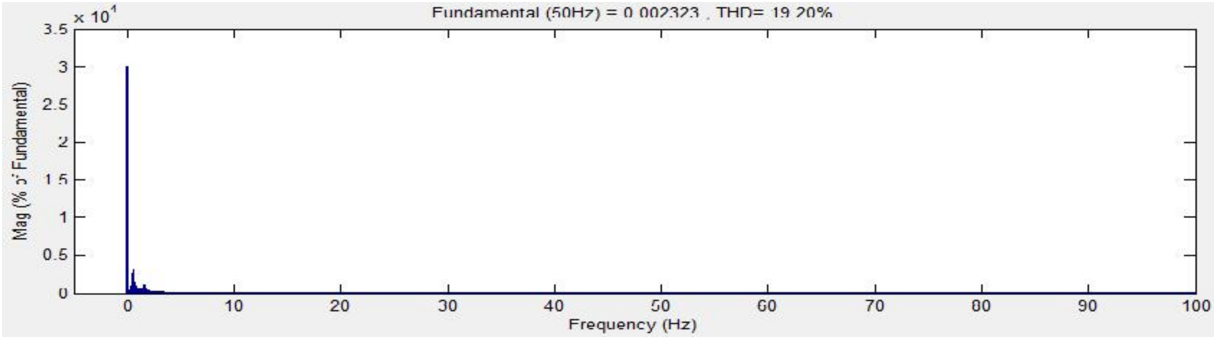

(b)

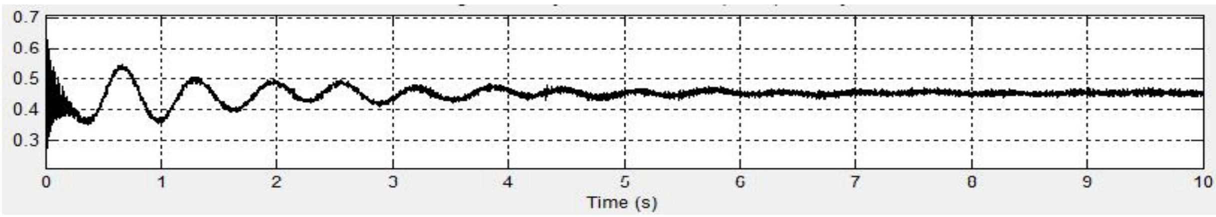

(c)

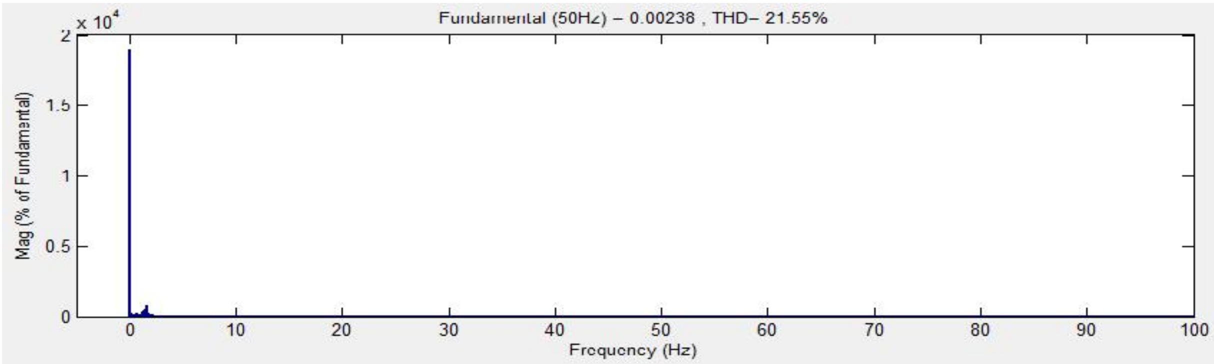

(d)

Figure 6.4 *d*-and *q*-axis current componets at Raozan generating unit withour EAF in the system (a) *d*-axis currnet i_d, (b) FFT of currnet i_d, (c) *q*-axis currnet i_q, (d) FFT of currnet i_q

Figure 6.5 shows the *dq*-axis current components when there are EAFs connected in the power grid. The EAFs are considered as source of three frequencies such as 14, 20.7 and 26.1 Hz. It is expected that those frequencies would be present in the figure 6.5(b) and (d) which show the FFT of *dq*-axis current waveforms. Although those frquencies are not dominating in *d*-axis current, they are more dominating in *q*-axis current as shown in figure 6.5(d)

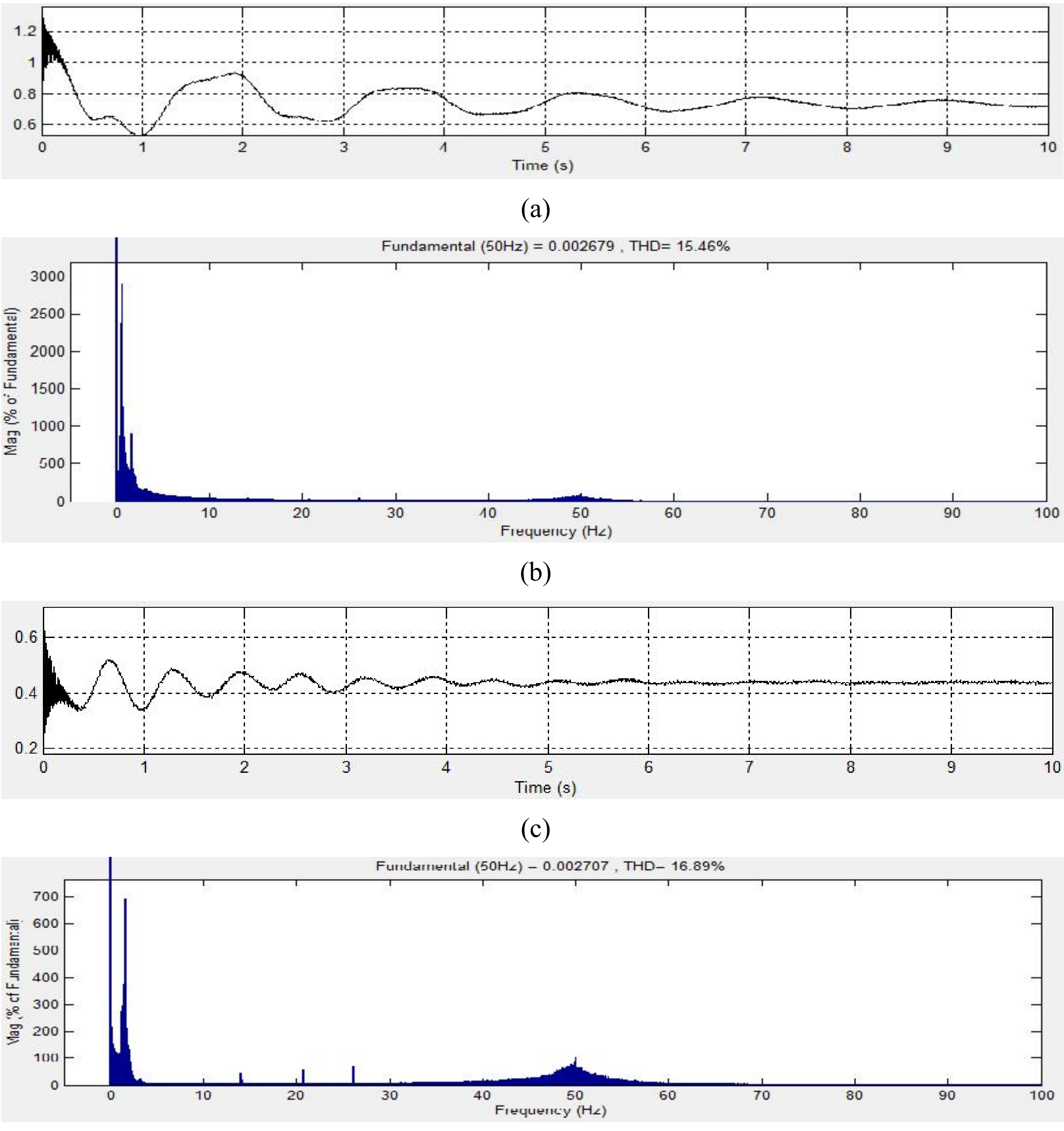

Figure 6.5 *d*-and *q*-axis current components at Raozan generating unit with EAF in the system (a) d-axis current i_d, (b) FFT of current i_d, (c) q-axis current i_q, (d) FFT of current i_q

6.5.2 Analysis of Electromagnetic Torque

Previously, it has been shown that the electromagnetic torque of synchronous generator is perturbed if the stator currents contain signals of frquency in the subsynchrous range. Because of the operatoin of EAFs, their feeders are spreading signals of subsynchronous frequencies, which cause amplification of torsional oscillating torques.

Figure 6.6 shows the air gap torque when there is no EAF in the system. It is seen that after 6 seconds of starting the generator, the torque become constant. It is also seen from FFT of air-gap torque in figure 6.6(b) that there is no other frquency component as dominant.

When there are EAFs in the system, the air gap tourque is perturbed. The EAF produces signals of subsynchronous frequencies such as 14, 20.7, 26.1 Hz which perturb the air-gap torque. The presence of those frequencies in the air-gap toruqe is shown in the FFT, figure 6.7(b).

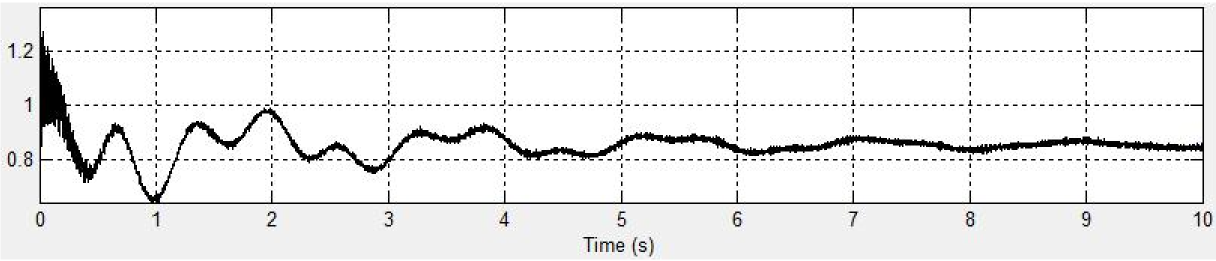

(a)

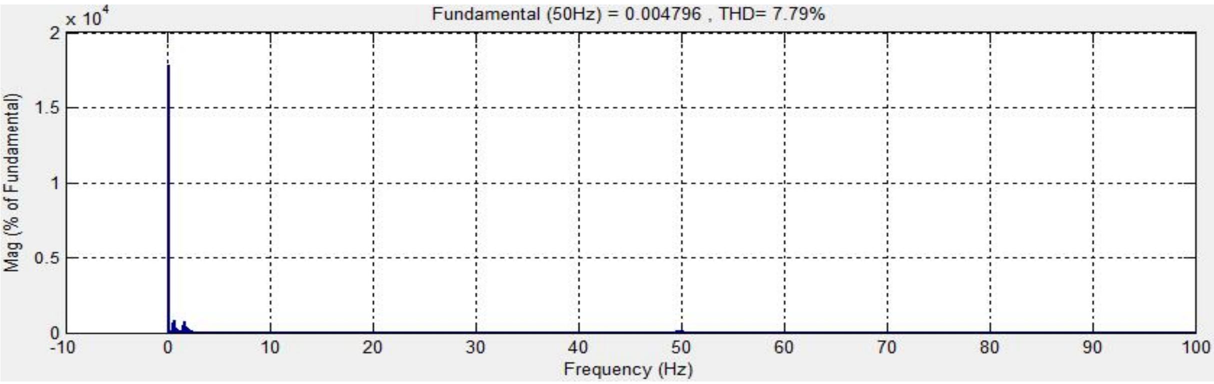

(b)

Figure 6.6 Air-gap torque without EAF in the system (a) torque T_e, (b) FFT of T_e

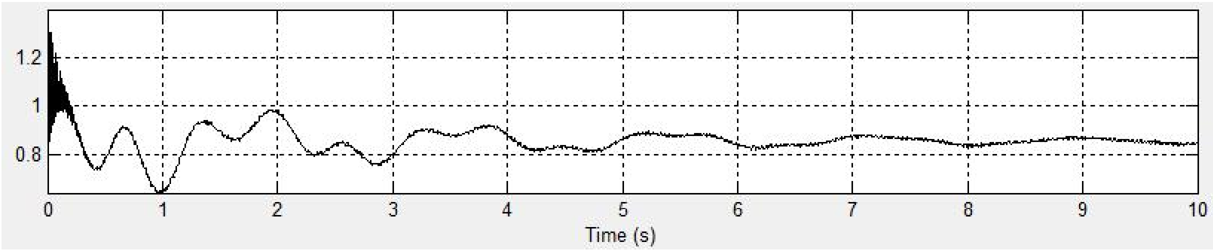

(a)

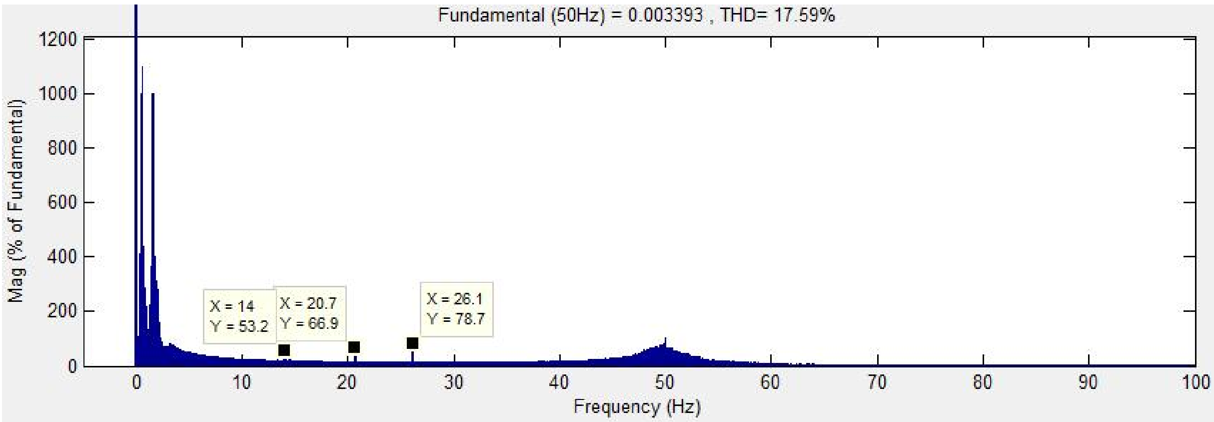

(b)

Figure 6.7 Air-gap torque with EAF in the system (a) torque T_e, (b) FFT of torque T_e

6.5.3 Analysis of Torsional Torque Amplification

The disturbance of generator air-gap torque perturbs the generator rotor, and through which farther disturbs the turbine-generator-exciter mechanism. From simulation using MATLAB power library in section 6.4, it has been shown that the turbine-generator-exciter system usually has torsional modes in the subsynchronous frequency range. Again, there are possibilities that EAFs produce signals of frequencies in that range. Thus, there occurs resonant excitation of the oscillating torques between different mass sections of the turbine-generator shaft.

For analyzing resonant excitaion of torsional modes, here only the turbine-generator unit at Raozan has been chosen. Figure 6.8(a) shows the torsional torque transmission between generator and LP_A section of the turbine when there is no EAF connected in the power system. It is seen that the torsional torque reach to an almost steady value after 9 seconds of starting generator.

Figure 6.9(a) represents the transmitted torque between generator and LP_A section when there are EAFs connected in the power system but there occurs no torsional resonance at turbine-generator shaft. It is seen that the torsional oscillation tends to be steady/constant after some times of starting generator. It implies that although there are EAFs operating in the system, they are not threat for generating unit if they don't produce signal of frequencies equal to any frequency of torsional modes

Figure 6.10(a) represents the transmitted torque between generator and LP_A section when there are EAFs connected in the power system and there occurs torsional resonance at turbine-generator shaft. From figure 6.10(a), It is seen that amplitude of oscillation of torsional torque is amplified. Figure 6.8(b), 6.9(b) and 6.10(b) represent the FFTs of the corresponding wave of torsional torque as shown in figure 6.8(b), 6.9(b) and 6.10(b). Comparing those FFTs, the amount of torque amplificaton can be calculated which will be described in next section. Figures 6.11 to 6.19 describe transmitted oscillating torque between LP_A to HP with/without EAFs connected in the power system and with/without torsional resonance. They clearly show the amplification of torsional torque.

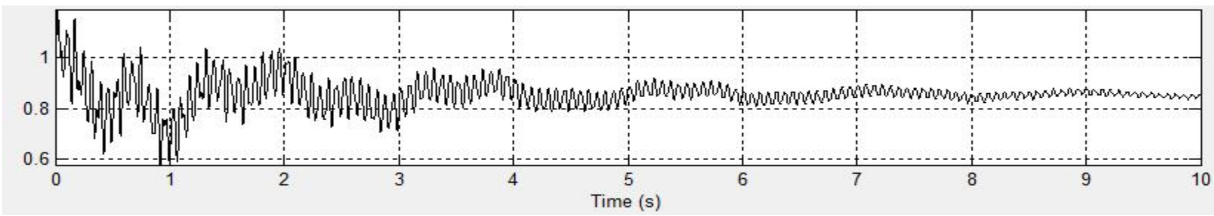

(a)

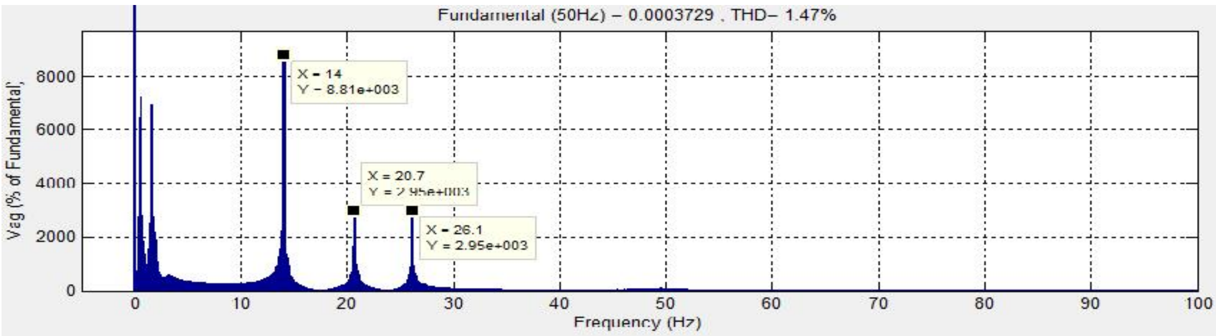

(b)

Figure 6.8 Torsional torque between generator and LP_A section at Raozan without EAFs connected in the grid (a) torsional torque waveform, (b) FFT of torsional torque waveform

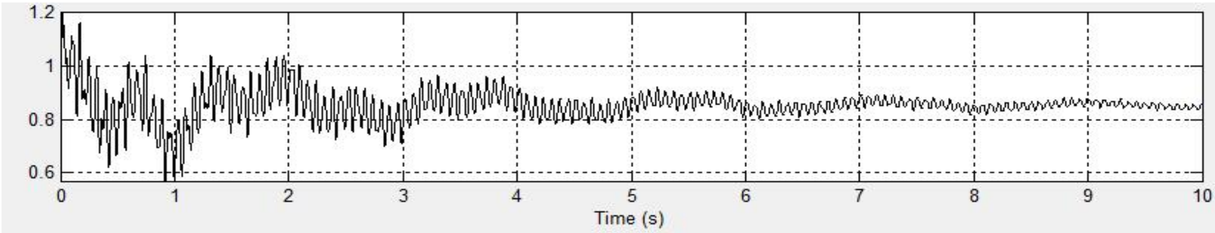

(a)

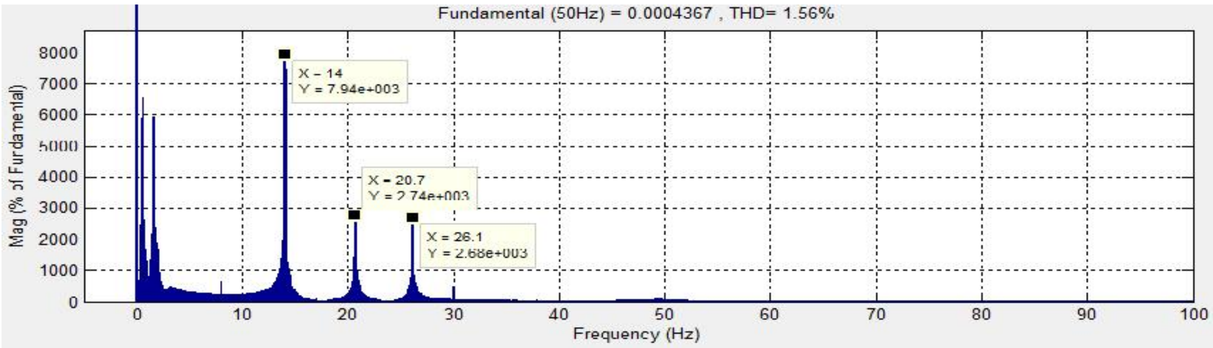

(b)

Figure 6.9 Torsional torque between generator and LP_A section at Raozan with EAFs connected, but without resonance (a) torsional torque waveform, (b) FFT of torsional torque waveform

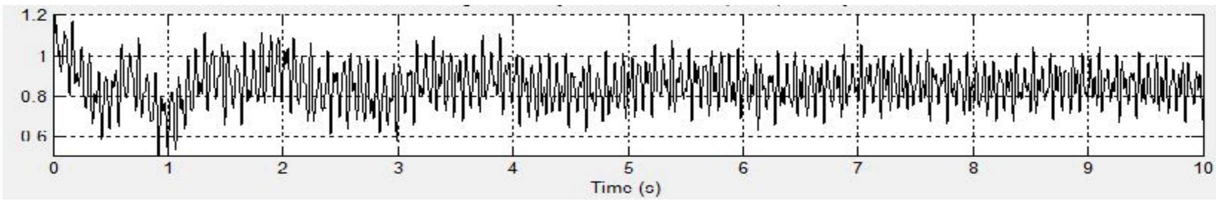

(a)

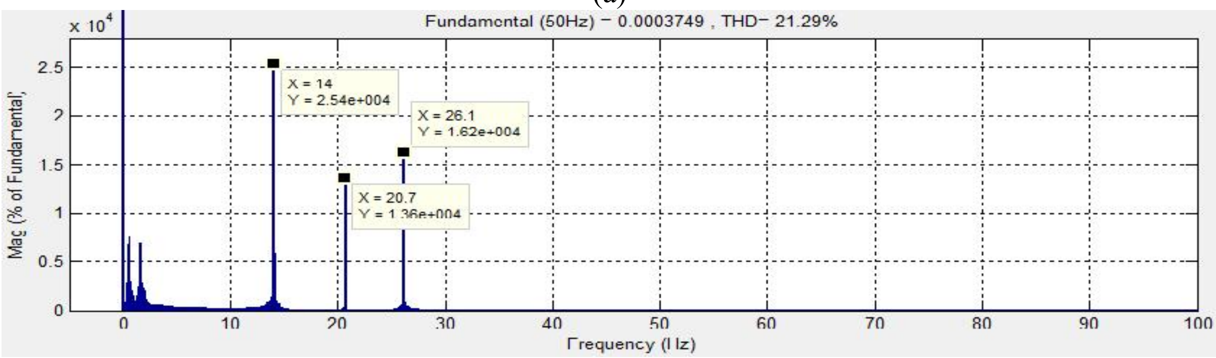

(b)

Figure 6.10 Torsional torque between generator and LP_A section at Raozan with EAFs connected, and with torsional resonance (a) torsional torque waveform, (b) FFT of torsional torque waveform

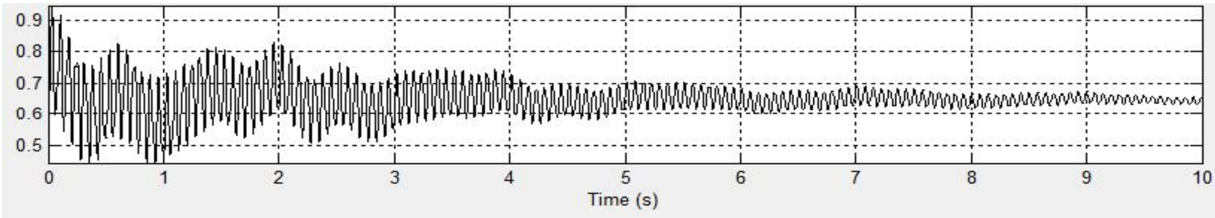

(a)

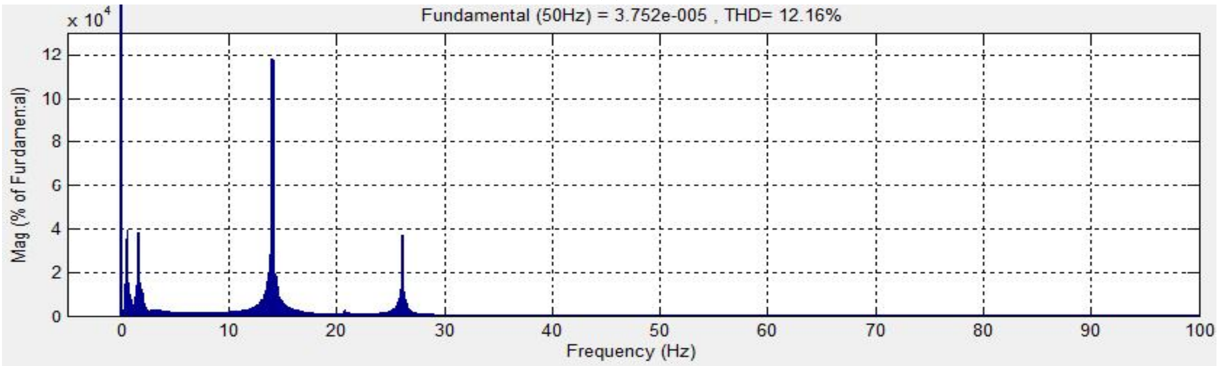

(b)

Figure 6.11 Torsional torque between LP_A and LP_B section at Raozan without EAFs connected the grid (a) torsional torque waveform, (b) FFT of torsional torque waveform

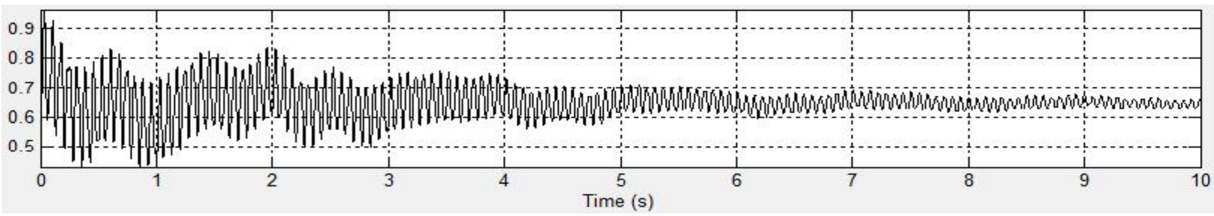

(a)

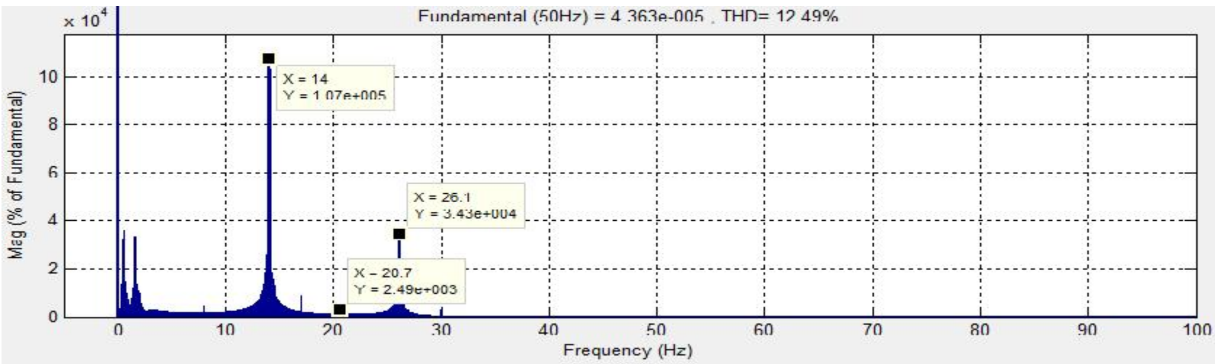

(b)

Figure 6.12 Torsional torque between LP_A and LP_B section at Raozan with EAFs connected, but without resonance (a) torsional torque waveform, (b) FFT of torsional torque waveform

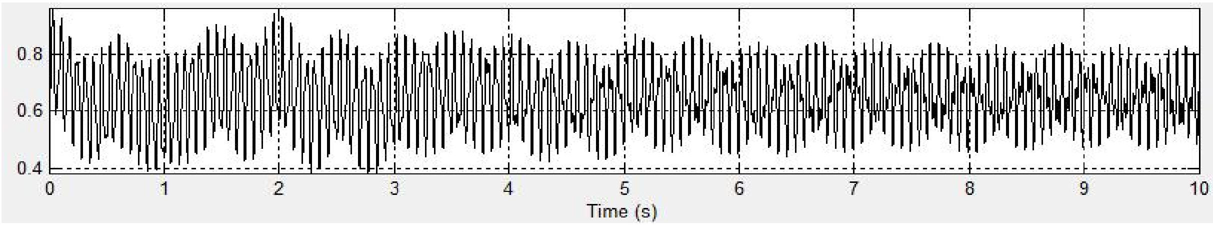

(a)

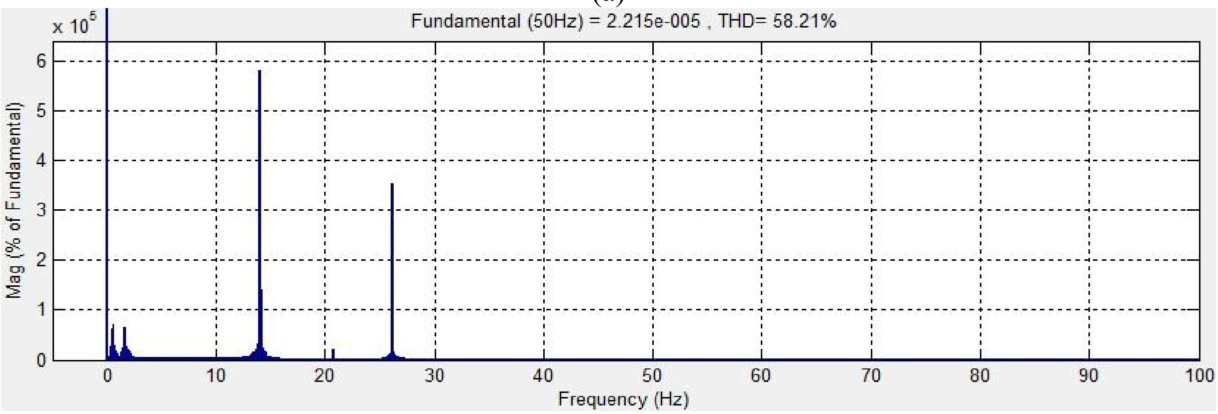

(b)

Figure 6.13 Torsional torque between LP_A and LP_B section at Raozan with EAFs, and with resonance (a) torsional torque waveform, (b) FFT of torsional torque waveform

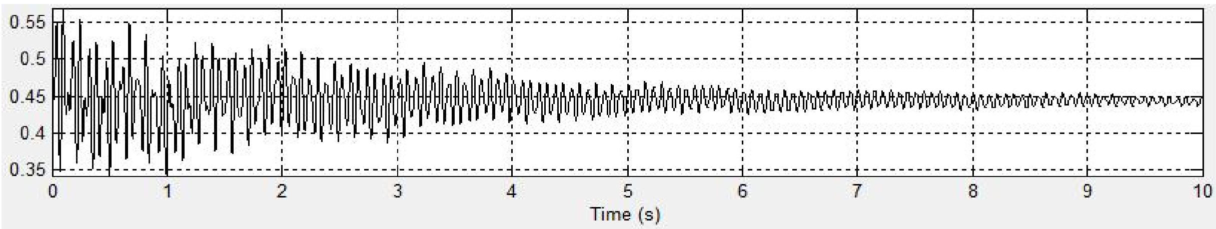

(a)

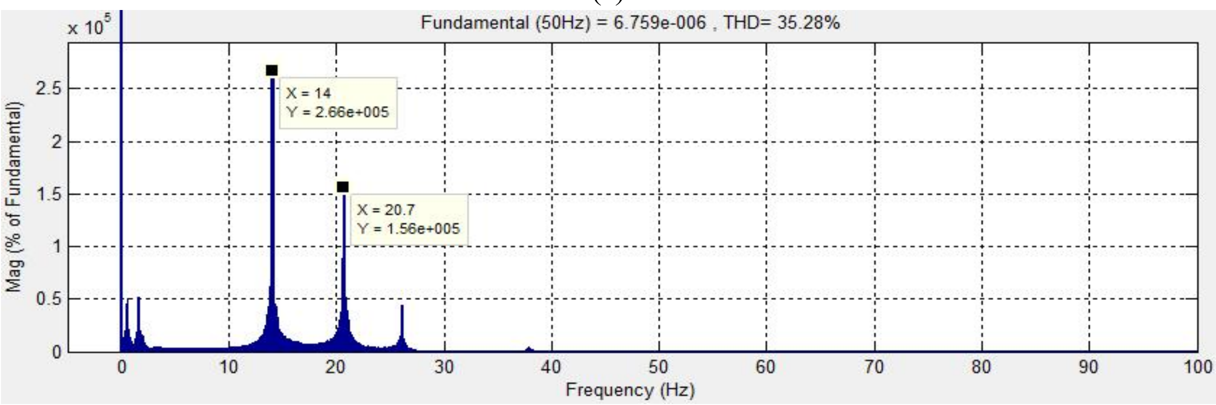

(b

Figure 6.14 Torsional torque between LP_B and IP section at Raozan without EAFs (a) torsional torque waveform, (b) FFT of torsional torque waveform

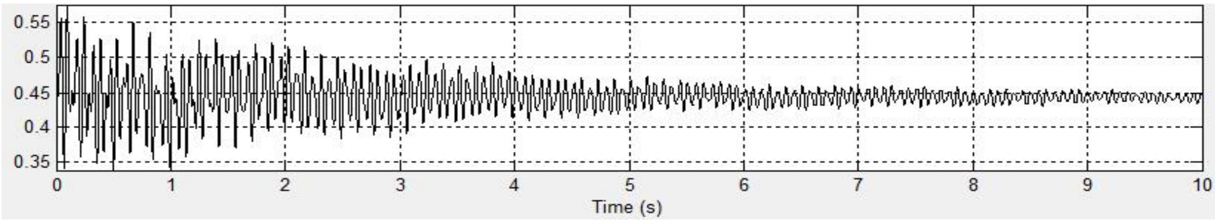

(a)

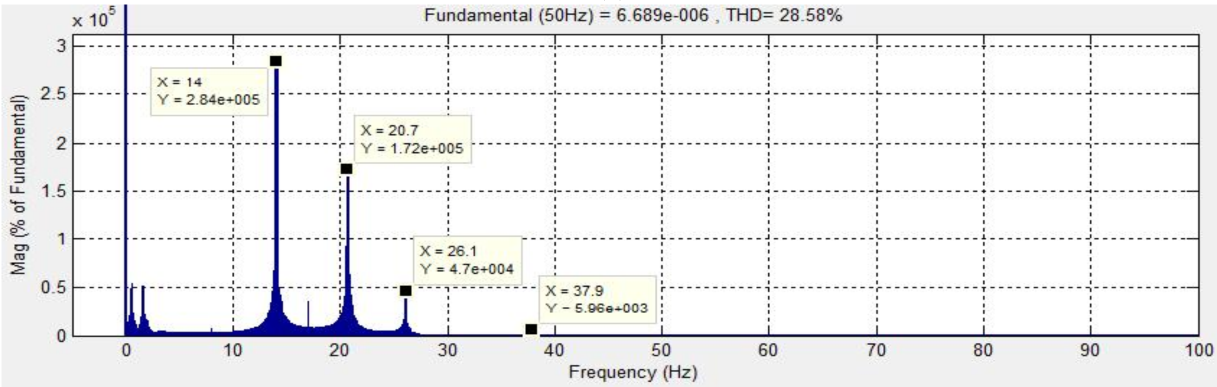

(b)

Figure 6.15 Torsional torque between LP_B and IP section at Raozan with EAFs connected, but without resonance (a) torsional torque waveform, (b) FFT of torsional torque waveform

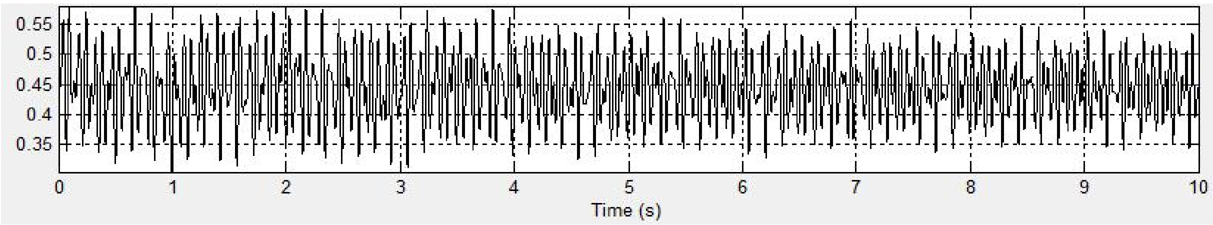

(a)

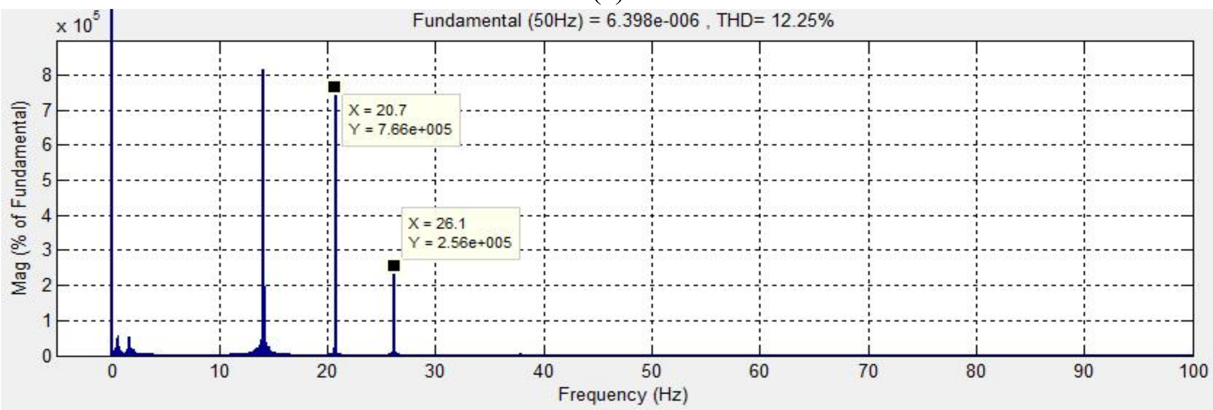

(b)

Figure 6.16 Torsional torque between LP_B and IP section at Raozan with EAFs connected, and with resonance (a) torsional torque waveform, (b) FFT of torsional torque waveform

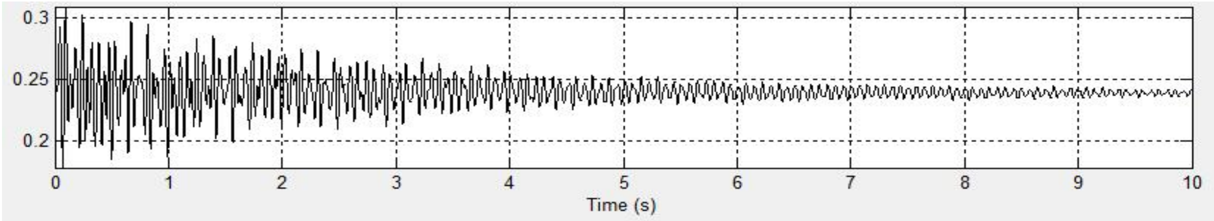

(a)

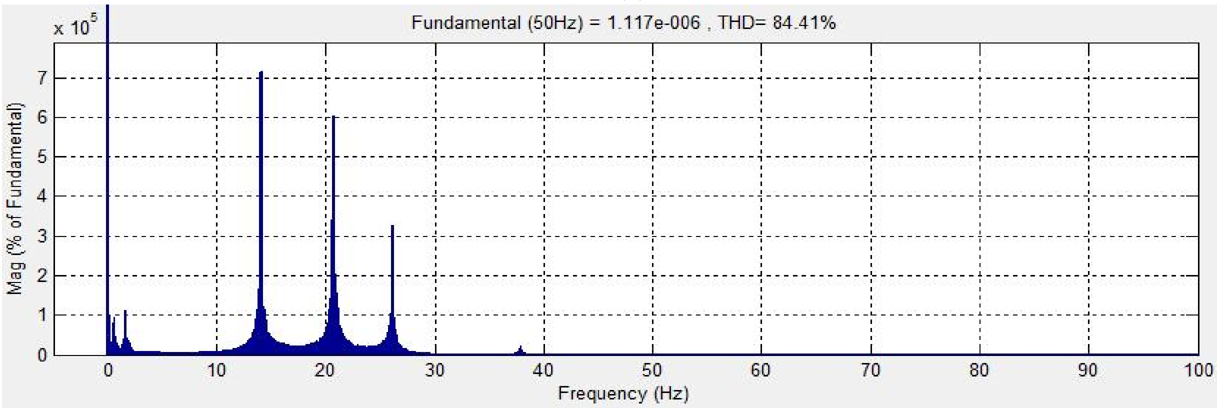

(b)

Figure 6.17 Torsional torque between IP and HP section at Raozan without EAFs connected (a) torsional torque waveform, (b) FFT of torsional torque waveform

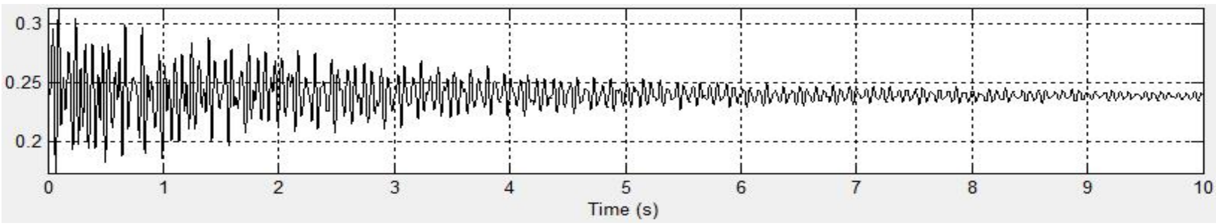

(a)

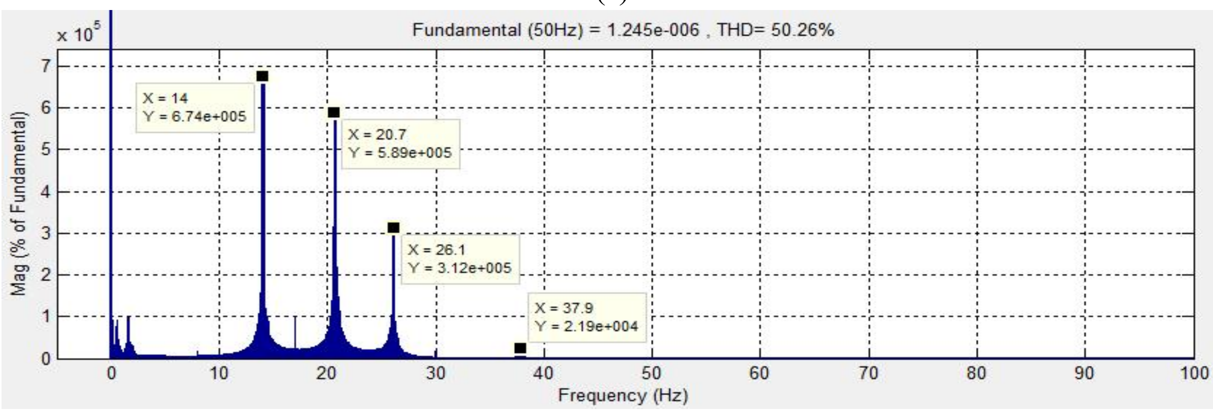

(b)

Figure 6.18 Torsional torque between IP and HP section at Raozan with EAFs connected, but without resonance (a) torsional torque waveform, (b) FFT of torsional torque waveform

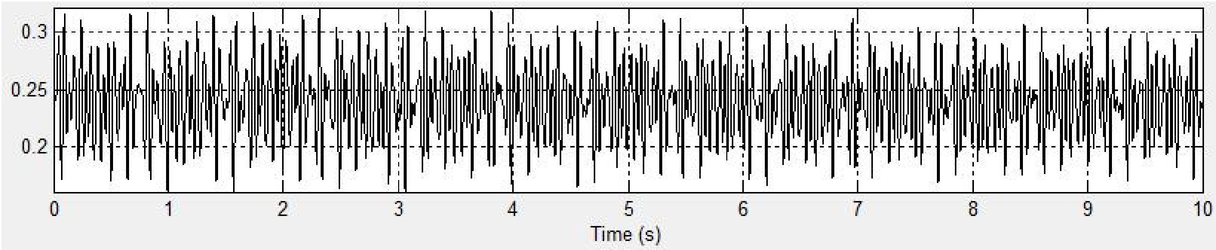

(a)

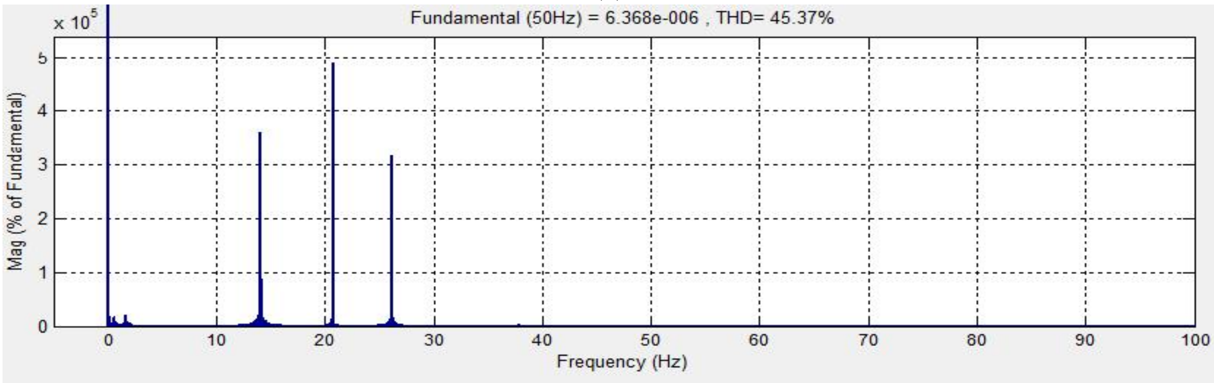

(b)

Figure 6.19 Torsional torque between IP and HP section at Raozan with EAFs connected, and with resonance (a) torsional torque waveform, (b) FFT of torsional torque waveform

6.6 Hydro Generator Torsional Characteristics

The rotor of hydro turbine-generating unit consists of a generator rotor and a turbine runner. There is an additional rotor mass, if the hydro-power generating unit has a shaft driven exciter. In any turbine-generator rotor shaft, if there are *n* number of masses, there are *n-1* number of torsional modes of oscillation. So, in hydro-turbine-generator unit with shaft driven exciter, there are two torsional modes of oscillation. Generally, the inertia of the generator rotor is about 10 to 40 times higher than that of the turbine runner (waterwheel). The frequencies of torsional modes lie in the range of 6 Hz to 26 Hz [30].

There are no reported cases of adverse dynamic interaction between the hydro generator rotor and the electrical network. The reasons for the absence of adverse interaction are as follows:

1. The inertia of the rotor is remarkably higher than that of turbine runner and exciter rotor. This causes them to behave as a single mass section and effectively guards the rotor

mechanical system. For this reason, disturbances in the network can not excite torsional modes.

2. Damping due to viscous waterwheel. This makes the inherent damping of torsional oscillations for hydro units significantly higher than for steam-turbine generators.

6.7 Quantification of Torsional Torque

In the simulation, the characteristics of the two AC EAFs are considered similar. The capacities of them are different. To investigate the torsional torque amplification, the worst case condition is considered, i.e. all frequencies equal to torsional mode frequencies are generated from both EAFs. It is done because, in test system, it is shown that excitation of one torsional mode does not affect other modes.

The FFT analysis technique is used to quantify the magnitude of the torsional torque between different mass sections. The magnitude of torsional torque of generating unit at Raozan Power Plant is shown in Table 6.7 to 6.9 where $T_{(LPA\text{-}Gen)}$ represents torsional torque between generator and LP_A, $T_{(LPB\text{-}LPA)}$ between LP_A and LP_B, $T_{(IP\text{-}LPB)}$ between LP_B and IP, and $T_{(HP\text{-}IP)}$ between IP and HP. Table 6.7 shows the magnitude of torsional torque when there is no EAF connected to the power system. Table 6.8 shows the magnitude of torsional torque without torsional resonance although there is EAF connected to the power system. Table 6.9 shows the magnitude of torsional torque when there occurs torsional resonance due to operaton of EAFs in the power system. To measure the amount of torsional torque amplification, data in Table 6.8 and data in Table 6.9 are compared. The amount of torsional torque amplification due to torsional resonance is shown in Table 6.10.

Raozan Power Plant:

Table 6.7: Torsional torque in Raozan plant without EAF in the system

Torque(pu) \ f(Hz)	0	14	20.7	26.1	37.9	50	THD%
$T_{(HP\text{-}IP)}$	2.40E-01	8.01E-03	6.75E-03	3.64E-03	2.36E-04	1.12E-06	84.41
$T_{(IP\text{-}LPB)}$	4.45E-01	1.80E-02	1.05E-02	2.95E-03	3.43E-04	6.76E-06	35.28
$T_{(LPB\text{-}LPA)}$	6.49E-01	4.43E-02	9.94E-04	1.40E-02	9.98E-05	3.75E-05	12.16
$T_{(LPA\text{-}Gen)}$	8.54E-01	3.29E-02	1.10E-02	1.10E-02	1.33E-04	3.73E-04	1.47

Table 6.8: Torsional torque in Raozan plant with existing EAF but without resonance

f(Hz) / Torque(pu)	0	14	20.7	26.1	37.9	50	THD%
$T_{(HP-IP)}$	2.40E-01	8.39E-03	7.33E-03	3.88E-03	2.73E-04	1.25E-06	50.26
$T_{(IP-LPB)}$	4.45E-01	1.90E-02	1.15E-02	3.14E-03	3.99E-04	6.69E-06	28.58
$T_{(LPB-LPA)}$	6.50E-01	4.67E-02	1.09E-03	1.50E-02	1.16E-04	4.36E-05	12.49
$T_{(LPA-Gen)}$	8.56E-01	3.47E-02	1.20E-02	1.17E-02	1.64E-04	4.37E-04	1.56

Table 6.9: Torsional torque in Raozan plant with existing EAF and with resonance

f(Hz) / Torque(pu)	0	14	20.7	26.1	37.9	50	THD%
$T_{(HP-IP)}$	2.40E-01	2.31E-02	3.13E-02	2.02E-02	2.52E-04	6.37E-06	45.37
$T_{(IP-LPB)}$	4.45E-01	5.23E-02	4.90E-02	1.64E-02	3.73E-04	6.40E-06	12.25
$T_{(LPB-LPA)}$	6.49E-01	1.29E-01	4.52E-03	7.80E-02	1.55E-04	2.22E-05	58.21
$T_{(LPA-Gen)}$	8.55E-01	9.52E-02	5.10E-02	6.07E-02	1.28E-04	3.75E-04	21.29

Table 6.10: Torsional torque amplification in Raozan plant with existing EAFs

f(Hz) / Torque ratio between sections	0	14	20.7	26.1	37.9
HP-IP	9.99E-01	2.75E+00	4.26E+00	5.20E+00	9.23E-01
IP-LP_B	1.00E+00	2.75E+00	4.26E+00	5.21E+00	9.36E-01
LP_B-LP_A	9.98E-01	2.76E+00	4.16E+00	5.21E+00	1.34E+00
LP_A-Gen	9.99E-01	2.75E+00	4.26E+00	5.19E+00	7.79E-01

From Table 6.10, it is seen that the amount of average amplified torsional toque due to resonant excitation of mode 1 is 2.75 times of its non-resonant torsional torque. Torsional torque of mode 2 is amplified, on an average, 4.26 times of its non-resonant value and mode 3 is amplified, on an average, 5.20 times of its non-resonant value.

The torsional torque quantifications of generating unit at Sikalbaha Power Plant are given in Table 6.1 to 6.13 which explain torques at different conditions. The amount of torsional torques at resonant condition is compared with torsional torques at non-resonant condition and the comparison is shown in Table 6.14.

Sikalbaha Power Plant:

Table 6.11: Torsional torque in Sikalbaha plant without EAF

f(Hz) / Torque(pu)	0	14	20.7	26.1	37.9	50	THD%
$T_{(HP-IP)}$	2.31E-01	8.75E-03	9.36E-03	5.32E-03	2.91E-04	1.02E-06	70.81
$T_{(IP-LPB)}$	4.28E-01	1.99E-02	1.47E-02	4.32E-03	4.23E-04	8.08E-06	27.44
$T_{(LPB-LPA)}$	6.26E-01	4.89E-02	1.36E-03	2.05E-02	1.13E-04	5.97E-05	11.8
$T_{(LPA-Gen)}$	8.22E-01	3.62E-02	1.53E-02	1.61E-02	1.77E-04	5.59E-04	0.63

'able 6.12: Torsional torque in Sikalbaha plant with existing EAF but without resonance

f(Hz) / Torque(pu)	0	14	20.7	26.1	37.9	50	THD%
$T_{(HP-IP)}$	2.31E-01	9.33E-03	9.50E-03	5.45E-03	2.64E-04	1.55E-06	62.44
$T_{(IP-LPB)}$	4.28E-01	2.12E-02	1.50E-02	4.42E-03	3.86E-04	8.74E-06	30.7
$T_{(LPB-LPA)}$	6.26E-01	5.21E-02	1.39E-03	2.10E-02	1.05E-04	6.28E-05	10.39
$T_{(LPA-Gen)}$	8.26E-01	3.86E-02	1.55E-02	1.65E-02	1.53E-04	5.94E-04	0.65

Table 6.13: Torsional torque in Sikalbaha plant with existing EAF and with resonance

f(Hz) / Torque(pu)	0	14	20.7	26.1	37.9	50	THD%
$T_{(HP-IP)}$	2.31E-01	2.19E-02	2.40E-02	1.39E-02	2.69E-04	3.07E-06	37.69
$T_{(IP-LPB)}$	4.28E-01	4.97E-02	3.76E-02	1.12E-02	3.00E-04	9.48E-06	9.76
$T_{(LPB-LPA)}$	6.23E-01	1.22E-01	3.43E-03	5.34E-02	1.44E-04	4.95E-05	14.63
$T_{(LPA-Gen)}$	8.22E-01	9.06E-02	3.91E-02	4.17E-02	4.00E-05	5.60E-04	10.43

Table 6.14: Torsional torque amplification in Sikalbaha plant with existing EAFs

f(Hz) / Torque ratio between sections	0	14	20.7	26.1	37.9
HP-IP	9.98E-01	2.35E+00	2.52E+00	2.54E+00	1.02E+00
IP-LP_B	1.00E+00	2.35E+00	2.52E+00	2.53E+00	7.78E-01
LP_B-LP_A	9.96E-01	2.35E+00	2.47E+00	2.55E+00	1.37E+00
LP_A-Gen	9.96E-01	2.35E+00	2.52E+00	2.54E+00	2.62E-01

From Table 6.14, it is seen that mode 1 is amplified, on an average, 2.35 times of its non-resonant value, mode 2 is amplified, on an average, 2.52 times of its non-resonant value and mode 3 is amplified 2.54 times of its non-resonant value.

6.8 Torsional Torque in Chittagong Region with Additional EAFs.

In section 6.2, it has been discussed that there are many steel industries in Chittagong region and few of them are using AC/DC EAFs. Others are using induction or ladle furnaces. As the production capacity of EAFs is higher than any other furnace, many EAFs may be installed in that region in future. Again, demand of good quality steel is increasing day-by-day, which trends to higher possibility of installing EAFs in steel industry. Considering this, four AC EAFs of equal capacity (100 MVA each) with same characteristics are assumed to be connected to the grid of BPS-Chittagong region. Among these, one is connected at Abul Khair, one at Modern and other twos are connected to Khulsi grid. These locations are indicated in the figure 6.1.

Table 6.15 shows the amplitude of torsional torque when there are four AC EAFs connected to the grid and there occurs resonance in the turbine-generator shaft at Raozan. Here also, the worst case condition is considered, i.e., all frequencies equal to torsional mode frequencies are generated from EAFs and their impact on generating unit is investigated. To quantify the amount of torsional torques amplification at Raozan plant, the torsional torques at resonance (Table 6.15) are compared with torsional torques at non-resonance (Table 6.7). The amplified torques are presented in Table 6.16.

Generating Unit at Raozan Power Plant:

Table 6.15: Torsional torque at resonance in Raozan plant with additional EAFs

f(Hz) / Torque(pu)	0	14	20.7	26.1	37.9	50	THD%
$T_{(HP-IP)}$	2.41E-01	4.60E-02	5.85E-02	3.66E-02	2.57E-04	1.15E-05	49.31
$T_{(IP-LPB)}$	4.46E-01	1.05E-01	9.17E-02	2.95E-02	3.88E-04	9.98E-06	22.99
$T_{(LPB-LPA)}$	6.51E-01	2.57E-01	8.38E-03	1.41E-01	2.44E-04	1.70E-05	76.34
$T_{(LPA-Gen)}$	8.58E-01	1.90E-01	9.50E-02	1.10E-01	3.67E-04	3.43E-04	53.64

Table 6.16: Amount of torsional torque amplification in Raozan plant with additional EAFs

f(Hz) / Torque ratio between sections	0	14	20.7	26.1	37.9
HP-IP	1.00E+00	5.74E+00	8.66E+00	1.00E+01	1.09E+00
IP-LP_B	1.00E+00	5.83E+00	8.70E+00	1.00E+01	1.13E+00
LP_B-LP_A	1.00E+00	5.81E+00	8.43E+00	1.00E+01	2.44E+00
LP_A-Gen	1.00E+00	5.79E+00	8.64E+00	9.98E+00	2.77E+00

Table 6.16 shows the amount of torque amplification when there occurs torsional resonance. It is seen that when mode 1 is excited, the torsional torque is amplified 5.78 times of its non-resonant torque. When mode 2 is excited, the torsional torque is amplified, on an average, 8.61 times of its non-resonant torque. When mode 3 is excited, the torsional torque is amplified, on an average, 10 times of its non-resonant torque. So it is deducible that higher the mode is excited, higher the amplification occurs.

Table 6.17 shows the amount of torsional torque in same turbine-generator shaft at Sikalbaha plant when four AC EAFs are connected to the grid. To quantify the amount of torsional torques amplification at Sikalbaha plant, the torsional torques at resonance (Table 6.17) are compared with torsional torques at non-resonance (Table 6.11). The amplified torques are presented in Table 6.18.

Generating Unit at Sikalbaha Power Plant:

Table 6.17: Torsional torque at resonance in Sikalbaha plant with additional EAFs

f(Hz) / Torque(pu)	0	14	20.7	26.1	37.9	50	THD%
$T_{(HP-IP)}$	2.32E-01	5.23E-02	7.87E-02	5.35E-02	3.32E-04	1.70E-05	49.97
$T_{(IP-LPB)}$	4.30E-01	1.19E-01	1.23E-01	4.33E-02	4.71E-04	1.30E-05	11.53
$T_{(LPB-LPA)}$	6.28E-01	2.92E-01	1.14E-02	2.06E-01	2.38E-04	5.77E-05	54.61
$T_{(LPA-Gen)}$	8.23E-01	2.16E-01	1.28E-01	1.61E-01	3.97E-04	7.28E-04	31.23

Table 6.18: Amount of torsional torque amplification in Sikalbaha plant with additional EAFs

f(Hz) / Torque ratio between sections	0	14	20.7	26.1	37.9
HP-IP	1.01E+00	5.98E+00	8.41E+00	1.00E+01	1.14E+00
IP-LP_B	1.00E+00	5.97E+00	8.40E+00	1.00E+01	1.11E+00
LP_B-LP_A	1.00E+00	5.98E+00	8.35E+00	1.00E+01	2.11E+00
LP_A-Gen	1.00E+00	5.98E+00	8.37E+00	1.00E+01	2.25E+00

Table 6.18 shows the amount of torsional torque amplification in the turbine-generator shaft at Sikalbaha plant. It is seen that the torque amplification is similar to that of turbine-generator shaft at Raozan power plant.

Torsional torque amplification of system with additional EAFs is compared with that of system with existing EAFs and the comparison is presented in Table 6.19. From Table 6.19, it is seen that torsional torques with additional EAFs are larger than that of torsional torques at present. In the simulation, it is considered that there are no protection schemes for subsynchronous resonance. So, protection schemes for any additional EAFs should be installed.

From the analysis, it can be assessed that if there are no protection schemes, may be, the shaft of the turbine-generator unit at Raozan and Sikalbaha will not be broken/cracked immediately due to torsional resonance but it will lose its fatigue life. And in the long run, the shaft system may be damaged.

Table 6.19: Comparison of torsional torque amplification between systems with additional EAFs

and existing EAFs

Power plant	f (Hz)	Torque amplification at present	Torque amplification with additional EAFs	Torque increment (%)
Raozan	14	2.7525	5.7925	110.5
	20.7	4.2350	8.6075	103.3
	26.1	5.2025	9.9950	92.1
Sikalbaha	14	2.3500	5.9775	154.4
	20.7	2.5075	8.3825	234.3
	26.1	2.5400	10.0000	293.7

CHAPTER 7

CONCLUSION

7.1 Conclusion

The EAF load causes power quality problems such as flicker, voltage imbalances, harmonics and interharmonics. It is the source of subsynchronous frequencies. Because of subsynchronous resonance, the torsional oscillating torques in a turbine-generator shaft are amplified which may induce torsional stress to the shaft system. It may reduce fatigue-life and even cause severe damages to turbine-generator shaft. The magnitude and risk of damage due to torsional stress have to be carefully analysed in advance to ensure undisturbed operation and to preclude any damage from the unit. The assessment of impacts of multiple EAF operation on turbine-generator shaft is done in this work.

Since the interaction between EAF operation and turbine-generator mechanical system is in sub-synchronous frequency range, the shaft system can be designed by a simple lumped-mass model having five torsional masses such as generator rotor, two low-pressure turbine sections, an intermediate-pressure turbine section and a high pressure turbine section. The three-phase EAFs were modeled using MATLAB/Simulink from mathematical model of electric arc, where the resistances of the EAFs were varied deterministically in the frquency range of 1.2-45.5 Hz to meet the actual characteristics of EAF.

For the test system, upto five EAFs were connected at the same PCC and its effect on turbine-generator shaft was observed with/without resonant excitation of torsional modes. From investigation of the test system, it has been found that large amplitude amplification of torsional oscillations occurs when higher modes are excited. It is also observed that the torsional torques increase non-linearly to higher magnitude due to multiple EAF operation at the same PCC. The location of a single EAF was varied to investigate its impact on turbine-generator shaft. From the observation, it is found that greater the distance between EAF and PCC, lesser its impact. The magnitude of torsoinal torques decreased non-linearly with increasing distance from PCC to EAF.

Finally, the Chittagong region of the BPS with two steel mills using AC EAFs was modeled and simulated including all the large power plants in that area. The three torsional modes (modes 1, 2, 3) of both generators at Raozan and Sikalbaha were excited by the simultaneous operation of EAFs. It is observed that the turbine-generators in the Raozan plant face a greater impact than those at Sikalbaha plant. The hydro generators at Kaptai face nominal impact. Impacts of simultaneous operation of aditional EAFs in the region was also investigated. In all simulations, it is assumed that there are no protection schemes for subsynchronous resonance.

Since the physical parameters of the turbine section are not available and that are collected from different sources, the actual torsional mode frequencies in BPS may be different. To find the actual mode frequencies, acurate parameters of turbine section are required. The subsynchronous frequencies produced by EAFs may also be obtained from the field measurement data.

Since there are no subsynchronous resonance protection schemes in the BPS at present, it can be assessed that the turbine-generator shafts at Raozan and Sikalbaha power plants may not get broken/cracked immediately due to torsional resonance, but will lose their fatigue life. In the long run, the shaft systems may be damaged.

7.2 Scope of Future Works

In this work, only the torsional torque amplification due to multiple EAF operation has been investigated. There are many other areas of impact on Bangladesh power system because of EAF operation which needs to be studied. Following are the suggestions for future works related to BPS:

(a) This work may be extended for the whole of BPS.

(b) During torsional excitation, energy is absorbed by the oscillations/vibrations. Calculation of this amount of energy and investigation of its source should be studied.

(c) Subsynchronous resonance may also affect other rotating equipments which should be considered for further investigation.

(d) Only deterministic model of EAF was considered; stochastic model of EAF should be studied for comparison.

(e) Solutions to the problems caused by the operation of EAFs in the BPS should be studied.

REFERENCES

[1] Song-Manguelle J., Sihler C., Schramm S., "A General Approach of Damping Torsional Resonance Modes in Multi-megawatt Applications", *IEEE Transaction on Industry Application*, Vol. 47, No. 3, pp. 1390-1399, May-June 2011.

[2] Lambrecht D. and Kulig T., "Torsional performance of turbine generator shafts especially under resonant excitation", *IEEE Transactions on Power Apparatus and Systems*, Vol. PAS-101, No. 10, October 1982

[3] Smith K.S., Ran L., "Torsional Resonance Risk Management in Islanded Industrial Power Systems Supplying Large VFDs", Industry Applications Conference, 42nd IAS Annual Meeting. Conference Record of the 2007 IEEE, pp. 2429-2438, 23-27 September 2007

[4] Meckel C., "Mechanical damage of a subsynchronous cascade drive due to torsional resonance", *Cement Industry Technical Conference, IEEE-IAS/PCA* , pp. 133-150, 29 Apr 2001-03 May 2001

[5] Ta-Peng Tsao, Jong-Ian Tsai, "Torsional interactions between an electrical arc furnace load and a turbine-generator set", *Proceedings of the 2004 IEEE International Conference on Electric Utility Deregulation, Restructuring and Power Technologies (DRPT)*, Vol. 2, pp. 627-632, 2004

[6] Jong-Ian Tsai, Chi-Hshiung Lin, Ta-Peng Tsao, "Assessment of long-term life expenditure for steam turbine shafts due to non-characteristic subharmonic currents in asynchronous links", *IEEE Transactions on Power Systems*, Vol. 19, No. 1, Pp. 507 - 516, 2004

[7] Jong-Ian Tsai, Ta-Peng Tsao, "Restricting Turbine Blade Vibrations by a Series Compensation Capacitor", *Fourth International Conference on Innovative Computing, Information and Control (ICICIC)*, pp. 942-945, 2009.

[8] Lin, W.M., Tsai, C.C., Lin, C.H., Tsao, T.P., "Alleviating shaft torsional vibrations caused by electric arc furnaces for a low capacity turbine generator by using a flywheel coupler", *IEEE International Conference on Industrial Engineering and Engineering Management (IEEM)*, pp. 1771-1775, 2010

[9] Baker, D.H., Boukarim, G.E., D"Aquila, R., Piwko, R.J., "Subsynchronous resonance studies and mitigation methods for series capacitor applications", *IEEE Power Engineering Society Inaugural Conference and Exposition in Africa*, pp. 386 – 392, 2005

[10] Clark, K., "Overview of subsynchronous resonance related phenomena", *IEEE PES, Transmission and Distribution Conference and Exposition (T&D)*, pp. 1-3, 2012

[11] Lei, X., Buchholz, B.M., Retzmann, D.W., Jiang, D., Yang, Y.T., Zhou, X.X., "Analyzing subsynchronous resonance using a simulation program", *IEEE Proceedings, International Conference on Power System Technology (PowerCon)*, Vol. 2, pp. 775 – 781, 2000

[12] Kumar, R., Harada, A., Merkle, M., Miri, A.M., "Investigation of the influence of series compensation in AC transmission systems on bus connected parallel generating units with respect to subsynchronous resonance (SSR)", *Power Tech Conference Proceedings*, *IEEE* Bologna, Vol. 3 , 2003

[13] Kumar, R., Harada, A., Merkle, M., Schwab, A.J, "A new approach for determining series compensation ratio for transmission systems with bus connected parallel generating units considering subsynchronous resonance as a constraint", *CIGRE/IEEE PES International Symposium on Quality and Security of Electric Power Delivery Systems*, pp. 22, -27, 2003

[14] Ramey, D.G., Sismour, A.C., Kung, G.C., "Important Parameters in Considering Transient Torques on Turbine-Generator Shaft Systems", *IEEE Transactions on Power Apparatus and Systems*, Vol. PAS-99, Issue: 1, pp. 311-317, 1980

[15] Varadan, S., Makram, E. B., and Girgis, A. A., "A New Time Domain Voltage Source Model for an Arc Furnace Using EMTP," *IEEE Transactions on Power Delivery*, vol. 11, no. 3, pp. 1685–1690, July 1996

[16] Mayordomo, J.G., Beites, L.F., Asensi, R., Izzeddine, M., Zabala, L., Amantegui, J., "A New Frequency Domain Arc Furnace Model for Iterative Harmonic Analysis", *IEEE Transactions on Power Delivery*, Volume 12, Issue 4, pp.1771 – 1778 October 1997

[17] Collantes-Bellido, R., Gomez, T., "Identification and Modelling of a Three Phase Arc Furnace for Voltage Disturbace Simulation", *IEEE Transactions on Power Delivery*, Vol. 12, No. 4, pp. 1812-1817, October 1997

[18] Ozgun, O., Abur, A., "Flicker Study Using a Novel Arc Furnace Model", *IEEE Transactions on Power Delivery*, Vol. 17, No. 4, pp.1158-1163, October 2002

[19] Tongxin Zheng, Makram, E. B., ''An Adaptive Arc Furnace Model'', *IEEE Transactions on Power Delivery*, Vol. 15, No. 3, pp. 931-939, July 2000

[20] Cano Plata, E.A., Tacca, H.E., " Arc Furnace Modeling in ATP-EMTP", *Presented at the International Conference on Power Systems Transients(IPST'05) in Montreal*, Canada, June 19-23, 2005

[21] Panoiu, M., Panoiu, C., Sora, I., Rob, R., ''Simulation of the Flicker Phenomenon Based on Modeling the Electric Arc'', *WSEAS Transactions on System*, Vol. 7, No. 10, pp. 1132-1142, ISSN: 1109-2777, October 2008

[22] Solanics, P., Kozminski, K., Bajpai, M., Esztergalyos, J., Fennell, E., Gardell, J., Mozina, C., Patel, S., Pierce, A., Skendzic, V., Waudby, P., and Williams, J., "The Impact of Large Steel Mill Loads on Power Generating Units", *IEEE Transactions on Power Delivery*, Vol. 15, No. 1, pp. 24-30, January 2000

[23] Tsai, T., Wang, J., Lin, C. ''Effect of Small Power Disturbances on Turbine-Generator Mechanism Torsional Torque and Fatigue'', *IEEE ICSS2005 International Conference on System & Signals*, 2005.

[24] Owen, E. L., ''Intregation of Steel Mills into Electric Power Systems'', *A Power Quality Newsletter (EPRI, Signature)*, Vol. 6, No. 2, pp. 1-7, Spring 1996.

[25] Robert, A., Janssens, N., Couvreur, M., Ledoux, P., Boon, G., Demaret, H., Nedden, L. Z., Deuse, J., Dubois, J., ''Electromechanical Oscillations and Torsional Stresses of Generating Units near Arc Furnaces'', cigre, http://www. cigre.org, 1998

[26] Manchur, G., Erven, C.C., ''Development of a Model for Predicting Flicker from Electric Arc Furnace'', *IEEE Transactions on Power Delivery*, Vol. 7, n.1, pp. 416-426, January 1992

[27] Montanari, G.C., Loggini, M., Cavallini, A., Pitti, L., and Zaninelli, D., ''Arc furnace model for the study of flicker compensation in electrical networks'', *IEEE Transaction on Power Delivery*, Vol.9, No. 4, pp. 2026-2033, October 1994

[28] Chang, W., Wu, C., Yen, S., ''A Flexible Voltage Flicker Teaching Facility for Electric Power Quality Education'', *IEEE Transactions on Power Systems*, Vol. 13, No. 1, pp. 27-33, February 1998

[29] Logar, V., Dovzan, D., and Skrjanc, I., ''Mathematical Modeling and Experimental Validation of an Electric Arc Furnace'', *ISIJ International*, Vol. 51, No. 3, pp. 382-391, 2011

[30] Kundur, P., *Power System Stability and Control*. New York: McGraw-Hill, 1994

[31] Acha, E., Semlyen, A., Rajakovic, N., ‘‘A Harmonic Domain Computational Package for Nonlinear Problems and its application to electric Arcs’’, *IEEE Transactions on Power Delivery*, Vol. 5, No. 3, pp. 1390-1397, July 1990

[32] Alonso, M.A.P., Donsion, M.P., ‘‘An Improved Time Domain Arc Furnace Model for Harmonic Analysis’’, *IEEE Transactions on Power Delevery*, Vol. 19, No. 1, pp. 367-373, January 2004.

[33] Andrei H., Cepisca C. and Grigorescu S., ‘‘Power Quality and Electrical Arc Furnaces’’, *Valahia University of Targoviste, Politehnica University of Bucharest, Romania.*

[34] Jones J., ‘‘Understanding Electric Arc Furnace Operations’’, The EPRI Center for materials production, *Carnegie Mellon Research Institute, Pittsburgh, Pennsylvania*, February, 1997

[35] Ryff, P.F., ‘‘Calculation of Arc-Circuit Asymmetry in Electric Arc Furnaces’’, *IEE Proc*., Vol. 130, Pt. B, No. 3, May 1983

[36] Tsai, J., Zhan, T., Wu, R., “A Random Subsynchronous Resonance in a Turbine Generator Set”, *Proceedings of the IASTED International Conference Energy and Power Systems*, Chiang, Thailand, March 29-31, 2006

[37] Vervenne, I., Van Reusel, K., Belmans, R., ‘‘Electric Arc Furnace Modelling from a ‘‘Power Quality’’ Point of View’’, *3rd IEEE Benelux Young Researchers Symposium in Electrical Power Engineering*, Ghent, Belgium, April 2006

[38] A.M.O. Haruni, Kashem M. Muttaqi, M. Negnevitsky, “Analysis of harmonics and voltage fluctuation using different models of arc furnace”, *Porwer Engineering Conference*, ustralasian Universities, AUPEC 2007

[39] Stade D., Schan H. and Kramer S., “Modelling of the electrical behaviour of arc furnace”, in Proc. *29th Universities Power Engineering Conference*, Vol. 1, pp. 125-128, 1994.

[40] Carpinelli G., Iacovone F., Russo A. and Varilone P., “Chaos-bsed modelling of DC arc furnaces for power quality issues,” in *IEEE Transactions on Power Delivery*, Vol. 19, No. 4, pp.1869-1876, October 2004

[41] Peterson H.M., Koch R.G., Swart P.H. and Van Heerden R., ‘‘Modeling arc furnace flicker and invesitigating compensation techniques’’, *IEEE Proceedings of Industrial Applications Soc. Annu. Meeting*, Vol. 2, pp. 125-128, 1995

[42] Mayordomo J.G., Beites L.F., Asensi R., Izzaddine M., Zabala L. and Amantegui J., ‘‘ A new frequency domain arc furnace model for iterative harmonic analysis,’’ *IEEE Transactions on Power Delivery*, Vol. 12, pp. 1771-1778, October 1997

[43] IEEE Subsynchronous resonance working group, "Second benchmark model for computer simulation of subsynchronous resonance," *IEEE Transactions on Power Apparatus and Systems*, vol. PAS-104, no. 5, pp. 1057-1066, 1985

[44] IEEE Working Group on Prime Mover and Energy Supply Models for System Dynamic Performance Studies, "Hydraulic Turbine and Turbine Control Models for Dynamic Studies," *IEEE Transactions on Power Systems*, Vol.7, No.1, pp. 167-179, February 1992

[45] Power Grid Company of Bangladesh (PGCB) Ltd, ‘‘Existing 230 kV and 132 kV grid network of Bangladesh’’, Available: http//www.pgcb.org.bd

APPENDIX A

The following system was used to find the torsional modes and its frequencies where there was no EAFs connected in the power system. Where E_t represents terminal voltage, E_B represents the infinite bus voltage, P_t represents MW output from the generator Q_t represents MVar output from the generator. *LV* represents the primary side of the transformer, *HV* represents the secondary side of the transformer. R_L and X_L represent line resistance and reactance respectively. All the parameters are in pu.

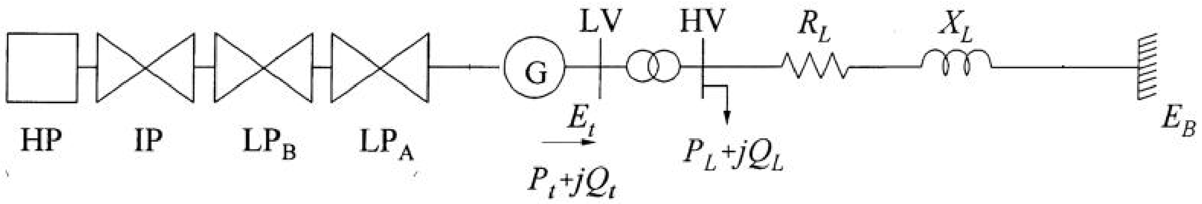

Figure A-1 Turbine-generator system used to calculate torsional modes and its frequencies in test system

MATLAB Programming:

```
%Physical parameters of Turbine-generator shaft%
%Damping constants
D1 = 0.02*8;
D2 = 0.3104*8;
D3 = 0.05*8;
D4 = 0.05*8;
D5 = 0.04*8;
%Inertia constants
H1 = 0.556;
H2 = 0.775;
H3 = 0.751;
H4 = 0.151;
H5 = 0.081;
%Stiffnes between mass sections of Turbine-generator shaft
K12 = 51.92;
K23 = 63;
K34 = 40.33;
K45 = 18.17;

f0 = 50; %System frequency in Hz
w0 = 2*pi*f0; % angular frequency in rad/sec.
```

```
%Calculation of Synchronizing torque coeffcient, Ks%

Pt = 0.9360; % Generator terminan real power in pu
Et = 1.08;% generator terminal voltage in pu
Eb = 1.0;% Infinite bus voltage in pu

Xt = 0.13;% Transformer winding reactance in pu
XL = 0.75;% Line reactance in pu

Ra = 0.003;% Generator armature resistance in pu
Rt = 0.008;% Transformer winding resistance in pu
RL = 0.008;% Line resistance in pu

Xl = 0.13;% Generator Leakage reactance in pu
Xd = 1.51;% Generator d-axis reactance in pu
Xq = 1.47;% Generator q-axis reactance in pu
Xd1p = 0.257;% Generator d-axis transient reactance in pu
Xq1p = 0.6;% Generator q-axis transient reactance in pu
Xd2p = 0.203;% Generator d-axis subtransient reactance in pu
Xq2p = 0.229;% Generator q-axis subtransient reactance in pu

% Consideration of magnetic saturation effect
Asat = 0.008;% Magnetic saturation constant
Bsat = 9.6; % Magnetic saturation constant
SiT1 = 0.8;

RE = Rt+RL;
Xadu = Xd-Xl;% Unsaturated mutual reactance of stator-rotor circuit
Xaqu = Xq-Xl;% Unsaturated mutual reactance stator-rotor circuit
XE = Xt+XL;% total line reactance in pu

deltatb = (180/pi)*asin(Pt*XE/(Et*Eb));%angle between generator
                                terminal and infinite bus
Qt = Et*(Et-Eb*cos(deltatb*pi/180))/XE;% Reactive power output
                                 from generator

It = conj(Pt+i*Qt)/conj(Et); %Generator stator current
                       considering Et as reference, %
Ir = real(It); % real part of It%
Ii = imag(It); % imaginary part of It%
Im = sqrt(Ir^2+Ii^2); %magnitude of generator internal current%
fi = abs((180/pi)*atan(Ii/Ir));%angle of It, considering Et as   reference %

Ea = Et+i*Xd1p*It;% Generator internal voltage
```

```
a = real(Ea); % real part of Ea%
b = imag(Ea); % imaginary part of Ea%
Eam = sqrt(a^2+b^2); %magnitude of generator internal voltage%
angleEa = (180/pi)*atan(b/a);%angle o1f Ea%

deltaib = deltatb+angleEa;% Angle between generator internal
                          voltage and infinits bus voltage

Siat = Eam;
Sii = Asat*exp(Bsat*(Siat-SiT1));
Ksd = Siat/(Siat+Sii);% degree of magnetic saturation in d-axis
Ksq = Ksd;% degree of magnetic saturation in q-axis

Xds = Ksd*Xadu+Xl;
Xqs = Ksq*Xaqu+Xl;
deltai=(180/pi)*atan((Im*Xqs*cos(fi*pi/180)-
    Im*Ra*sin(fi*pi/180))/(Et+Im*Ra*cos(fi*pi/180)+Im*Xqs*sin(fi*pi/180)));

ed0 = Et*sin(deltai*pi/180);
eq0 = Et*cos(deltai*pi/180);
id0 = Im*sin(deltai*pi/180+fi*pi/180);
iq0 = Im*cos(deltai*pi/180+fi*pi/180);
EBd0 = ed0-RE*id0+XE*iq0;
EBq0 = eq0-RE*iq0-XE*id0;
delta0 = (180/pi)*atan(EBd0/EBq0);

Ks = (Eam*Eb/XT)*cos(delta0*pi/180);% Synchronizing torque
                                    coefficient

%Calculation of Eigenvalues%
Elements of State Matrix:
```

a11 = 0;
a12 = 0;
a13 = 0;
a14 = 0;
a15 = 0;
a16 = w0;
a17 = 0;
a18 = 0;
a19 = 0;
a110 = 0;
	a41 = 0;
	a42 = 0;
	a43 = 0;
	a44 = 0;
	a45 = 0;
	a46 = 0;
	a47 = 0;
	a48 = 0;
	a49 = w0;
	a410 = 0;
		a71 = K12/(2*H2);
		a72 = -(K12+K23)/(2*H2);
		a73 = K23/(2*H2);
		a74 = 0;
		a75 = 0;
		a76 = 0;
		a77 = -D2/(2*H2);
		a78 = 0;
		a79 = 0;
		a710 = 0;

a21 = 0;
a22 = 0;
a23 = 0;
	a51 = 0;
	a52 = 0;
	a53 = 0;
		a81 = 0;
		a82 = K23/(2*H3);
		a83 = -(K23+K34)/(2*H3);

a24 = 0;
a25 = 0;
a26 = 0;
a27 = w0;
a28 = 0;
a29 = 0;
a210 = 0;
	a54 = 0;
	a55 = 0;
	a56 = 0;
	a57 = 0;
	a58 = 0;
	a59 = 0;
	a510 = w0;
		a84 = K34/(2*H3);
		a85 = 0;
		a86 = 0;
		a87 = 0;
		a88 = -D3/(2*H3);
		a89 = 0;
		a810 = 0;

a31 = 0;
a32 = 0;
a33 = 0;
a34 = 0;
a35 = 0;
a36 = 0;
a37 = 0;
a38 = w0;
a39 = 0;
a310 = 0;
	a61 = - (K12+Ks)/(2*H1);
	a62 = K12/(2*H1);
	a63 = 0;
	a64 = 0;
	a65 = 0;
	a66 = -D1/(2*H1);
	a67 = 0;
	a68 = 0;
	a69 = 0;
	a610 = 0;
		a91 = 0;
		a92 = 0;
		a93 = K34/(2*H4);
		a94 = -(K34+K45)/(2*H4);
		a95 = K45/(2*H4);
		a96 = 0;
		a97 = 0;
		a98 = 0;
		a99 = -D4/(2*H4);
		a910 = 0;

	a101 = 0;
	a102 = 0;
	a103 = 0;
	a104 = K45/(2*H5);
	a105 = -K45/(2*H5);
	a106 = 0;
	a107 = 0;
	a108 = 0;
	a109 = 0;
	a1010 = -D5/(2*H5);	

```
A = [a11 a12 a13 a14 a15 a16 a17 a18 a19 a110;...
    a21 a22 a23 a24 a25 a26 a27 a28 a29 a210;...
    a31 a32 a33 a34 a35 a36 a37 a38 a39 a310;...
    a41 a42 a43 a44 a45 a46 a47 a48 a49 a410;...
    a51 a52 a53 a54 a55 a56 a57 a58 a59 a510;...
    a61 a62 a63 a64 a65 a66 a67 a68 a69 a610;...
    a71 a72 a73 a74 a75 a76 a77 a78 a79 a710;...
    a81 a82 a83 a84 a85 a86 a87 a88 a89 a810;...
    a91 a92 a93 a94 a95 a96 a97 a98 a99 a910;...
    a101 a102 a103 a104 a105 a106 a107 a108 a109 a1010];

[REV lamda] = eig(A);% REV= right eigen vector, lamda=   % eigenvalues
LEV = inv(REV);%LEV= Left eigen vector
LEVt = transpose(LEV);
P = REV.*LEVt;%
```

APPENDIX B

Table B-1: Some constants for steam-turbine and its controlling units

Name of Constants	Value
Regulator gain, Kp	1
Perm.droop Rp(pu)	0.05
dead zone Dz(pu)	0
Speed relay time constant Tsr(s)	0.001
Servo-motor time constant Tsm(s)	0.15
Gate opening limits	
Vgmin(pu/s)	-0.1
Vgmax(pu/s)	0.1
gmin(pu)	0
gmax(pu)	4.496
Steam turbine time constant	
T2(s)	3.3
T2(s)	7
T3(s)	7
T4(s)	3.5
Turbine torque fracton	
F2	0.24
F3	0.24
F4	0.24
F5	0.28

Table B-2: Constants for hydro-turbine and its controlling units

Name of constants	Value
Servo-motor	
Ka	10/3
Ta(s)	0.07
Gate opening limits	
gmin(pu)	0.01
gmax(pu)	0.97518
vgmin(pu/s)	-0.1
vgmax(pu/s)	0.1
Permanent droop and regulator	
Rp()	0.05
Kp()	1.163
Ki()	0.105
Kd()	0
Td(s)	0.01
Hydraulic turbine	
beta()	0
Tw(s)	2.67

Table B-3: Constants for excitation system for hydro-turbine unit

Name of constants	Value
Low-pass filter time constant Tr(s)	20e-3
Regulator gain and time constant	
Ka()	300
Ta(s)	0.001
Exciter	
Ke()	1
Te(s)	0
Transient gain reduction	
Tb(s)	0
Tc(s)	0
Damping filter gain and time constant	
Kf()	0.001
Tf(s)	0.1
Regulator output limits and gain	
Efmin(pu)	-11.5
Efmax(pu)	11.5
Kp()	0